ELEVATED RECHARGE OF ELECTROCHEMICAL CELLS

by

PETER NOVAK

Presented to the Faculty of the Graduate School of

The University of Texas at Arlington in Partial Fulfillment

of the Requirements

for the Degree of

DOCTOR OF PHILOSOPHY

THE UNIVERSITY OF TEXAS AT ARLINGTON

December 2013

Acknowledgements

I would like to thank everyone on my committee. I would like to thank Dr. Dillon for helping me navigate the bureaucracy. I would like to thank Dr. Kenarangui for persuading me to get a doctorate. I would like to thank Dr. Lee for teaching me not to over engineer things, and more importantly for putting up with me. I would like to thank Dr. Liu for always taking time to answer my questions. Lastly, I would like to thank Dr. Wetz for taking me on as a student. I was your first doctoral candidate, and hopefully I shall not be your last. Though I think neither of us knew what we were getting into, somehow we managed to work together.

I would also like to give a huge thanks to my colleagues and lab-mates, Jay, James, Isaac, Clint, Greg, Anthony, Simon, and especially Biju. Looking back I am amazed at all the things we did, and how we managed do half of them. I would also like to thank Jamila, Nathan, and Nadim for putting up with some of the more tedious tasks as well. Your presence greatly assisted our research efforts. Also, thanks to Mike for suffering through the senior design with me. Isaac W, thanks for suffering through micro with me. Lastly, I would like to thank my mom and dad, who have always supported me. Also, thanks to my sister for looking out for me.

November 09, 2013

Abstract

ELEVATED RECHARGE OF

ELECTROCHEMICAL

CELLS

Peter Novak, PhD

The University of Texas at Arlington, 2013

Supervising Professor: David Wetz

Electrochemical cells are energy dense storage devices used to power everything from small portable electronics such as cell phones, to larger systems including electric and hybrid-electric vehicles or even electric utility backup supplies. In recent years, the electrochemical community has analyzed many aspects of cell performance with papers covering the influence of temperature, humidity, pressure, and various other factors on the aging of different types of cells. Despite the abundance of information on various issues, very little work has been presented in the area of high rate elevated charge and even less work regarding high rate pulsed elevated charge.

This thesis starts by giving a basic overview of batteries and pulsed power systems, a specific type of load used in a variety of defense and civilian applications, before moving on to a more detailed technical background on a number of different types of cells with a focus on lithium-ion batteries. Prior work investigating the aging mechanisms of lithium-ion batteries will also be presented and examined. The aim of the work performed here is to further demonstrate how high-rate pulsed and continuous recharge impacts the aging of lithium-ion batteries. The development of the experiments

performed and the results obtained will be discussed along with the results of a cell modeling exercise. Conclusions are then drawn in the final chapter.

Table of Contents

List of Illustrations

List of Tables

List of Equations

Chapter 1

Introduction

To myself I am only a child playing on the beach,
while vast oceans of truth lie undiscovered before me.
-Sir Isaac Newton

Electrochemical cells are energy dense storage devices used to power everything from small portable electronics such as cell phones to larger systems including electric and hybrid-electric vehicles or even electric utility backup supplies. In recent years, the electrochemical community has analyzed many aspects of cell performance including the influence of temperature, humidity, pressure, and various other factors on the aging of different types of cells. Despite the abundance of information on various issues, very little work is presented in the area of high rate elevated charge and less work is presented regarding high rate pulsed elevated charge.

This thesis focuses on the aging of lithium-ion batteries when they are recharged using high currents along with a minor emphasis on the elevated rate recharge of other types of electrochemical cells. The first chapter will cover methods of charging batteries, the difficulties with charging batteries at high rates, and some applications of high current charging. The second chapter will discuss more specifics concerning a number of different chemistries. The third chapter will cover prior work in the literature concerning electrochemical cells and the mechanisms which cause them to age. As part of this thesis, experiments were performed in which a 3Ah nickel cobalt aluminum oxide (NCA) lithium-ion battery was recharged at elevated and nominal rates. The fourth chapter discusses the results of those experiments and the fifth chapter will provide insight as to how aging evolves when high rate recharge currents are used. In the sixth chapter, modeling efforts performed using the experimental data will be discussed. The seventh

chapter will briefly highlight some additional elevated rate recharge experiments which have been performed and finally the eighth chapter will present conclusions and future work.

1.1 Basic Electrochemical Cell

A battery consists of two electrodes and an electrolyte separated by a porous membrane that allows positive ions to flow from the cathode to the anode. In the case of lead acid batteries and metal-hydride batteries, hydrogen ions are generated by the governing chemical reactions. Advances in the manufacturing of electrochemical materials has allowed battery makers to develop higher energy batteries which use lithium-ions rather than hydrogen. Battery chemistries are considered to be of either the primary or secondary type. Primary cells undergo polarization, meaning that either the chemical reaction governing the cell is non-reversible or that the ions cannot easily traverse the cathode material. In either case, this prevents further work from being performed once the cell has been discharged and the cell must either be thrown away or recycled. This means that under normal operating conditions, primary batteries cannot be recharged. Primary cells have a wide penetration in the battery market due to their maturity as well as their fiscal advantages. Most conventional AA, AAA, 9V, C, and D sized cells used by the majority of consumer electronic devices are primary cells since their raw materials are not hard to acquire and cheap to procure. On the other hand, secondary cells offer the advantage of being rechargeable. These cells include lithium-ion, nickel metal hydride, and lead acid, among many others. The work presented here focuses on secondary chemistries due to their ability to be recharged multiple times without significant degradation to their materials. An illustration showing the motion of lithium ions and electrons during the charge and discharge processes of a lithium-ion battery is shown in Figure 1.

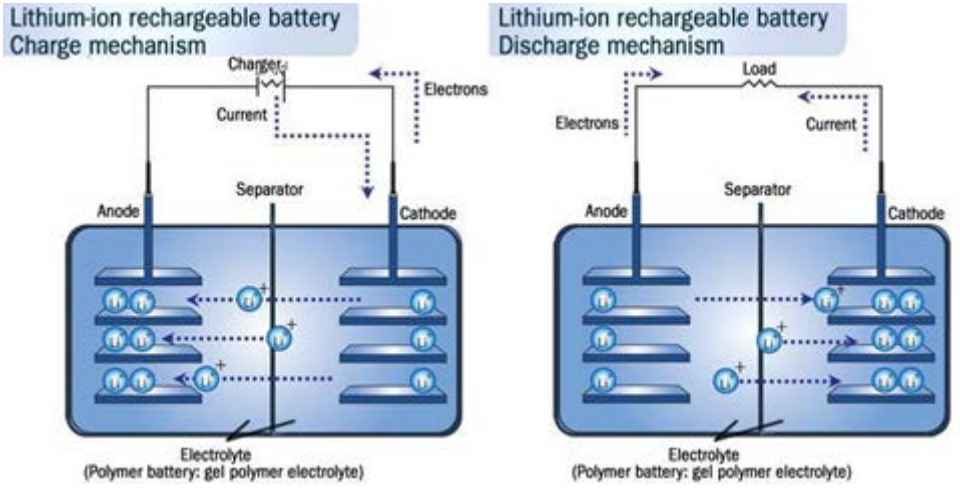

Figure 1 A secondary cell showing a secondary lithium-ion cell undergoing charge and discharge [1].
During the charge process, the charger extracts electrons from the cathode while lithium-ions migrate from the cathode to the anode. During the discharge process, electrons are sourced out of the anode and through the load while ions migrate from the anode back into the cathode.

Independent of whether a cell contains a primary or secondary chemistry, batteries are sized in units of ampere hours (Ah) or watt hours (Wh). These ratings provide an estimate of the cell's capacity. For example, a 3Ah battery is notionally able to source 3 A of current for one hour. Performing the aforementioned discharge is referred to as a 1C discharge. The 1C term in the prior sentence refers to the cell's C-rate. The C-rate is defined as the current sourced out of or placed into the cell divided by its nominal capacity in ampere hours. For example, if the same 3Ah cell undergoes a 2C discharge, the cell will source 6 A of current to the load for slightly under half an hour before being fully discharged. Unfortunately, the relationship between C-rates, capacity discharged, and the time to complete discharge is not completely linear. In the case of new, advanced lithium-ion batteries with low internal resistances, the useable capacity

remains relatively consistent as the C-rate increases. This is shown in the voltage vs. capacity curves of a 5Ah lithium-ion battery in Figure 2.

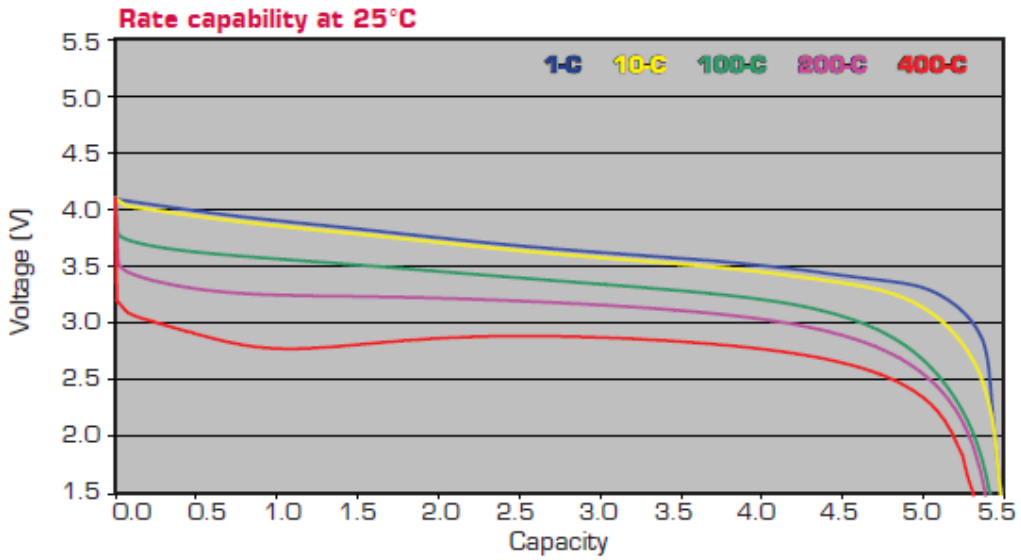

Figure 2 Voltage vs. capacity curves measured from a 5 Ah NCA lithium-ion battery at various C-rates [2].

Generally, a simple linear relationship usually makes a decent approximation for the amount of time a cell should be able to discharge a particular current with respect to its nominal C-rate. The rate dependency varies strongly for different chemistries and how much it varies depends upon the conditions in which they are used. Because operation at high rates can create a host of concerns ranging from degraded cycle life to severe safety hazards, they are seldom operated at extreme current rates. This means that little literature is available beyond 5C recharges.

Energy storage technologies that are available today include lead-acid batteries, nickel-metal hydride batteries, sodium-sulfur batteries, lithium-ion batteries, electric double layer capacitors, and lithium-ion capacitors among countless others. Each has advantages and disadvantages. Some of the characteristics that are used to determine the application of these technologies include the nominal voltage, surge current, energy

density, power density, cost per unit energy, cycle life, calendar life, self-discharge rate, and overall efficiency. Among two of the most critical properties listed above are the energy and power density, respectively. An energy dense cell is able to store considerable energy in a small package. These types of cells are usually designed to source a large amount of energy for a longer period of time at a lower rate. On the other hand, power dense cells are able to supply energy to the load quickly, requiring them to source current at high C rates. Ideally, manufacturers and chemists would like to make a cell that has both the maximum energy density and power density in a single chemistry and form factor, but this is difficult due to physical and/or chemical limitations. A Ragone plot comparing the power and energy densities of some of these different technologies is shown in Figure 3. As shown in the aforementioned figure, supercapacitors are a textbook example of a power dense electrochemical cell. They can be charged and discharged at high rates with the only side effects being mild cyclic aging, as well as heating. A fuel cell, on the other hand, is an energy dense technology. This means that it may supply a steady load for a long time, but is unable to supply current at high rates.

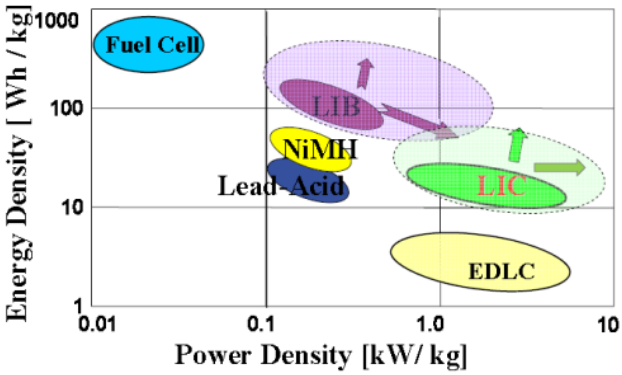

Figure 3 Ragone plot comparing the power and energy density of various conventional off-the-shelf energy storage technologies (typical values when these devices are used to power electronic systems in steady state operation) [3].

While lithium-ion batteries are not the most mature energy storage technology, they are being used, or considered for use, in a wide variety of applications due to their

high energy density, high power density, or both. These include consumer electronics, hybrid/all electric vehicles, and even pulsed power systems being developed for the US Department of Defense (DoD). These devices have been previously used in many applications and have shown to be reliable and efficient. Many of the aging mechanisms that lead to the end of life for these devices, when used at their rated conditions, are well understood and documented. What has not yet been studied, however, is how these devices perform and degrade when they are charged and discharged over many cycles at rates that greatly exceed their nominal ratings. In other words, at the conditions that will be required to drive high power applications such as vehicles and pulsed power applications.

Commercially available lithium-ion batteries are typically very energy dense (100 Wh/kg) but only moderately power dense. Their low power density is a consequence of the time needed for electrochemical reactions to occur, coupled with a high internal resistance (several mΩ) that only increases as cells age and are cycled. It is widely considered that a lithium-ion battery reaches the end of its life when the cell's energy and power capability are at 80% of their original values [2]. The lifetime of lithium-ion batteries can be as short as a few hundred cycles or as long as several hundred thousand cycles depending on the application, the depth of discharge, and the rate of recharge.

1.2 Charging of Batteries

There are a number of different standard procedures used to recharge electrochemical cells. This includes the trickle charge, float charge, and the constant current-constant voltage charge. In the case of a trickle charge, a constant current with a low magnitude is sourced to the cell until fully charged. This is a low rate procedure and does an extremely good job of charging batteries if time is not a major constraint. Many

“overnight” chargers utilize this method of charging to charge cell phones and other portable electronic devices. Float chargers are similar to trickle charges, except they provide a constant voltage to the battery rather than a constant current. The difference in voltage between the battery and the charger causes a current to flow from the source to the electrochemical cell, thus adding capacity. This makes the cell voltage appear as if it is “floating’ upward to the same voltage as the power supply. Though useful, this method of charging only controls the current rate by potential difference. The most common method of charging lithium-ion batteries is known as the constant current – constant voltage charge procedure. As the name implies, this method of charging uses a constant amount of current to charge the battery until the voltage reaches a critical cutoff value. After reaching the cutoff voltage, the charger regulates its output voltage to the desired charge voltage and it continues to apply that voltage until the current drops below a specified value, meaning that the cell has accepted all of the charge it is capable of receiving. This process is shown graphically in Figure 4.

One reason this method of charging is widely used today is because it is a standard that can easily be replicated and normalized over a wide range of battery capacities. Like discharge procedures, recharge procedures are usually defined by the C-rating used relative to the cell(s) under test. The magnitude of the constant current (CC) is typically referred to as N*C, where N is an integer greater than zero. The higher the recharge rate, the higher the value of N. When CC magnitudes less than 1C are used, they are typically documented as a C/N charge. A sample plot of the current and voltage recorded when recharging a 3Ah lithium-ion battery is shown in Figure 4. Note that the cell voltage is plotted as a function of time as opposed to capacity as was shown in Figure 2 above. This better illustrates what happens during a 1C, CC-CV charge than a plot vs. capacity would. High currents can be used in the CC charge phase as a means

to recharge fully discharged batteries up to roughly eighty percent state of charge (SOC) relatively quickly. Once high SOCs (roughly 80%) are achieved, the charge rate must be decreased to lower rates in order to prevent excess electrical stress on the electrolyte.

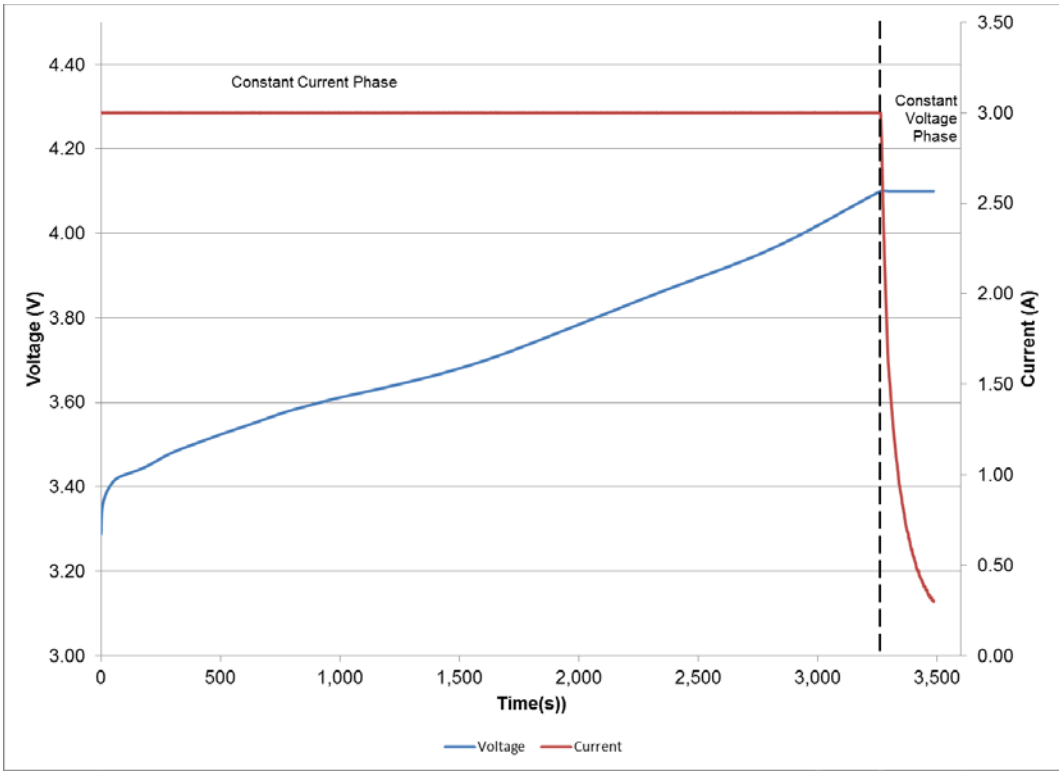

Figure 4 A 1C CC/CV charge on a 3Ahr cell until the current drops to C/10.

This plot demonstrates a simple 1C, CC/CV charge of a 3Ah cell. Current is supplied at a constant current rate of 3 A until the maximum cell voltage of 4.1V is reached at which point the charge converts to a 4.1V constant voltage charge until the current supplied by the source into the cell decreases below 0.3 A or C/10.

In more recent years, induction has become a popular method of charging batteries. This is a market response to industry having a number of proprietary connections for their small electronic devices. Charging by induction works largely like a transformer with a large air gap. A coil in the primary device is magnetically linked to a coil in the secondary device, permitting current to flow even though no wires connect the

two inductors. This method prevents corrosion and allows circuits to be electrically isolated from each other, but has a large amount of waste energy, typically in the form of flux loss in the air gap. Another drawback includes the lack of IEEE standards regarding charge by induction for small electronic devices, though a committee for this task was formed in 2012 [4]. At the time of this writing, the standard has yet to be finalized. Even though IEEE standards are not present, charge by induction typically takes in a 50/60 Hz power supply, rectifies that signal, and then inverts it to a high frequency AC signal before going to an inductive coil. The high frequency AC signal is then magnetically coupled into a coil on the device being charged. At that point the charge is rectified and DC current is fed through a charger which charges the electrochemical cell in one of the manners described above, dependent upon the control circuitry.

The last method of charging, known as pulsed charging, refers to applying current to the cell in a pulsed manner. The current rate can be either high or low depending on the application. Typically, low current pulsed charging might be used to keep a cell-phone fully charged after the trickle charge has been completed. Depending on the author, small pulsed charging may itself be referred to as a trickle charge. This method of charging does not increase the state of charge, but will instead periodically refresh the charge which batteries naturally lose over time. Large current pulsed (LCP) charging methods can be used to recharge fully discharged batteries up to roughly eighty percent state of charge (SOC) relatively quickly. Once high SOCs (roughly 80%) are achieved, the charge rate must be decreased to lower rates in order to prevent excess electrical stress on the electrolyte. Pulsed charging has previously been investigated at nominal rates in the literature. Though this will be discussed in further detail later, the types of acceptable pulsed charging methods and rates generally depends upon the

chemistry. Table 1 displays a summary of the charging methods advantages and disadvantages.

Table 1 Summary table of various advantages and disadvantages of charging methods.

Charge Type	**Major Advantage**	**Major Disadvantage**
Trickle Charge	Very safe	Extremely slow rate.
Float Charge	Safe	Charge rate dependent upon potential difference.
LCP Charge	Very Fast	Faster aging. May not fully charge cell.
CC-CV Charge	Standard	Requires two stages.
Charge by Induction	Electrical Isolation	Heat loss, inefficient

1.3 Concerns with High Current Recharging of Electrochemical Cells

The recharge of electrochemical cells at elevated current rates presents a number of potential cell life and safety issues. The cell's equivalent series resistance plays a pivotal role. All of the components of the battery: the cathode, electrolyte, separator, anode, and the current collectors contribute to the cell's internal resistance. Electrochemists and electrical engineers typically lump all of these different resistive contributions into one value, referred to as the ESR. When recharging at high rates, a voltage rise in the cell's potential, proportional to $I*R_{ESR,}$ is measured in series with the cell' charge potential at the cell's terminals. If the total cell voltage rises above the bandgap of the electrolyte, the cell can begin to fail thermodynamically.

In order to achieve the maximum cell potential possible, electrolyte bandgaps are generally stressed near their limits in normal operating conditions. Unfortunately, exceeding the electrolyte bandgap potential is not difficult, especially during high rate recharges. If the voltage of the electrochemical cell exceeds the bandgap of the

electrolyte, the cell can become thermodynamically unstable. Even when charging at 1C rates, the voltage rise across the ESR is significant and cannot be ignored, making it vital to understand the limitations before elevated rate charge currents are used.

High rate recharge also increases the heat generated internal to the cell. Any time current travels through a resistance, joule heating occurs at a rate proportional to the square of the current. This means that even small resistances can generate a significant amount of heat when high currents flow through them. Though elevated temperatures cause the ionic resistance of the electrolyte to decrease, the ratcheting effect of repeated high rate charge and discharge can cause the cell to reach its maximum safe operating temperature. If the temperature of the cell gets too hot, a non-reversible chemical reaction may occur. At the minimum, this non-reversible reaction can greatly diminish the functionality of the battery.

The ionic diffusion rate is also a concern when high rate recharge procedures are used. If the charge rate is too high, it may not be possible to extract and intercalate the ion out of and into each respective electrode. For lithium-ion batteries, the presence of a solid-electrolyte interface (SEI) layer prevents ions from quickly intercalating in and out of the carbon anode. The inability of the ion to work its way into the structure can lead to phenomena such as lithium plating and dendrite growth. In the case of lithium plating, a thin layer of lithium is formed on top of the SEI layer, which further prevents the intercalation of ions. Dendric growth refers to a physical structure that forms on the electrode surface. The dendrite is essentially a buildup of lithium on the electrode surface. A scanning electron microscope (SEM) image of one such dendrite is displayed in Figure 5.

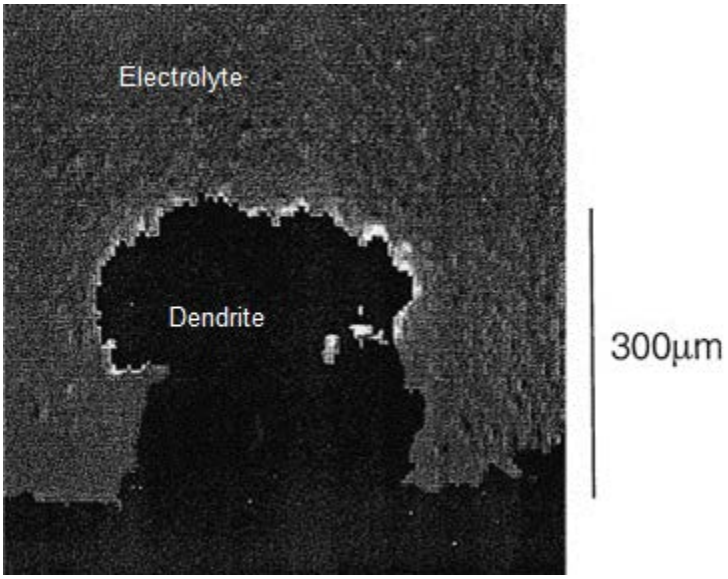

Figure 5 SEM image of dendric growth on a graphite anode [6].

Figure 5 shows an example of how the structure builds. If allowed to build long enough, these structures may protrude from the surface. If it extends too far, the dendrite may pierce the separator which will short circuit the cell internally.

Diffusion may also lead to another form of failure, known as salt formation. In normal operation, the salt allows the ion to travel from the anode to the cathode. If there are too many ions present however, the highly electropositive ion will form a compound with a free anion. What salt is formed depends greatly on which electrolyte is used. As an example, the electrolyte might form a compound such as lithium fluoride rather than the lithium phosphorous hexaflouride it would under normal operation [7]. Regardless of the salt formed, the lithium-ion is no longer available to intercalate, decreasing the overall capacity of the cell.

1.3.1 Applications Benefiting from the implementation of high rate recharge

High current charging offers a benefit to a wide a number of different applications. Any electronic device that uses an electrochemical cell as its power supply

will benefit from having reduced downtime or reduced charge time. Many of those are high power applications which require the energy storage to accept a large amount of current in a short period of time. One involves the harvesting of transient energy from renewable generation sources such as wind turbines. On the electrical grid, the generation must be able to match the load at all times. When the load does not match the amount of power generated, either generation must ramp up or load shedding must occur. The wind is unreliable, as well as unpredictable, which Figure 6 and Figure 7 illustrate. Since the energy harvested by wind turbines must be used at the moment it is generated, their ability to charge an energy storage device in a pulsed, high-rate manner is critical in order for the energy to be used eventually by the loads connected to the grid. Harvesting this energy greatly assists utility operators and allows wind farms to participate in the day ahead market since a set amount of energy is stored for use in their energy storage device. While a lack of wind is never good, an abundance of wind is also problematic as these temporary events supply a great deal of energy which can almost never be used fully at the time it occurs. While the use of batteries alone is optimal due to their high energy density, their low power density often makes them impractical thereby requiring them to be combined with more power dense technologies such as electric double layer capacitors (EDLCs). The increase in the power density from newer lithium-ion batteries helps to alleviate this redundancy. Despite this, it is still unclear how the repeated application of high pulsed currents to the newer lithium-ion batteries will impact the aging of the devices.

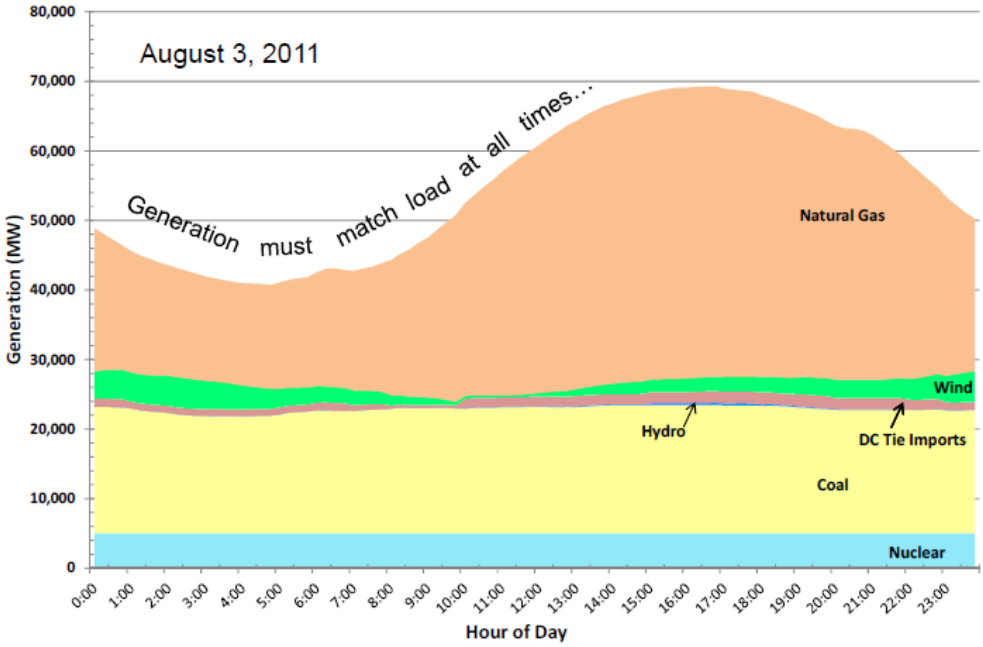

Figure 6 The generation provided by ERCOT on August 3rd, 2011. This shows one of the major issues with wind, in that it cannot be dispatched.[8]

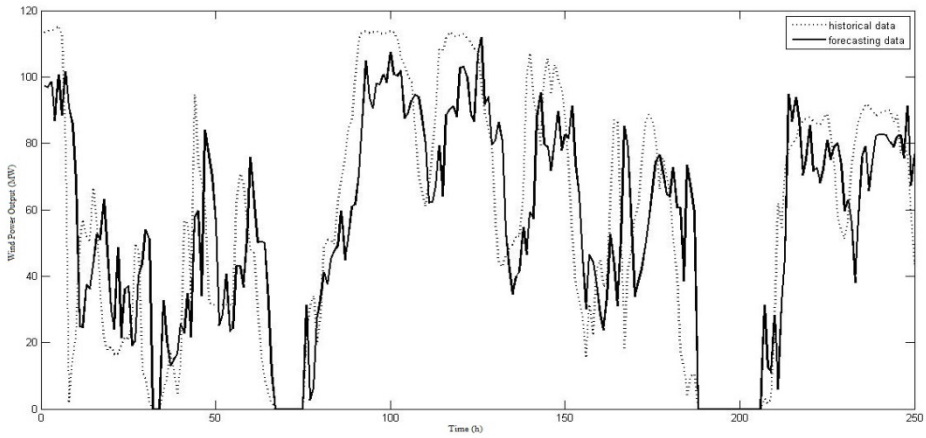

Figure 7 Transients inherent in wind power generation [9].

The ability to recharge batteries at high pulsed and continuous rates is also of great benefit to the wide spread adoption of hybrid electric vehicles (HEVs) and all electric vehicles (EVs). A schematic showing the drivetrain of a hybrid electric vehicle is

shown in Figure 8. One of the major obstacles these automobiles face deals with the fact that they require a large amount of time to 'refuel' when batteries must be recharged at low, nominal rates. In order to sell these vehicles in the United States, the Department of Transportation has a number of safety regulations and tests that all light-duty vehicles must pass. As expected, large battery banks are needed to give HEVs and EVs a feasible driving range. With this comes a long recharge time, as long as 8-10 hours in some cases. By comparison, most conventional internal combustion engines take less than ten minutes to completely refuel at the local gas station. The ability to recharge the energy storage at a high continuous rate is critical to reduce the recharge times. Though this is beneficial, even if it is possible, a large infrastructure burden prevents widespread adoption at the time of this writing. Electric utilities would have to greatly improve their grid as well as provide significantly more generation in order to accommodate a large number of electric vehicles.

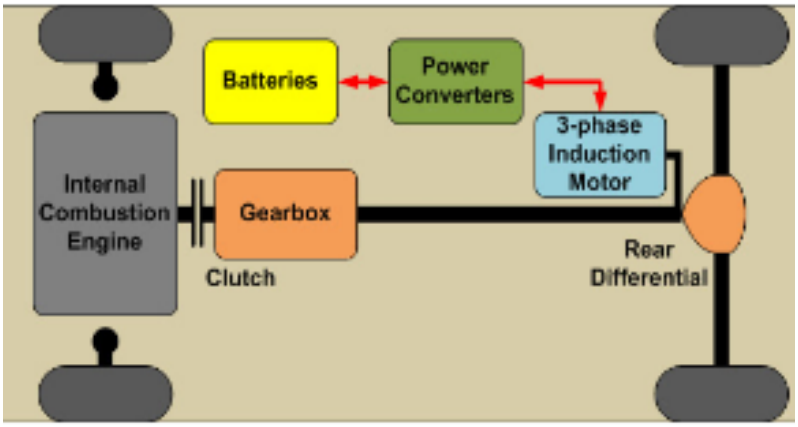

Figure 8 Powertrain of a hybrid electric vehicle [11].

Because of the large mass most vehicles have, it is possible to make use of regenerative braking. Note in Figure 8, the electric power train has arrows pointing

towards and away from the batteries, meaning that this particular vehicle utilizes energy harvesting from regenerative braking, as shown in Figure 9.

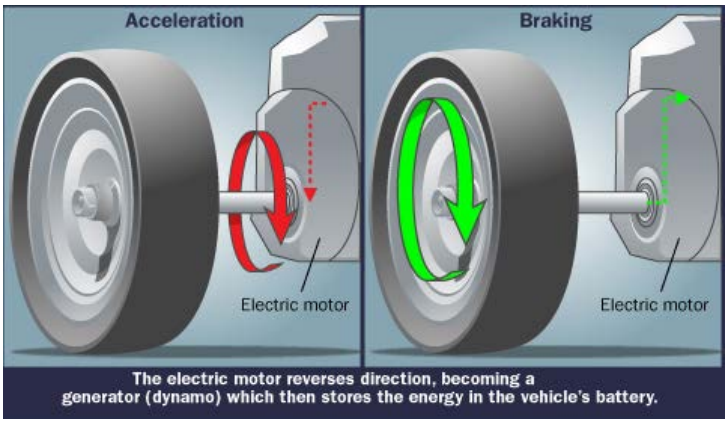

Figure 9 – A simple schematic of regenerative breaking.
When accelerating, the engine provides power to spin the wheels one direction. Reversing the direction of motion temporarily turns the motor into a generator, and feeds current back into the batteries[10].

The idea behind regenerative breaking is relatively simple. Rather than use discs or drums to generate friction and stop the vehicle, regenerative breaking primarily utilizes the electromagnetic force, greatly reducing the amount of waste heat as shown in Figure 9. In order to achieve this, engineers simply take advantage of induction (asynchronous) motors. When two of three phases on an AC induction motor are switched, the motor rotates in the opposite direction that it was previously going. In other words, if an induction motor was spinning counter-clockwise, and an operator switched phases A and B, the induction motor would begin to spin clockwise. In a similar fashion, if a car is travelling down the road and the driver hits the breaks, the tires spinning the other way temporarily force the motor to act as a generator which provides a large amount of power to the batteries in a transient manner over a short amount of time. The entire regenerative breaking process approximates a single pulse temporarily charging a battery. The magnitude as well as duration of the pulse generally determines what

electrochemical cell or combination of electrochemical cells should be used in order to achieve optimum energy capture. This will be described further in Chapter 2.

Another potential area where large amounts of current could potentially be useful is in copper refinement. One of the more common methods of refining copper is to put thin sheets of copper into an electrolyte and let current flow through it for days or weeks at a time. For those unfamiliar with the process, copper refinement via electrolysis has a pure plate and an impure plate acting as the cathode and anode of an electrochemical cell. As large amounts of current flow through the electrolytic solution (typically a copper sulfate), the impurities such as zinc and iron are dissolved into the solution. Obviously, this requires a large amount of current over a long period of time, and there are other bottlenecks in the copper refining process so research in this area is somewhat slow going. However, it still remains a potentially viable application that could be done in a pulsed form. Unfortunately, at the time of this writing very little literature exists on copper plating done on a large scale, though a fair amount of literature exists for a similar process called copper electroplating, particularly for MEMs, circuit boards, and other various silicon fabrication techniques [12,13].

Finally, the last application that will be discussed involves the use of batteries as as the prime power source in pulsed power systems. Pulsed power systems have many applications, such as high power microwave sources [14], electromagnetic launchers [15], improvised explosive device (IED) defeat [16], and environmental treatment systems [17] among others. Developing fieldable compact pulsed power systems for these various applications has been difficult. From a historical perspective, pulsed power research has been performed in large laboratories where size was not a limiting factor. Transitioning a large system into a compact device is challenging. As part of a US Air Force Multidiciplinary University Research Iniatiative (MURI), Schamiloglu, et al. found that the

critical needs for developing a compact pulsed power device include advancements in materials research and development, electromagnetic modeling, and thermal management [5]. While their work was focused on improving the state of the art in high power microwave devices, these needs closely align with the needs for improvement in all areas of compact pulsed power.

A typical pulsed power system is made up of a prime power source, intermediate energy storage, pulsed forming line(s) (PFL), switch(es), and a load. What the load is determines the pulsed power system. A simplified schematic of this is shown in Figure 10. Note that this hardware allows a large amount of power to be compressed down into a relatively short amount of time, shown by Figure 11.

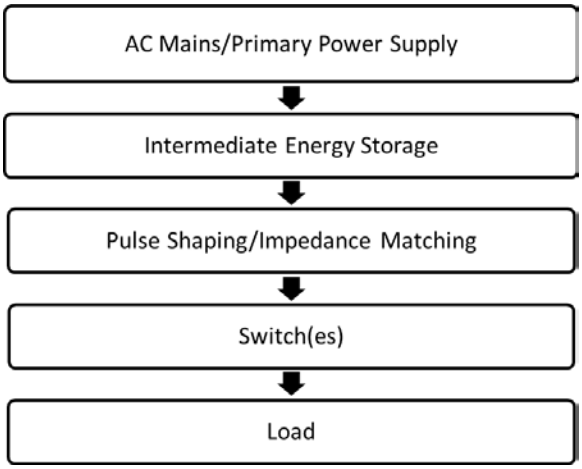

Figure 10 A typical pulsed power system setup.

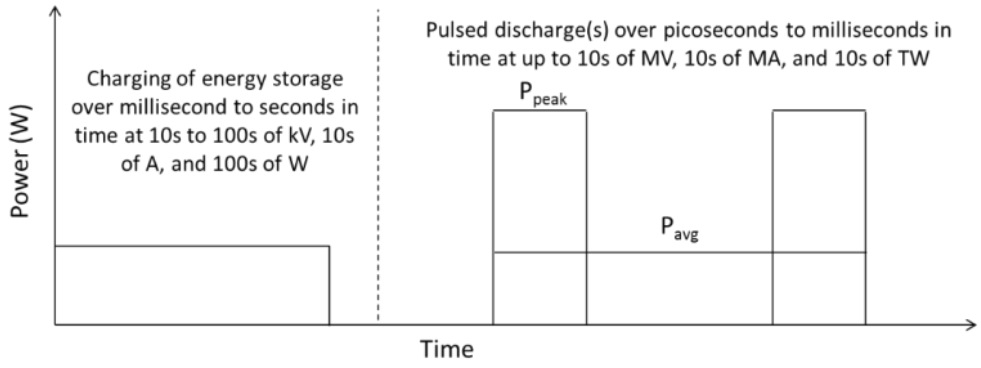

Figure 11 - The theoretical basis of pulse power. Pulsed Power compresses the energy of a relatively steady state pulse into a short amount of time.[18]

The ability to reduce the size of a pulsed power system depends on how small each of these respective components can become. The intermediate energy storage is most often made up of either capacitive or inductive elements. The energy density of both capacitors and inductors have advanced significantly over the past decade with improvements in dielectrics [20], electrode structures [21], and ferrite core materials [22]. The size of the pulsed forming lines depends upon the dielectric used, and many dielectrics such as sulfur hexafluoride [23] have been extensively characterized. These advances have improved pulse forming lines in many applications. The considerable advances in solid state switch technologies have perhaps had the most influence on the size of pulsed power systems. In the early days of pulsed power technology, the switches used to control the flow of energy were large, heavy, and often hazardous. The ability of solid state switches to function as pulsed power switches has greatly increased in recent years [24,25] largely due to the increases in hold off voltages and hold off currents. As one may expect, transitioning from ignitrons and mechanical switches to solid state devices such as insulated gate bipolar transistors (IGBTs) greatly decreases the foot print of traditional pulsed power devices. Despite the reductions in the volume and mass of switching technologies, prime power sources remain relatively large. Very little work has

been done on reducing the size of prime power sources for pulsed power applications in the pulsed power community. However, the electrochemical community has placed a large amount of work into increasing the power and energy density of electrochemical cells. The large volume of research, as well as the concurrent advancement in manufacturing of electrochemical materials, has made it possible for batteries to possess a small foot print while still being able to charge and discharge pulsed power loads. The reduction in footprint and weight has made batteries particularly suited for mobile applications, where having a secondary generator to provide a pulsed power load would incur too large a cost either in volume, mass, fuel consumption, expense, or a combination thereof. Due to the nature of pulsed power loads, they generally discharge quickly. If one needs to quickly charge a primary power supply or intermediate store consisting of electrochemical cells, one must have a knowledgeable risk assessment of how the electrochemical cell will tolerate the elevated charge. A specific charge profile will be discussed in chapter 5, and chapters 2 and 3 should provide sufficient information to make predictions for other charge profiles and with varying cell chemistries.

Chapter 2

Technical Background on Selected Electrochemical Cells

He who knows best knows how little he knows
-Thomas Jefferson

As stated in Chapter 1, the materials and manufacuring of electrochemical cells has greatly improved over the past two decades, particularly with respect to lithium-ion cells. However, lithium-ion cells are not the only type of secondary cell that can be recharged at either nominal or high rates. A few technical specifics of the recharge characteristics of nickel cadmium (NiCad), Nickel-metal hydride (NiMH), supercapacitors, and asyemmetric capacitors will be presented in this chapter, however, the primary focus will be cast on the recharge of lihtium-ion batteries. Figure 12 contains a Ragone chart which displays typical volumetric and gravimetric energy density many different types of secondary batteries. A similar chart displaying the gravimetric power and energy density of the cells is shown in Figure 3.

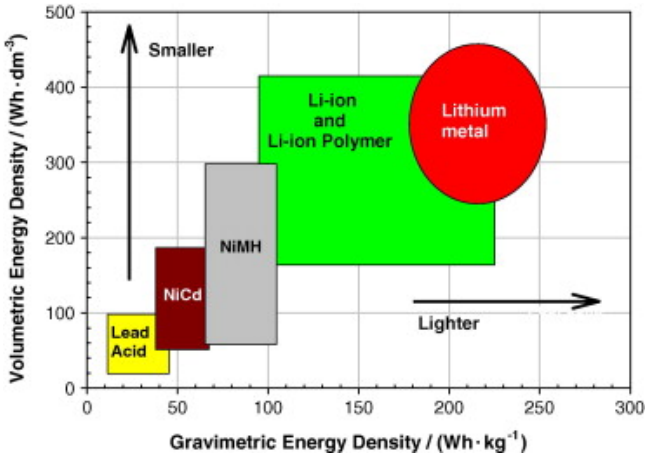

Figure 12 - A comparison of volumetric and gravimetric energy density of various electrochemical cells. Note that the lithium-metal battery is a primary cell [26]

Combined, the two figures present a nearly complete picture of the vast differences in the energy and power density of today's electrochemical cells. As one can

surmise, even though lithium-ion batteries have the highest energy density, other chemistries have use in a number of applications in which even lithium-ion batteries are not optimal.

2.1 Lead Acid Batteries

Lead-acid batteries are regarded as the first rechargeable battery [27]. The century and a half in research and development has allowed the lead acid battery to mature into a multibillion dollar industry. Though lead acid batteries have had significant alterations made to them over the years, the major chemical equations governing the cell have not significantly changed. The major chemical equations governing the operation of lead acid cells are shown in Equation 1. Equation 1a describes the overall chemical equation of a lead acid cell, and equations 1b and 1c describe the chemical reactions that occur at the cathode and anode respectively. The toxicity of lead has been a known issue for a long time [28]; however, wide-scale recycling of these batteries technology has largely alleviated the problem [29].

$$Pb + PbO_2 + 2H_2SO_4 \leftrightarrow 2PbSO_4 + 2H_2O \qquad [1a]$$

$$3H^+ + PbO_2 + HSO_4^- + 2e^- \leftrightarrow PbSO_4 + 2H_2O \qquad [1b]$$

$$Pb + HSO_4^- \leftrightarrow PbSO_4 + 2e^- + 3H^+ \qquad [1c]$$

Equation 1 - The overall equation for the lead acid cell [1a], the cathode half-cell-reaction [1b] and the anode half-cell-reaction [1c]. Note that the electrons do not participate in overall equation, but are an important part of each half reaction.

The relative simplicity and abundance of materials (water, sulfuric acid, and lead) have made these batteries extremely popular and affordable for many years now. Lead has a relatively low melting point and high density, making it easy to shape electrodes using lead foil. A detailed look at Figure 3 and Figure 12 show that lead acid batteries are

considerably power dense but lack energy density compared to other battery technologies. Unfortunately, lead is one of the largest and heaviest atoms on the periodic table. This makes it hard to achieve high gravimetric energy density (kW/kg), as shown in Figure 12. When considering their use in high power applications, the high currents that can be sourced in a relatively short amount of time makes these batteries look extremely viable at first glance. The lack of energy density is a drawback if long operation at high rates is needed. While lead acids are used in countless applications, one often thinks of their use as energy sources to start devices such as automobiles. In this mode of operation, the devices source little overall energy and instead are only used in a pulsed power operation. Therefore, recharge is typically performed using a float charge procedure. Manufacturers generally recommend a constant voltage recharge procedure with a specific peak current allowable. For example, the EnerSys Genesis XE series specifies a constant voltage with a maximum current of 3C10, which is three times the nominal 10 hour rate. In the case of the XE16, which is a 16 Ah battery, the peak current rate of 48 A is recommended. A sample constant voltage recharge of an XE16 battery is shown in Figure 13.

The figure shows a noticeable voltage decrease at the start of the procedure. This is believed to occur as a result of the high initial impedance of the battery. Initially, the cell is fully discharged, the electrolyte is primarily water, and the cell's temperature is low. The complete discharge of the cell caused a fixed amount of sulfation (sulfonation), meaning that the amorphous lead-sulfate that typically appears while discharging transformed into a more stable crystalline solid. Breaking up the crystalline solid requires more energy than simply changing the lead sulfate back into lead oxide, or pure lead as described in Equation 1. Note that sulfation may be overcome by slightly overvoltaging each individual cell in a lead acid battery, colloquially referred to as performing a

saturation charge. As the charge is initiated, the high impedance is unable to accept the high current charge causing the power supply supplying the charge to briefly collapse. As the cell starts to recharge, the electrolyte becomes more acidic and the impedance drops as a result of this, as well as the increasing cell temperature. Eventually, the battery is able to accept the high current causing its voltage to rise.

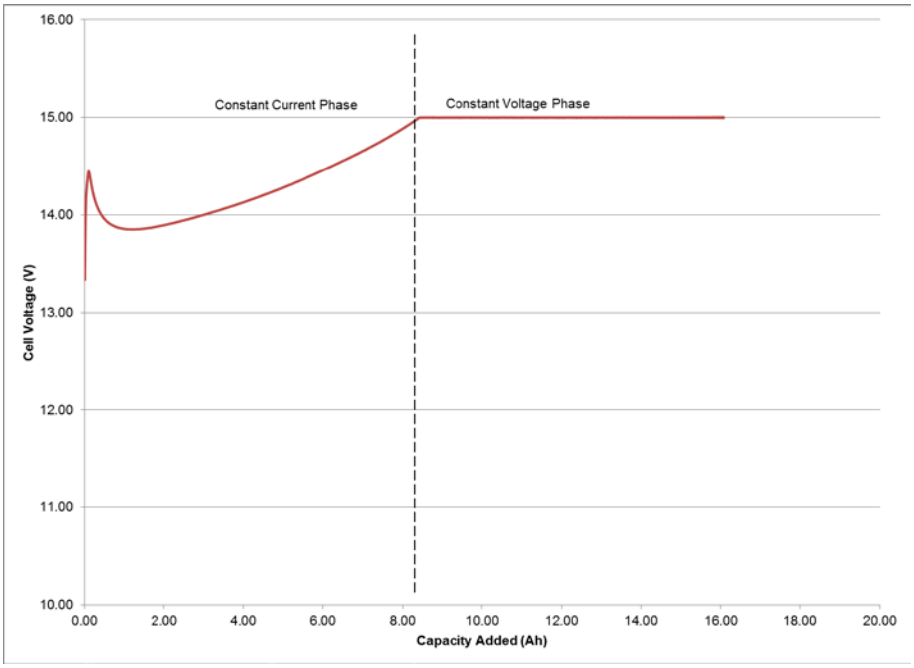

Figure 13 - A sample 3C CC/CV of a 16Ah lead acid battery charge until C/10 is reached. The voltage dip in the beginning is due to the sulfonation of the lead.

In order to preserve the cycle life of lead acid batteries, it is typically recommended that they not be discharged below 80% DoD and that they be recharged at low currents. Due to their widespread use, the IEEE has developed a large number of standards related to lead acid batteries, such as IEEE SA 450 which has practices and recommendations for the maintenance of vented lead acid batteries. Numerous other IEEE standards also exist regarding lead acid batteries. In short, the maturity and cost of these batteries makes them extremely feasible for high rate recharge, especially where

volume and mass are not a major constraint and economic concerns override all other considerations. Though the high-rate recharge may alter the cycle life of a lead acid battery slightly, it is not significant compared to how deep the battery discharges during use.

Despite the inherent issues with mass, high power systems which utilize lead acid batteries as their prime power source have been previously documented. For example, [30] used lead acid batteries to power a 21 kW pulse to start an aircraft engine, and [31] used lead acid cells as the prime power source of an electromagnetic launcher.

2.1.1 Bipolar Lead Acid Batteries

When a higher combined energy and power density is needed, one may consider the use of a different type of lead-acid battery known as a 'bipolar' lead-acid battery. In this type of cell, a singular electrode is made with a conductive layer on either side of it. One side of the surface is coated with a negative active material, making up the anode of a cell, while the other side is coated with a positive active material, making up the cathode of the next adjacent cell to the cathode on the other side [32-36]. This method of construction greatly reduced the amount of interconnecting material, and therefore the interconnection impedance, of traditional lead acid batteries. The reduction in electrodes and tab connections reduces the volume and mass of these cells compared to their traditional counterparts as shown in Figure 14.

Though the footprint of bipolar lead acid batteries has been reduced over the years [38], no feasible way to substantially reduce the mass of these cells much further exists since they require one of the heaviest elements. The high number of electron orbitals allows relativistic effects to add a large amount of efficiency to the electrochemical process [39], but this prevents construction of cells with high energy or power density. Bipolar lead acid batteries have a slightly reduced lifetime compared to

their conventional counterparts [40]. Another reason bipolar lead acids have not become popular is their large current decline within the first 200 microseconds of a pulse discharge, as shown in Figure 15.

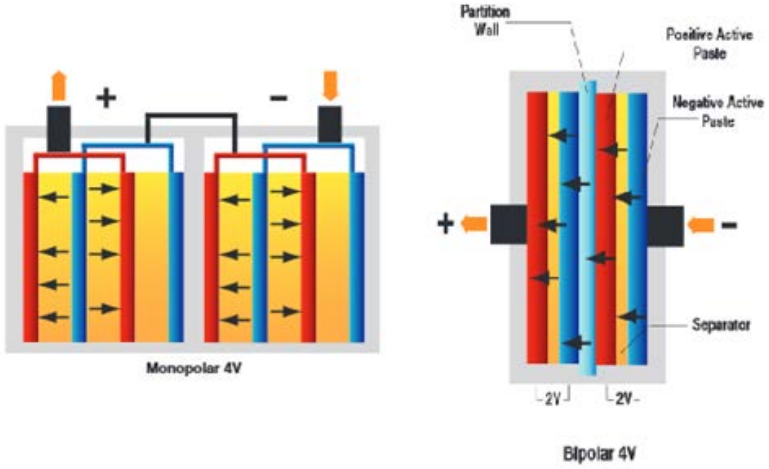

Figure 14 - The difference between traditional construction and bipolar construction [37]. These active materials take the function of an anode and cathode respectively,

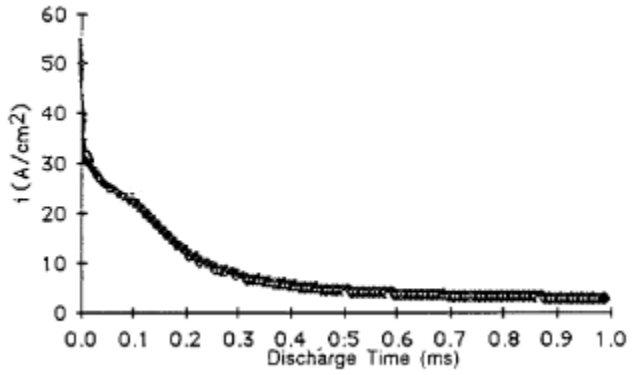

Figure 15 - The current profile of a bipolar lead acid cell undergoing discharge, taken form [41]. Note the significant current decrease within the first 200 µs.

2.1.2 Elevated Rate Recharge of Lead Acid Batteries

As shown earlier, the elevated rate recharge of lead acid cells is possible and advantageous when fast recharge time is needed. Note that high rate recharge does decrease the energy and coulombic efficiency of a charge [42], but lead acids will generally form smaller particle sizes with higher current charges, as seen in Figure 16.

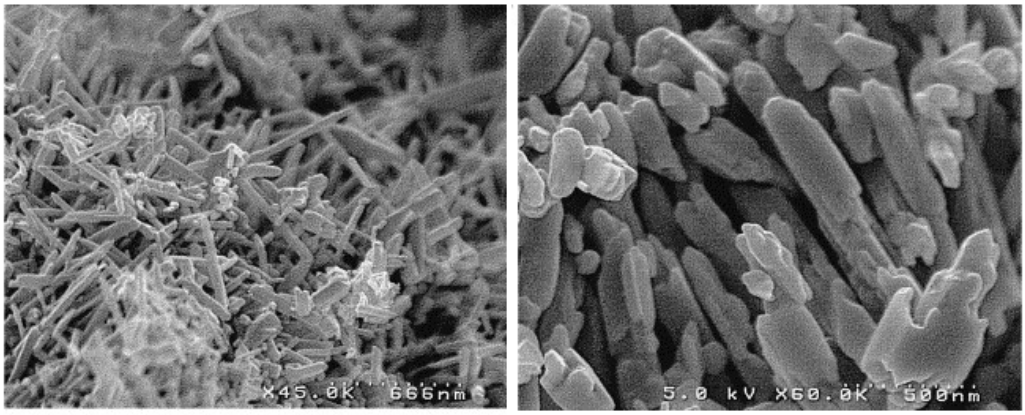

Figure 16 A SEM image showing difference in particle sizes in elevated recharge (a) and low rate charge (b) [43].

These smaller particle sizes produce a larger surface area, and will increase cycle life as long as the lead acid cell does not gas during the recharge [44]. Also, the high current charge may cause some heating to occur. Bipolar lead acid cells may be charged at higher magnitudes than their traditional counter parts, though further work needs to be performed in order to conclusively determine how bipolar cells age as a function of cycle life. In the case of pulsed elevated charge of traditional lead acid cells, there are both benefits and drawbacks. The drawbacks are increased oxygen evolution at the cathode [45], and an increase in the ESR of the lead acid cell as a function of cycle life [46]. The advantage to pulsed charging, however, is lead acid batteries increasing charge acceptance [45,48].

2.2 Nickel Cadmium and Nickel Metal Hydride Batteries

Nickel Cadmium (NiCAD) and Nickel Metal Hydride (NiMH) cells operate off of similar governing equations, seen in Equation 2. NiMH was designed largely as a replacement for NiCad batteries because of the toxicity of cadmium, as well as the alleged memory effect which stems from the formation of cadmium crystals. As a result, and when possible, most engineers prefer to use NiMH.. However, NiCAD's greatest strength is their cycle life, but NiMH has a good cycle life as well. To illustrate the point about cycle life, two examples follow. In 1997, [48] reported that NiCAD batteries functioned well in orbit for just under 1700 days with discharge rates varying from C/2 to 3C/4, and a variety of depth of discharges with a CC-CV charge of C/2 until C/20 was reached, sunlight permitting. By comparison, [49] reported that nickel metal hydride cells had 10% capacity loss in 1000 cycles with an HEV simulation profile 2001, which had discharges of 2.5C down to 20% SOC and a C/4 CC charge. Though the two profiles vary slightly, they both functioned for a prolonged period of time for their designated applications.

$$Ni(OH)_2 + M \leftrightarrow NiOOH + MH \qquad [2a]$$

$$Ni(OH)_2 + OH^- \leftrightarrow NiOOH + H_2O + e^- \qquad [2b]$$

$$H_2O + e^- + M \leftrightarrow OH + MH \qquad [2c]$$

Equation 2 - Equations for NiMH cell
(a) is the overall equation, (b) is the cathode half-cell reaction, and the anode half-cell reaction is (c). Note that M in this formula stands for a metal or a metallic compound. The equation for a NiCAD battery merely replaces the M Cd for cadmium.

NiCADs and NiMH have been used extensively in portable electronics and other applications such as cordless power tools. Similar to lead acid batteries, NiCad batteries have been around for approximately one century and consequently have a large amount

of literature available about them. This is illustrated by IEEE SA 1635-2012, which is the standard for thermal management of NiCad and lead acid cells. Many more standards exist for NiCad cells than NiMH cells though NiMH cells do have a fair amount of literature written about them as well.

2.2.1 Bipolar Nickel Metal Hydride Batteries

Another type of bipolar battery has also shown some promise for use in high power applications. Bipolar NiMH cells have performed well when used in high power aerospace applications [50,51]. The technique that differentiates bipolar cells from standard NiMH batteries is approximately the same as that which differentiates the traditional and 'bipolar' lead acid batteries above. The use of one electrode with the two coatings again greatly reduces the mass and volume of the cells. Compared to traditional NiMH batteries, a bipolar battery offers significantly more gravimetric power density, even though it has approximately the same gravimetric energy density. A more complete electrochemical description of a 'bipolar' NiMH battery may be found in [52]. A 1.2kW/kg, 70 Wh/kg, 154 Wh/L 'bipolar' nickel metal hydride battery has been previously constructed and used by NASA for satellite applications [53]. Because of these characteristics, the air force has seriously considered using these cells to replace lead acid cells on some of their aircraft [54].

2.2.2 Nickel Metal Hydrides and Nickel Cadmium Cells in Elevated Rate Recharge

In summary, NiCAD cells should be used in elevated rate recharge applications when cycle life is a driving concern. NiMH cells should be used when lead acids do not provide enough power or energy, but restrictions prevent the use of lithium-ion cells due to their hazardous handling requirements. An elevated rate charge on these batteries tends to heat them to temperatures measurably above ambient temperature, increasing their charge acceptance [55, 56]. Both cells also perform well when exposed to pulse

charging as well. The high current pulse charging decreases crystalline dendrite growth on NiMH cells [57], and provides the cell chemistry a little bit of time to diffuse and recover [58].

2.3 Supercapacitors & Asymmetric Capacitors

Supercapacitors are sometimes referred to as ultracapacitors or electric double layer capacitors (EDLCs). These electrochemical devices are dominated by the strong electromagnetic force, and have no governing chemical equations. EDLCs have an incredibly high power density. As the name states, supercapacitors have a large capacitance value as well. Recall that for a parallel plate capacitor, capacitance is directly proportional to the area and inversely proportional to the distance between the plates. Since EDLCs have a large surface area and only nanometers of separation between positive and negative charges, capacitance values in the kilo-farad range are easily achievable. Unfortunately, the short distance between charges does not allow large potentials to be built up, which limits their potential to approximately 2.7 V. Due to the energy density being directly proportional to the square of the voltage, supercapacitors are unable to store a large amount of energy relative to other electrochemical devices. For quick reference, Equation 3 shows the energy stored in a capacitor.

$$E = \frac{1}{2} C V^2$$

Equation 3 - The energy stored in a capacitor. E is the energy in Joules, V is the electric potential volts, and C is the capacitance in Farads.

Note that unlike batteries, most capacitors store joules of energy rather than watt hours of energy. For reference, one watt hour equates to 3600 joules. In an effort to alleviate some of the issues with energy density, some chemists have doped one of the carbon electrodes with lithium in order to achieve a higher energy density[59] Older

asymmetric cells might replace one graphite electrode with a $Li_4Ti_5O_{12}$ electrode [60]. In either case, one electrode is slightly different than the other, thus leading to the term "asymmetric" when describing the capacitor.

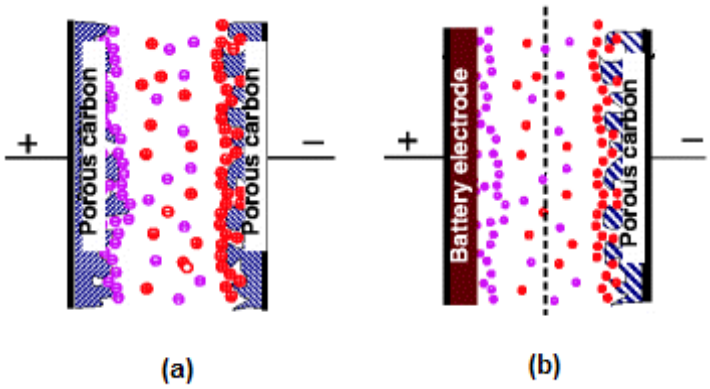

Figure 17 - The difference in electrodes of symmetrical (a) and asymmetrical (b) capacitors [61].

At the time of this writing, most asymmetric capacitors use lithium in one form or another. This has led to most asymmetrical capacitors being called lithium-ion capacitors. Regardless of the terminology, these asymmetric capacitors typically have 3-4 times the energy density of an EDLC due to the higher working voltage. In order to illustrate this, Figure 17 shows the electrodes of a typical EDLC, and an asymmetric capacitor. Asymmetric capacitors have approximately the same power density as EDLCs. In some cases a reduction in the reaction speed can result from the non-faradaic process with the electrode containing lithium [62], which takes time to diffuse. Generally speaking, this is a minor drawback. The major drawback to these asymmetric capacitors compared to EDLC originates from the fact that most manufactured cells cannot discharge to zero volts without permanently damaging the cell. Research grade cells may perform slightly better, as noted by one author when they discharged an asymmetric capacitor down to zero volts five hundred times without capacity loss [63]. However, manufacturers have

not been able to duplicate this feat at the time of this writing [64,65]. Though lithium is by far the most popular material to use in an asymmetric capacitor due to its weight, other elements, such as nickel, may be used to construct an asymmetric capacitor [66].

2.3.1 Supercapacitors & Asymmetric Capacitors in Elevated Rate Recharge

Asymmetric capacitors and EDLCs can adsorb and release electrons quickly in elevated charges, though the speeds of these processes are limited by the mass of their ions. Barring some notable extreme circumstances, both EDLCs and asymmetric capacitors do not significantly age when used in elevated rate recharge compared to nominal charge rates. Though these cells have very high power density, their lack of energy density means that they typically must be combined with other energy dense cells for most applications.

2.4 Lithium-ion Batteries

SNY originally commercialized lithium-ion batteries in 1991, though research into lithium batteries has gone on for a much longer time period [67]. Due to the possibilities in commercial use, a large amount of literature exists on lithium-ion batteries. Figure 18 shows a simplified graphic of a lithium battery undergoing discharge. The schematic itself consists of a graphite anode, an electrolyte, a separator, and a lithium metal oxide cathode material.

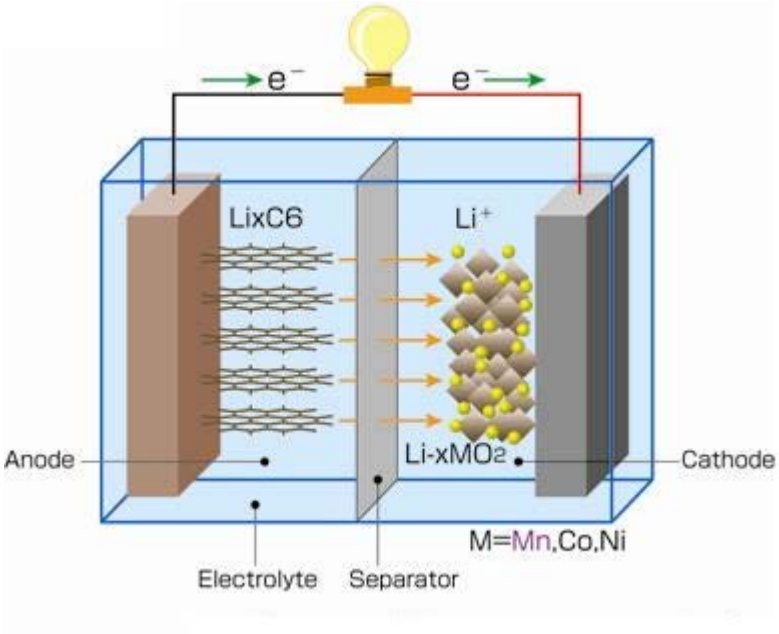

Figure 18 - A graphical representation of a lithium-ion battery undergoing discharge [68].

During discharge, the ion travels from the anode to the cathode, and vice versa when charging the cell. The material of the anode is typically graphite or a variation of carbon. The material of the cathode is typically a metal oxide and is typically used to describe the lithium-ion cell. The separator prevents internal electrical contact of the anode and cathode. Figure 18 shows a fairly simple cell, which of course has been modified over time. Transition of a simple cell into a consumer-grade product is a non-trivial process. Figure 19 displays four form factors that manufacturers typically provide for lithium-ion cells.

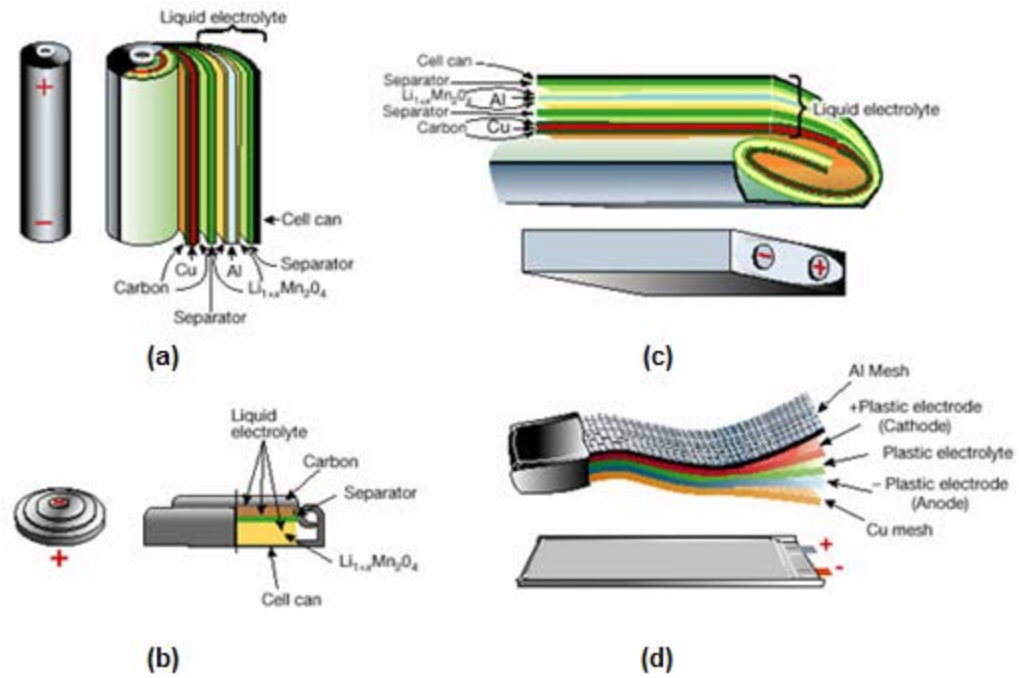

Figure 19 - How a manufacturer would typically construct a lithium-ion cell [69]. For the clarity, safety features are not shown on this particular figure. (a) shows an example of a jellyroll or cylindrical cell, (b) displays a coin cell, (c) presents a prismatic cell and (d) is a flat cell.

As stated previously, most lithium-ion cells utilize carbon, in particular graphite to form the anodes of their cells. This is because the lithium can be inserted and extracted relatively easily in the aforementioned structure, and because of the SP2 orbital hybridization allows higher conductivity[70]. Another anode material becoming popular is lithium-titanate, which will be discussed later. Future cells will likely contain silicon anodes [71], though that particular technology has not advanced enough at the time of this writing.

The next aspect of any battery is an electrolyte. An electrolyte allows ions to travel from the anode to the cathode and vice versa. Note that in Equation 1 and Equation 2, water was present due to its ability to dissociate salts. Unfortunately for

lithium cells, this is not an option due to the non-reversible exothermic reaction shown in Equation 4.

$$2Li + 2H_2O \rightarrow 2LiOH + H_2$$

Equation 4 - Exothermic Reaction of lithium in water

In Equation 4, the elementary reaction of lithium and water produces hydrogen gas and lithium hydroxide. This creates several problems. First, at room temperature and one atmosphere of pressure, an increase in the amount of hydrogen increases the flammability of the atmosphere. Second, a small amount of hydrogen would escape with each charge/discharge cycle. Though personnel refilling the electrolyte could alleviate this, one more problem remains in that the reaction itself is highly exothermic and could cause a rapid change of pressure due to the sudden increase in temperature. Consequently, lithium-ion cells typically have an organic solvent to act as their electrolyte. Although the solvation is still slightly exothermic, it does not cause a spontaneous chemical reaction like lithium and water would.

The last critical component of the lithium-ion battery is the cathode. Though mass produced cells tend to have current collectors, and other various parts as shown in Figure 19, a complete electrochemical cell only require a cathode, anode, electrolyte and separator as described in Figure 18. Generally, the cathode material determines the classification of the cell, e.g. lithium cobalt oxide ($LiCoO_2$) or a lithium manganese oxide ($LiMnO_2$). Regardless of the cathode choice, the electrolyte deposits and extracts lithium from the metal oxide. The two half-cell reactions of a lithium cobalt dioxide cell reaction is shown in Equation 5, as well as the overall chemical reaction. The chemical reactions described in Equation 5 take place in any lithium cobalt oxide cell. Lithium-ion cells have significantly more safety features than one would expect from a simple electrochemical

cell. Figure 20 shows a jelly roll cell that a manufacturer would typically provide off the shelf.

$$LiCoO_2 + 6C \leftrightarrow Li_{1-n}CoO_2 + Li_nC_6 \qquad [5a]$$

$$LiCoO_2 \leftrightarrow nLi^+ + ne^- + Li_{1-n}Co_2 \qquad [5b]$$

$$6C + nLi^+ + ne^- \leftrightarrow Li_nC_6 \qquad [5c]$$

Equation 5 - The equations for a lithium-cobalt oxide cell.
5a is the overall reaction, 5b is the cathode half-cell reaction and 5c is the anode half-cell reaction.

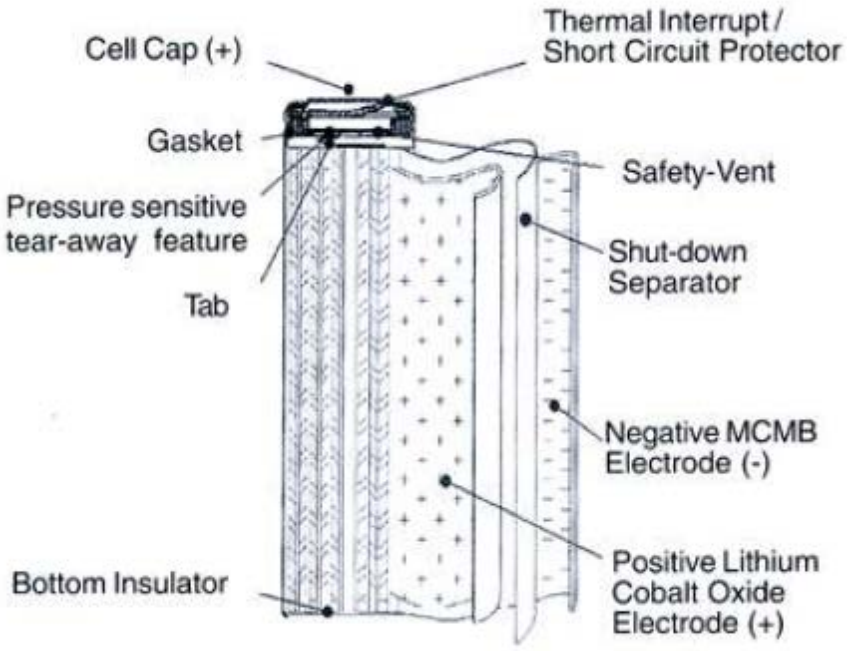

Figure 20 - A jellyroll cell with safety features [72].

One of the main reasons lithium-ion batteries have so many safety features comes from the negative press they have received [73] and the inherent danger of the cells. Unfortunately, when compressing a large amount of energy into a small unit of

volume, the possibility exists that a cell can quickly release its energy in an uncontrolled fashion. Though some chemistry may perform better with respect to safety, the price for increased safety means a decrease in capacity or other performance metric. Determining which tradeoff and chemistry works best for a particular application is a non-trivial task.

2.4.1 Lithium-ion Batteries, Anodes

As stated previously, lithium-ion batteries typically use graphite as the anode. The reason for this is that at an atomic level, graphite forms a hexagonal closed pack (HCP) structure. This structure permits small molecules and atoms to intercalate between its layers[74]. Because a lithium-ion is relatively small, this means they can be placed into and extracted from the crystal structure relatively easily. A picture of the crystal structure is shown in Figure 21.

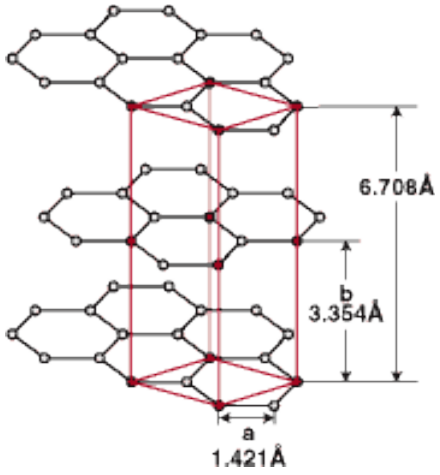

Figure 21 The graphite hexagonal crystal structure [75].

As of recently, lithium-titanate has recently increased in popularity as an anode material [76]. This is because of its ability to recharge and discharge incredibly quickly. Though lithium-titanate cells charge much quicker than their graphite counterparts, they

typically have lower operating voltages and require more cells in series to achieve the same voltage as a cell with a graphite anode. This will cause issues when higher voltages are required. It should be noted that manufacturers do have a number of these in production. E.g., Toshiba currently manufactures a twenty ampere hour lithium-titanate cell [77].

Though the technology has not yet sufficiently developed, silicon nano-wires may one day replace the carbon-based materials as anodes. Theoretically, tin and silicon have a higher capacity than graphite [78], though their issues with volume changes during cycling have prevented their widespread use [79,80]. At the time of this writing, no major manufacturer produces a lithium-ion cell with a silicon anode, but research into nanowires has alleviated a number of issues with respect to the large volume changes that occur in silicon anodes [81].

2.4.2 Lithium-ion Batteries, Electrolytes/Salts, SEI Layer, and Seperators

One of the major issues concerning electrolytes in lithium-ion batteries is cell balancing during recharge. In a typical lead acid car battery, anywhere from ten to fourteen electrochemical cells are connected in series to generate 12-16 V. Lead acid cells may do this because the aqueous electrolyte can automatically balance each individual cell voltage by gassing a little bit of hydrogen if one cell has a higher differential voltage than the other cells. Lithium-ion batteries do not have that luxury. Due to the inability of organic solvents to mimic water in this regard, most large battery systems consisting of more than two cells have battery management systems (BMS). Figure 22 shows a highly idealized BMS.

Though each BMS has slightly different features, most of them prevent any one cell from having a large potential difference from the other cells in the same series stack. BMSs typically prevent a large amount of current from suddenly entering or leaving the

cell as well. One drawback is that these systems are active and require power. Therefore, they can drain the capacity of the cell, even when not being used.

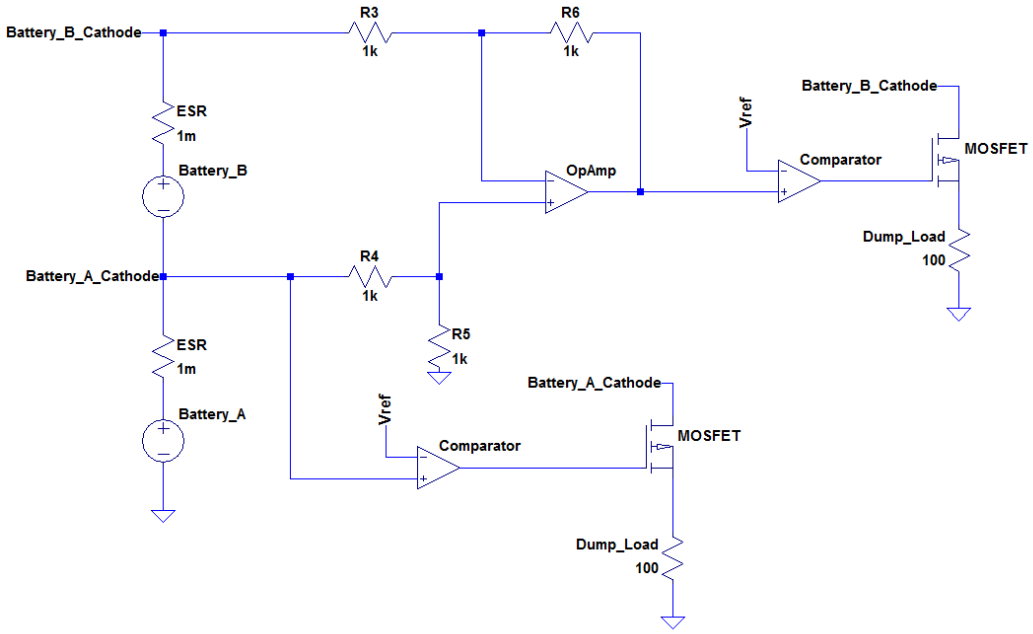

Figure 22 – A highly idealized cell balancing circuit for 2 batteries in series. A differential operational amplifier measures each individual cell voltage. When the cell voltage is too high, the comparator sends a signal to a MOSFET, draining the circuit. Typically the dump load resistance values slightly increase every ten volts in order to ensure that a large drain is not suddenly placed on the system. Note that this requires 3n-1 active components.

The salts dissociation in the in the electrolyte also presents a concern with respect to human health and safety. According to its material safety data sheet (MSDS) [82], $LiPF_6$ requires a full face shield and a respirator. It is also listed as an explosive. Most laboratories circumvent these requirements by flooding chambers with Argon or another inert gas, though that introduces other issues. Another lithium salt, $LiAsF_6$, has a number of immediate and chronic health effects associated with human contact [83]. Lithium perchlorate [84], can potentially cause blindness. All of these effects are compounded because the electrolyte must separate the salt in order to transport the

lithium-ions. Lithium has a Pauling electronegativity of slightly less than one, making it incredibly reactive. This limits electrolytes to organic solvents with a relatively wide band gap.

The typical lithium-ion electrolyte has a bandgap of around 5-6 Volts. Though the definition of bandgap may vary slightly from one application to another, in this particular instance it refers to the voltage range at which the electrolyte remains thermodynamically stable. Typical organic solvents include various ethylene and carbonate groups, such as ethylene . The negative effects listed in its MSDS include potential blindness, kidney failure, and also irritatation of the respiration tract if inhaled [85]. Despite these obvious hazards, the bandgap is slightly greater than 5V. This prevents the electrolyte from breaking down due to thermodynamic stability issues.

In addition to the salts and electrolytes being relatively hazardous themselves, they also typically retain a high degree of flammability. Laptop explosions and the Boeing Dreamliner fire both show that there is a significant amount of safety concerns with respect to lithium-ion batteries. Since the electrolyte is typically the component with the most volume, a significant amount of research has been directed at making these materials less combustible. Recently, a group of researchers developed a solid electrolyte that has potential (Li_3PS_4), though it is not on the market at the time of this writing [86].

Another important property of these electrolytes is that they are liquid, and therefore do not change volume easily. Given the rather volatile nature of these chemicals, limiting volume changes in the cell is a good thing. However, high current reactions can cause the electrolyte to ‘vent’ as if it were a gas. An example of this is shown in Figure 23. The particular procedure done to this cell was approximately 50C rapid charge (~75A), causing the cell to overvoltage. Though this particular cell did

feature a safety vent, it failed to act properly in the experiment due to the conditions of the test. This forced the electrolyte to find some other means of escaping, which the axial cut shows.

Figure 23 failed 26650 cell after a 75A (50C) charge.

Due to all of the safety concerns mentioned so far, it may seem like ionic conductivity is one of the last factors concerning an electrolyte. Unlike metals, electrolytes transport positive ions, which tend to be significantly larger than electrons and holes which are the typical carriers of current in electrical circuits. This means that an ionic conductor will not have the same conductivity that metals have, though still function by transferring charge and heat. The charge is transferred through ions, and the heat is generated by collisions within the electrolyte.

A number of researchers are currently trying to use various additives to gain different or additional electrolyte properties, but this particular process does not seem to be showing much progress with respect to adding energy or power density to the batteries [87]. In addition to the rather lackluster progress in that particular field, the

additives seem to only slightly modify the electrolyte and does not address the inherent safety/flammability concerns of the solvent. Other researchers have tried to use polymers as more stable electrolytes and have had a fair amount of success [88], but chemists generally have to change the salt as well as the electrolyte in order to make this possible. While polymers do seem to be slightly safer as a whole, there is a significant decrease in energy/power density compared to conventional liquid electrolytes. However, one particularly promising example of a salt used in a polymer electrolyte is lithium bis(trifluoromethane)sulfonimide. The salt rivals the performance of some liquid electrolyte/salt combinations and shows promise to reduce a number of safety concerns [89]; however, the problematic fluorine atom remains in its structure. Note that in ordinary use cases, the fluorine atoms would not be a concern because the potential of cell failure significantly decreases as less power flows through the cell. However, the large amounts of energy in pulsed power applications may give enough energy to the ionic liquid to break up its structure, leaving a large number of unbounded fluorine atoms. The amount of fluorine in the electrolyte, if unbounded is enough to cause concern both in terms of cell damage as well as human health and safety.

One other important characteristic of the electrolyte is that it forms a double layer. The double-layer phenomenon is dominated by the strong electromagnetic force. This means that the capacitive nature of the double layer allows charge to transfer relatively quickly compared to the chemical reactions of batteries. The chemical reaction, which involves the transfer of ions, as well as electrons, means that a battery cannot act as quickly as a system that solely transfers electrons. This reduction in speed stems from the fact that a lithium-ion has over 10,000 times the mass of an electron, making it extremely difficult to occur at high rates. For reference, power system IGBTs function at

approximately 4160V with a switching frequency of about 20 kHz and a rise time of about 10 microseconds [90].

Another issue with electrolytes is the (SEI) layer. As the name describes, the SEI layer is the boundary where the electrolyte first comes into contact with the electrode. If the SEI layer is formed properly, it will greatly aid the lifetime development of the cell [91]. The problem with the SEI layer though, is that it is greatly dependent on both the bulk and surface properties of the anode, as well as the properties of the electrolyte itself. Since such few things that can be done to the anode, a large amount of research has been performed to see if modifying if the electrolyte will improve SEI layer formation or stability.

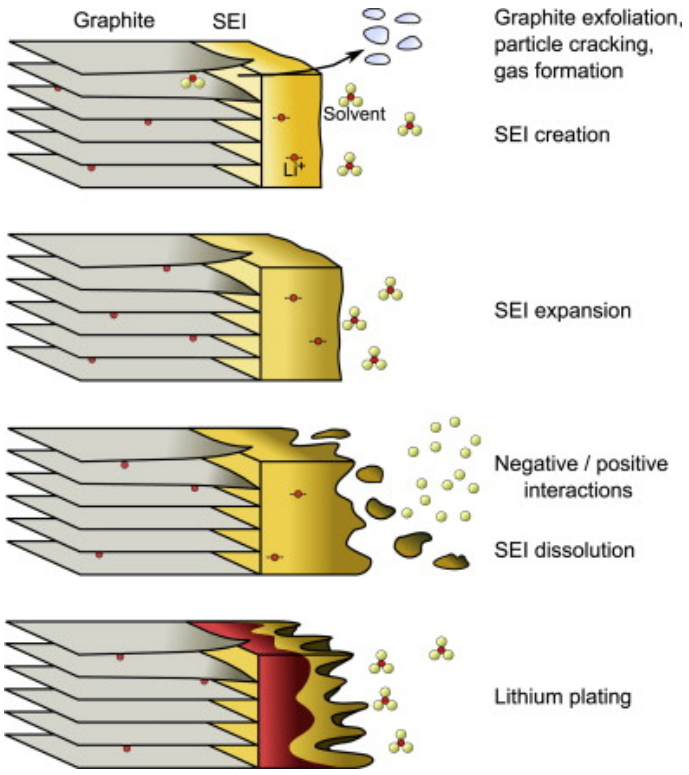

Figure 24 Growth of lithium plating over time [92].

This SEI layer is where lithium plating and dendrite growth occurs, as described in Chapter 1. High rate pulse charging directly affects lithium plating and dendric growth. As stated earlier, this stems from the diffusion rate. Because batteries are a non-nuclear chemical reaction, the conservation of mass applies. This means that the ions flowing form the cathode to the anode during charge must go somewhere. If the lithium goes into the SEI layer, but does not intercalate into the anode, the probability that lithium plating occurs greatly increases. Figure 24 displays this process[i].

Ideally, the separator should be extremely small in order to decrease the ESR of the cell. A good separator allows lithium-ions to flow through, but disallows the contact of the cathode and anode materials. Typical separators are polypropylene (PP) and polyethylene (PE). Depending on design criteria, they can either come in bulk or in monolayers. A thicker separator increases ESR, but increases cycle life. Most manufacturing techniques utilize a monolayer of PP or PE to act as the separator. Some manufacturers prefer a small number of PE and PP layers. These are simple enough to manufacture that various monolayers, duo-layers, and trilayers are available commercially [93]. Note that both polymers are relatively inert and allow lithium-ions to pass through easily.

2.4.3 Lithium-ion Batteries, Cathodes

In most cases, the cathode material describes the type of cell. Generally speaking, cathodes conform to a particular structure. For example, $LiAO_2$ compounds, where Li is lithium, A is a metal and O_2 refers to oxygen are classified as layered cathode structures [94]. A graphical representation of $LiCoO_2$, a common layered cathode, is shown in Figure 25 for clarity.

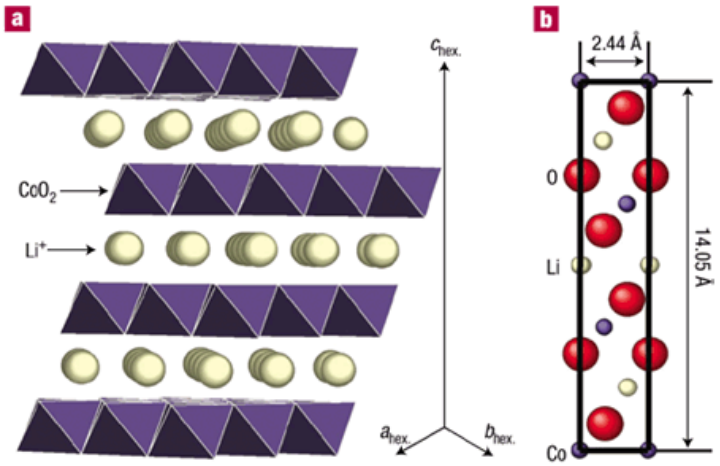

Figure 25 LiCoO2 structure taken from [95].
Part A shows the 'layering' of the cathode material. Part B shows a simplified unit cell.

As shown in Figure 25, the lithium intercalates between the cobalt oxide. This intercalation process allows lithium to flow in and out of the compound when charged and discharged. Though $LiCoO_2$ was one of the first compounds used as a cathode, its well documented safety issues have caused its popularity to drop. However, due to its status as the first commercial cathode, it still holds a significant portion of the lithium-ion battery market. Some manufacturers have added nickel, manganese, and aluminum to the compound, in order to slightly adjust the conductivity, capacity, and/or structural stability of the cathode. Consequently, $LiMnO_2$ and $LiMn_{0.5}Ni_{0.5}O_2$ compounds have gained popularity [96,97]. Another popular cathode with a layered structure is NCA. The main advantage of NCA comes from its working voltage compared to other layered cathode materials [98].

Spinel structures are used as cathodes in lithium-ion batteries as well. These compounds have the structure of AB_2O_4 where O is oxygen, and A and B are typically metals. However, they have the same structure as the mineral spinel $MgAl_2O_4$. In lithium-ion batteries, the A metal is always lithium.

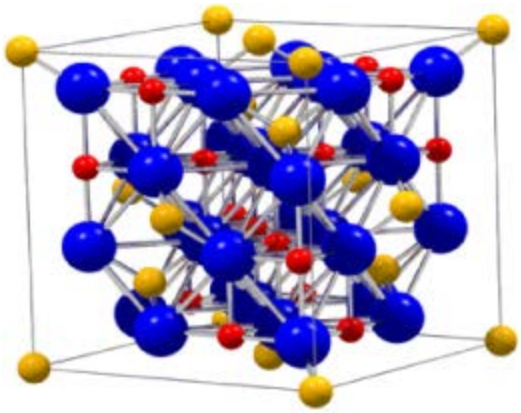

Figure 26 A spinel structure taken from [9998].
The yellow particles refer to the tetrahedral sites (typically metal A) and the red spheres coincide with the octahedral sites (typically metal B). The blue shperes represent the oxygen present in the mineral/cathode material.

A relatively popular spinel compound is $LiMn_2O_4$, due to its wide manufacturing base. Also note that the anode material lithium-titanate has a spinel structure. These generally have a face centered cubic structure with a tetrahedral and octahedral site. Figure 26 displays a common spinel structure for clarity. As with the layered cathode structures, researchers have utilized a number of compounds to try to improve performance of the spinel cathode [100]. Unfortunately, this type of cathode has relatively poor electrical conductivity and can undergo a distortion effect overtime. Formally, this refers to the John Teller Distortion, which causes $LiMn_2O_4$ cathodes to lose capacity overtime [101]. Research has alleviated these issues somewhat[102,103], though a number of problems remain with spinel cathodes.

One of the more promising cathodes with respect to safety is lithium-iron phosphate, shown in in Figure 27. This particular cathode has an olivine structure.

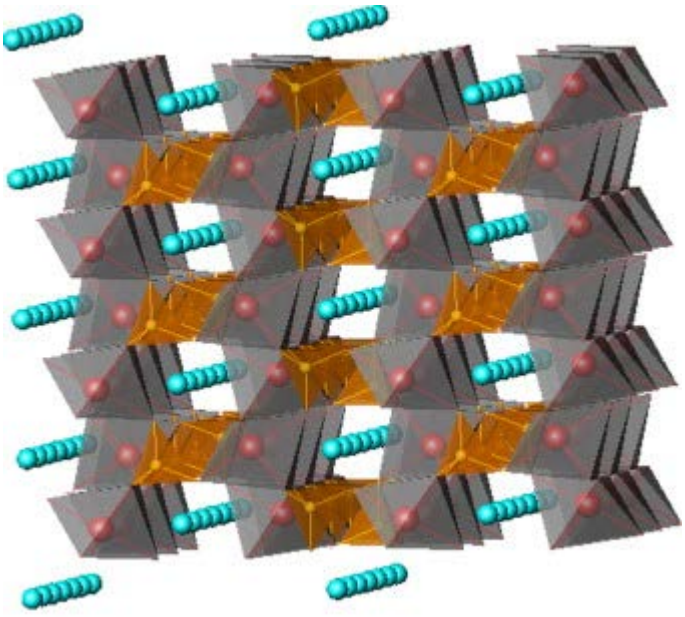

Figure 27 A typical $LiFePO_4$ structure taken from [104].

The lithium-ions are teal, and the phosphate tetrahedrons are colored brown. The FeO_6 octahedrons are colored gray.

Olivine's chemical formula is $M_2Si_2O_4$, where M is a metal (typically magnesium or iron), Si is silicon and O is oxygen. As an aside, olivines have been detected on Mars by the NASA rover Curiosity. Unlike the mineral, the cathode has lithium atoms. Because they are relatively small compared to the other atoms present (iron, oxygen, phosphorous), they form a 1D tunnel which allows ions to flow. This can be seen in Figure 27. As implied earlier, the most common olivine cathode is lithium iron phosphate ($LiFePO_4$). $LiFePO_4$, though significantly safer in terms of thermal runaway, has a couple of drawbacks. The largest drawback is the lack of conductivity compared to other electrodes. Unlike the separator, this cannot easily be circumvented by simply making the cathode thinner. One technique to increase conductivity involves adding carbon, but this comes at the expense of energy density. The other major concern with $LiFePO_4$ comes from its relative weight compared to other cathodes. The iron in the compound

makes it slightly heavier than various cobalt oxides, which may be a concern for astronautic and aerospace applications.

2.4.4 Lithium-ion Batteries in Elevated Rate Recharge

Lithium-ion batteries age faster when recharged at higher rates. A specific example of a pulsed elevated rate recharge will be covered in Chapter 5, and the specifics of how an elevated charge affects battery aging will be covered in Chapter 3. Elevated pulsed charging stresses the band gap more than normal operating conditions and a steady elevated rate charge is more likely to undergo lithium plating or dendrite growth. How much the lifetime is reduced depends on the magnitude of the current and the maximum potential of the cell during the charge. Smaller over-potentials and small magnitude currents will increase the lifetime of the cell, but will also increase the time to charge. Determining how much over-potential a cell can tolerate, as well as the amount of time to charge, is a function of application and chemistry. Generally speaking, lithium-ion cells may be charged at an elevated rate many times without issue, though a high number of repeated pulse charges may lead to premature failure.

Chapter 3

Prior Work and Aging Mechanisms

I'm not trying to get myself up a notch
on the ladder by shoving somebody else down
-George H.W. Bush

3.1 Prior Work

Despite the fact that power density in electrochemical cells has noticeably increased in recent years, most of the research recorded in the literature regards relatively small C-rates. For example, [105] built a 50kW charger for an electric vehicle. Though an impressive feat of engineering, the 50kW charge only provided an approximately 2C recharge. Another pragmatic system for charging lead acid batteries was built by [106], which can charge batteries with several hundred amperes of current. Unfortunately, the C-rate was still relatively low (~4C).

Currently, only some research has been done on pulsed charging. In lithium-ion cells, there is very little literature (aside from what the author has written) on the subject. In pulsed recharge of a lithium cell, Wang et al. [107] showed that elevated pulsed charging at 1C greatly reduced performance of the SEI layer. However, in this particular case, he was constructing the SEI layer, not performing lifetime measurements.

[108] published a conference paper where they charged a lead acid battery at 58C with what appeared to be very little issue, though no lifetime studies were made of that particular cell. This lead acid cell was designed to be used in pulsed power applications so it was designed for high current charge and discharge.

Nickel metal hydrides have some elevated charge research as well. [109] showed that the amount of capacity extracted after a 2C and 1C charge were approximately equal, though as the C-value increased the amount of energy extracted relative to the 1C charge dropped quickly. [110] showed that NiMH cells having a low

steady state drain of C/2 combined with a train of high current pulses of approximately 4C greatly decreases the lifetime of the cell to less than 300 cycles. Though NiMH cells tend not to discharge well under pulsed conditions, they do charge well under pulsed conditions. [111] showed that the increase in pulsed charge performance came from the reduction of pressure inside the cell.

There has also been some work done previously investigating the impact of high rate recharge on lithium-ion cells though the C-rates were relatively modest. [112] showed that though the difference was small compared to conventional charging methods, there was a subtle increase in resistance compared to lithium-ion cells over the cycle life of the battery. This is one reason that very few people pulse charge lithium-ion batteries. Another reason is that an extremely well cited report suggests that a low charge rate should be used when the cell is near 0% SOC [116].

The numbers above show some of the issues with elevated charge experiments. To increase the practicality of a rapid C charge, a significant amount of current must be delivered in a short amount of time. To compete with an internal combustion engine using fossil fuels, electric cars must be able to quickly recharge at a rate of 6C. Unfortunately, this takes a significant amount of infrastructure. The amount of increased generation and transmission required is beyond the scope of this work, though it is non-trivial.

Though information on high current charges seems to be relatively rare, high current discharging has a significant amount of literature. Unlike charging, discharging lithium-ion batteries is primarily limited by the diffusion rate of lithium-ions traversing across the cell. Since discharging decreases the potential of the electrochemical cell, the band gap of the electrolyte will not fail thermodynamically under discharge so long as it does not fail under steady state. Though there are still discharge limits that may cause a

concern, the risk of failure is significantly less so long as the voltage ratings are observed. In addition to the experiments done at UTA and others [117], there is a fair amount of literature available, especially with respect to automotive applications. For example, [118] did 50C discharge on a lithium-ion battery with fairly impressive results compared to the 1C discharge rate. [119] also did a 20C discharge on a lithium battery. There are a number of other papers on elevated discharging, but they summarize to stating the capacity extracted from the battery decreases as the discharge rate increases. However, the nonlinear relationship between the discharge rate and the extracted capacity varies from cell to cell. Most manufacturers provide a limited set of elevated discharge parameters on their datasheets, though the C-rates the manufacturers provide are typically low since they only provide a minimum safe value.

3.2 Aging Mechanisms

A large number of aging mechanisms exist in lithium-ion batteries. The most common methods of aging include calendar aging and cycling aging. As the name implies, calendar aging occurs when lithium-ion batteries are not in use. Because a discharge reaction is thermodynamically favorable, batteries self-discharge a little bit overtime. This self-discharge does not usually greatly affect things unless left alone for a prolonged period of time. As the amount of time a cell is left alone increases, the more the cell discharges. Also, calendar aging can cause impedance to increase in the cell, even though no high-rate chemical process occurs [120]. This means that in an ideal case, most batteries should be stored significantly below room temperature, but not so cold that the graphite anode becomes brittle and cracks. The typical temperature at which this occurs is approximately 253 K, so the recommended storage temperature is 273 K for most cells with an organic liquid electrolytes such as ethylene carbonate. In addition to lower ambient temperature, the other way to mitigate calendar aging is to

leave batteries at 50% SOC. The lower SOC value implies a lower electric potential of the cell, making the discharge reaction slightly less favorable than a fully charged cell. Lower SOCs and potentials will make the discharge reaction less likely, however there is a non-zero chance that the self-discharge of the cell may take the battery below its recommended limits, which is why most manufacturers recommend storing batteries in cool temperatures at approximately 50% SOC.

Calendar aging of the anode largely occurs due to the Van der Waals force. The Van der Waals force refers to a quick electric attraction formed because electrons move so quickly. Given enough time, the electrons will form a dipole, even if it is just temporary. This dipole force then attracts molecules to each other. The phenomenon has noticeable effect on small molecules and low temperatures. As either the molecule size increases or the temperature increases, the Van der Waals forces become insignificant compared to the other forces acting on the molecule. Because the lithium-ions are relatively small, Van der Waals forces play a significant role. In graphite or graphene intercalated lithium will move to the edge of the structure or to the electrolyte, causing capacity loss[123].

The other common aging mechanism in lithium-ion batteries is cycle aging. As the name implies, the cyclic aging process acts as a function of the number of cycles a lithium-ion battery has undergone. The typical methods of cyclic aging include metallic plating and mechanical degradation of the cell [121]. Unfortunately, there are very few ways to prevent cyclic aging if one actually wants to use a lithium-ion cell. About the only way to limit the cyclic aging process is to allow the lithium-ion battery to operate at higher temperatures (~303-323K) while being used, and not have a high rate discharge or charge. Depending on the applications such conditions may not be feasible. Though the higher temperature significantly helps the cyclic aging, it also degrades calendar aging.

This is because of the chemical nature of batteries. Higher temperatures allows processes to occur more readily due to the increase in average kinetic energy of the surroundings. This means that, ideally one wants to use lithium-ion batteries just below their thermal runaway temperature and then store them at low temperatures.

For lithium-ion batteries with graphite anodes, the SEI layer plays a major role in aging. If active material is lost or does not intercalate with the graphite easily, capacity fade will occur. If the SEI layer continues to grow unchecked, a noticeable power loss will occur due to the loss of contact area. If the SEI layer volume changes greatly, a noticeable power loss will occur again from the reduction of chemical area [122]. Determining what happens to the SEI layer outside of a specialized laboratory remains highly problematic. Typically, optically transparent electrodes and other various tricks may allow one to use various electromagnetic lithographies to diagnose cell aging conditions. Though incredibly useful, these electrodes are significantly harder to manufacture than non-optically transparent ones and consequently do not see much use in practical applications. With high rate charging, a particular concern comes from lithium plating of the SEI layer. This is because the amount of metal being extracted from the electrode occurs relatively quickly, and cannot enter and exit the graphite layers smoothly. This may either cause a short in the anode or may cause dendric growth, both of which reduce the capacity of the battery.

On the cathode side of the cell things are slightly different. Different cathode chemistries all age slightly differently. However, most cathodes have issues with hydrofluoric acid evolution. The acid can start dissolving the metal in the cathode, or it may simply gas leaving an unbounded fluorine atom. While recent research suggest that certain coatings may decrease the probability of this occurring [124], the problem does not go away due to the thermodynamic stability requirement of the electrolyte.

Besides fluorine, other gasses that may generate near the cathode are CO_2 and C_2H_2 for lithium cobalt oxide and lithium iron phosphate cathodes prospectively. Because the amount of gas generated depends on the overpotential of the electrochemical cell, these reactions are particularly important when pulse charging with large C-rates. This sort of gassing with large amounts of over potential typically means that the electrolyte has broken down, similar to the electrolysis of water. This is of particular concern for pulsed charging since the high C-rates typically induce a large voltage rise across the ESR of the cell. This failure mechanism, unlike others, typically causes cells to fail spectacularly and causes them to vent their electrolyte, thus destroying the cell.

On a less dramatic scale though, cathode degradation comes from structural change, electrolyte film formation, or chemical breakdown of the cathode compound itself [124]. As one might expect from a complex system such as a battery, none of these variables are independent from the others. High rate pulse charging likely affects this, especially with respect to structural breakdown and electrolyte film formation, though at the time of this writing no studies concur or dissent the above statement.

3.2.1 Tracking Aging Effects in a Non-invasive Manner

If a cell is well defined in terms of chemical composition and molecular structure, one may construct models that closely represent cells and their internal mechanisms [115]. However, if a large amount of chemical information is not known or provided, non-invasive techniques can provide a fair amount of insight as to how a cell ages. The simplest non-invasive technique is coulomb counting. Coulomb counting refers to the amount of charge extracted from a battery for a fixed discharge, which is calculated by integrating the current with respect to time for that particular discharge. Coulomb counting typically indicates when a cell has reached its most thermodynamically favorable state. Most lithium-ion batteries gain a minute, yet measurable amount of

capacity for approximately the first fifty cycles, though this does depend on their charge and discharge profile. Once this state has been reached, the cell begins to lose capacity and can never reach the maximum capacity it once achieved. The second simplest method is simply to measure the energy extracted from a fixed charge and discharge, referred to as joule counting. This method requires one to calculate the instantaneous power during each point in time and then integrate the power with respect to time. In most circumstances, the two values closely correlate with each other.

Though simple, these methods generally provide verification that a battery is aging and joule counting confirms that the battery did not produce more energy than it consumed during recharge, upholding the 2^{nd} law of thermodynamics. Coulomb and joule counting remain a relatively simple to way to determine the state of health of the battery, it does not provide a good insight as to what occurs internally in the cell. Electrochemical Impedance Spectroscopy (EIS) provides a good qualitative analysis of what may occur inside the cell.

EIS measures the AC frequency response in terms of impedance of a battery. In order to do this, EIS measurements are taken at open circuit potentials. All batteries slightly self-discharge; EIS measurements occur on a time scale that neither the SOC nor the state of health (SOH) of the battery significantly changes. In order to take an EIS measurement, a small AC sinusoid is fed to the battery on top of its open circuit potential. This small AC potential does not significantly alter the cell, but is large enough such that an impedance measurement can be made across the cell by comparing the AC input signal to the AC output signal. If the input signal is current, it is referred to as a galvanostatic EIS measurement. Likewise, EIS measurements taken with an AC voltage signal are called potentiostatic EIS measurement. These AC measurements are generally compared in a Bode plot (phase and impedance magnitude versus frequency)

or a Nyquist plot (real impedance versus imaginary impedance). The former plot is generally used to track impedance growth, while the latter has shapes that distinguish between different parts of a lithium-ion cell, which Figure 28 illustrates.

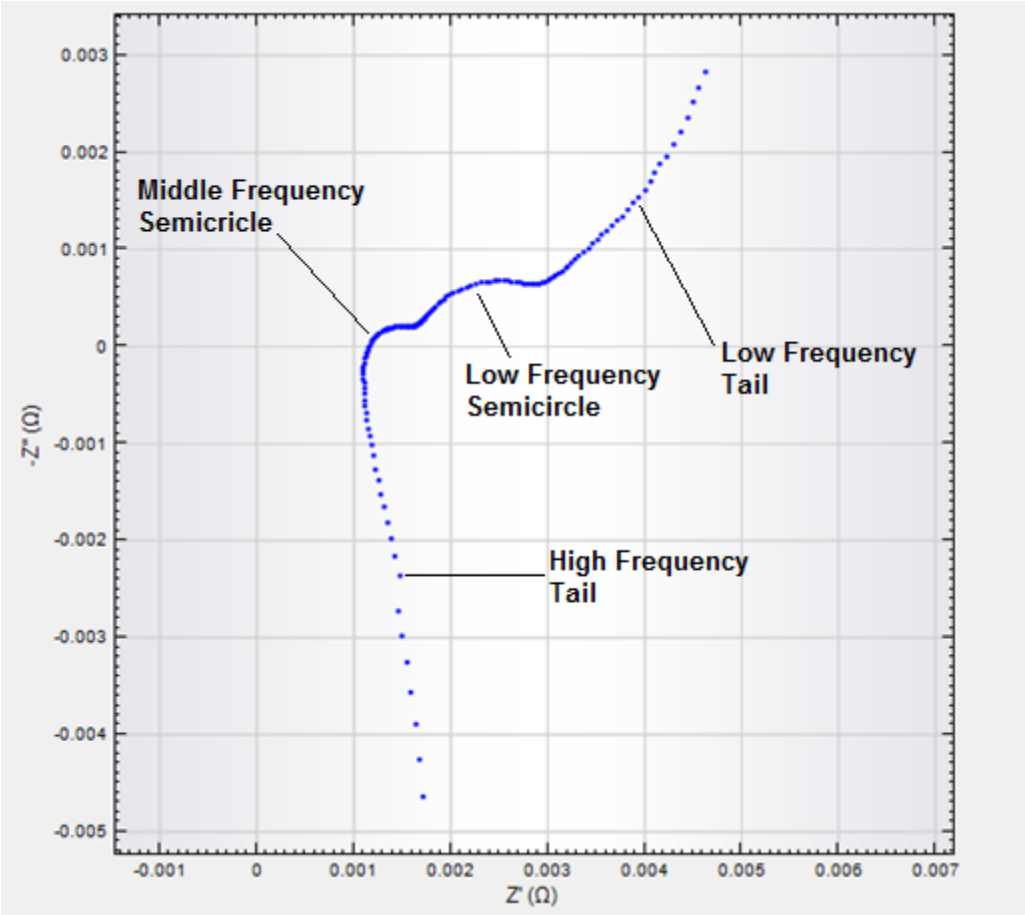

Figure 28 Typical structures in a Nyquist plot of a lithium-ion cell.

Each of these features typically corresponds to a particular aspect of a lithium-ion battery. In order of decreasing frequency, the high frequency tail models changes in the shape of the electrodes. This is because the high frequency tail typically models the inductive portion of the electrode, which is sensitive to geometry [146]. The middle frequency semicircle typically models changes the thin film or SEI layer, dependent upon one's choice of literature. The low frequency semicircle models the electric double layer

that has been discussed extensively, and the low frequency tail typically models semi-infinite diffusion.

It is important to note that EIS curves only give one point at a particular state of charge, temperature, and state of health. This is why when tracking the SOH, the SOC and temperature must be held at approximately the same level. This has led to the literature describing EIS curves at various voltages levels between a fixed percentage state of charge and fixed temperature. The two most common levels to take EIS measurements are at the near charged and near discharged states. In the literature, it would typically be written as between 90-100% SOC at X volts at room temperature and between 0-10% SOC at Y volts at room temperature, with X greater than Y. The exact values of the aforementioned variables depend upon chemistry of the cell in question. For lead acid car batteries, 11V and 13V are not uncommon. For individual lithium-ion cells with a graphite anode, 3 and 4V are standard for the charge and discharge state, though usually the discharge value may trend higher due to the voltage relaxation of the cell over time. Independent of the voltage values and temperature used, it is important to keep similar states of charge and temperature constant when tracking aging measurements.

Chapter 4

Experiment Development

Teach me and I remember. Involve me and I learn
-Benjamin Franklin

4.1 Experimental Setup

In order to perform high rate discharge and recharge experiments, initially, a novel test stand was designed. A circuit schematic of the test stand is shown in Figure 29. Figure 30 shows a CAD schematic of the stand and Figure 31 shows photograph of the test stand.

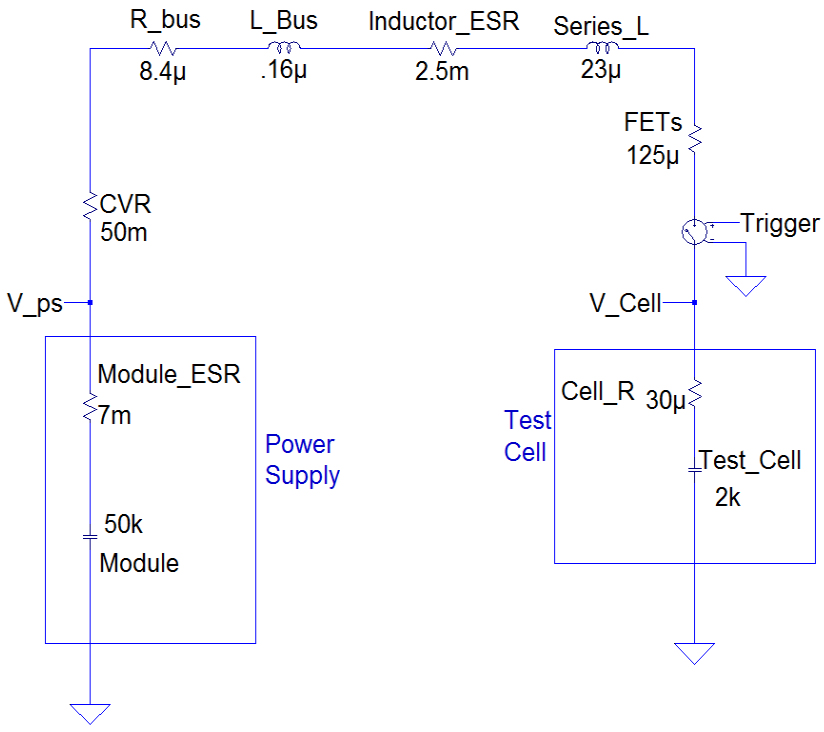

Figure 29 Original circuit of the charging test stand.

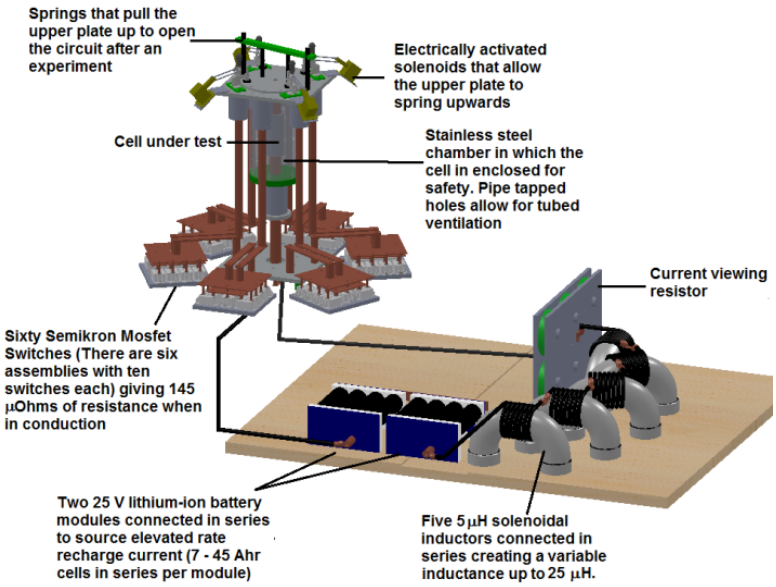

Figure 30 The original CAD schematic of the test stand in the charging configuration.

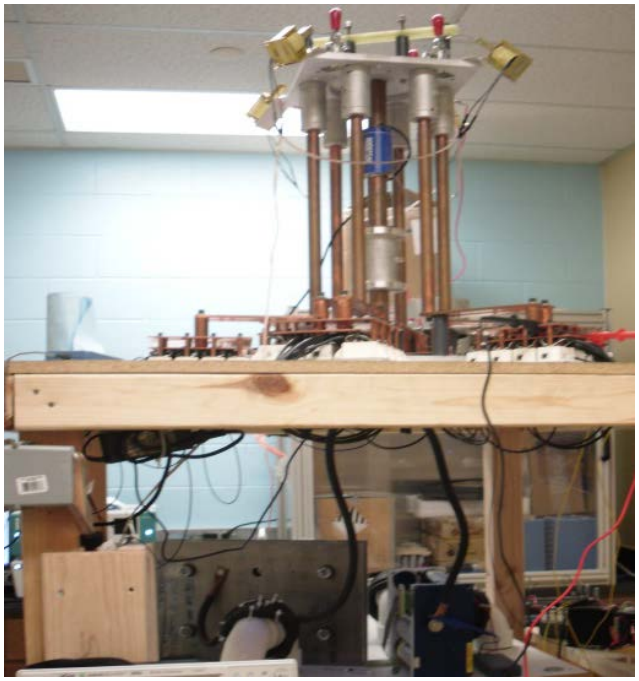

Figure 31 Original photograph of the test stand.

This design and the justifications for the stand have been well reported in the literature [125,126]. For completeness, the original design and justification for the various components thereof shall be explained forthwith. The stand was designed to switch pulsed currents up to 10 kA from a power supply module to the cell being charged. Since the cells are being stressed to levels beyond their respective ratings, thermal runaway is a concern. To maintain safety at all times, the test cell is housed in thick walled 304 stainless steel tube to ensure that any thermal runaway events are always contained. Additionally, the negative terminal of the battery is connected to a quick disconnect so that the circuit can be opened quickly during unexpected events, as well as providing a visible means to check to see if the stand is in open circuit condition after an experiment has completed.

The original power supply module, from which energy to recharge the battery comes from, consisted of up to fourteen GAIA 45Ahr lithium-ion battery cells connected in series or parallel. Their particular configuration determined the power supply voltage, and provided the current to charge the cell under test. The number of series connected cells can be adjusted as an easy way to set the voltage level, and calculate the approximate current from Ohm's Law. A series/parallel configuration of 100 mΩ HVR high energy disk resistors can also be connected in series with the source and the cell under test to limit the charge current as needed.

Beginning at the positive terminal of the current source, current travels through five series connected 5µH inductors, made of 11.7 mm diameter (4/0 AWG) stranded copper wire. The number of inductors used can be varied to shape the rise time of the current pulse being delivered to the cell. Next the current travels through the high energy resistors, and then flows into a parallel connection of up to 60 Semikron SKM111AR metal-oxide field-effect transistors (MOSFETs).

Each MOSFET has an on-state resistance of roughly 9 mΩ and has a hold off voltage of 100 V. The switches are rated to conduct 200 A at room temperature. The number of switches used to conduct current can be adjusted in increments of ten to control the series resistance of the circuit further if needed. From the MOSFETs, the current goes into the cell being charged and finally through a custom made 6061-T6 aluminum current viewing resistor (CVR), which measures the magnitude of the charging current, before returning to the negative terminal of the source. It should be noted that all of the stand's bus conductors are made of either C11000 copper or 6061-T6 aluminum and were sized so that a temperature rise of no more than 50 degrees C would occur during a full charge cycle of a 45 Ahr cell.

The diagnostics in the original test stand consisted of four high voltage differential voltage probes to monitor the cell voltage, the source voltage, the MOSFET voltage, and the voltage across the CVR. The resistance of the series CVR is roughly 2 μΩ making it difficult to very accurately measure the charge current when the amplitude falls below one kiloampere. Given the lack of resolution of the CVR, in the experiments presented here, the voltage across the larger high energy disk resistors has been used to measure the charge current. Since the charge currents applied to the cell are quite high, the power losses inside the cell can be quite large causing the cell to heat up considerably despite the low cell ESR. A LeCroy digital oscilloscope measured all of the voltage data. A 0.076 mm diameter, K-type thermocouple manufactured by Omega Engineering measured the temperature rise of the cell during and after the charge cycle. A small diameter thermocouple was chosen to minimize the thermal diffusion time. A National Instruments 9213 thermocouple module connected to a CompactRIO system collected the thermal data. The purpose of the results being presented here is to

highlight the capability of the test stand and briefly demonstrate the types of experiments that will be discussed later.

A number of experiments were performed initially to commission the test stand and evaluate the capability of the cells under consideration. In the first set of experiments that will be presented, the experimental recharge stand applied an elevated constant-current charge to a 18Ahr GAIA lithium-ion battery, a 2200 F JM Energy Low Resistance (LR) lithium-ion capacitor, and a 2000 F Maxwell supercapacitor. The data sheet properties of each of the cells tested is listed in Table 2.

Table 2 Data sheet properties of an 18Ahr lithium-ion battery, 2200 F lithium-ion capacitor, and 2000 F supercapacitor being tested during the commissioning experiments

Storage Device	Operating Voltage (VDC)	ESR (mΩ)	Mass (kg)	Power Density (kW/kg)	Energy Density (Wh/kg)
GAIA 18Ahr battery LiFePO4 [127]	2.1 – 3.8	< 1	0.93	2.1	62
2000F Maxwell Supercapacitor [128]	0 – 2.7	0.35	0.36	6.9	5.63
2200F (LR) Li-ion Capacitor [129]	2.2 – 3.8	1	0.2	9.8 (15 ms pulse)	11

The recharge current and cell voltage during the constant-current charge of each of the cells is shown in Figure 32 and Figure 33 respectively. The charge power and energy curves are shown in Figure 34 and Figure 35 respectively.

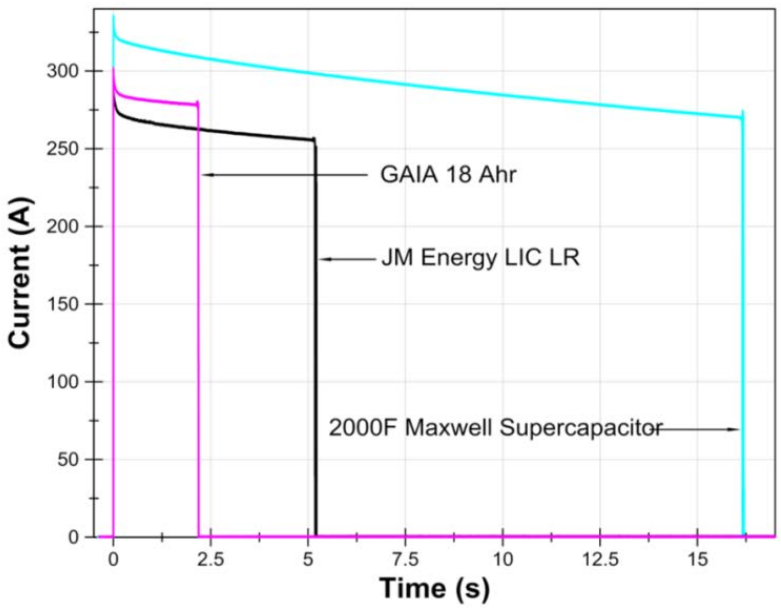

Figure 32 The constant current applied to the supercapacitor, asymmetric capacitor, and lithium-ion battery.

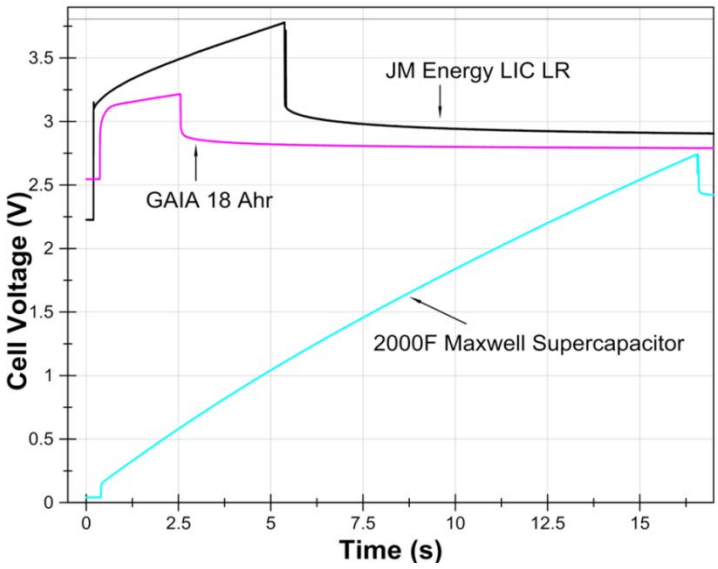

Figure 33 The voltage profile during the constant current charge during the commissioning experiments.

Note that the initial voltage of each of the cells was the lowest manufacturer recommended discharge value. The peak recharge currents are roughly 302 A (17C), 291 A, and 325 A for the lithium-ion battery, lithium-ion capacitor, and supercapacitor respectively. The recharge currents decrease as the cell under test is charged since the differential voltage between the source and cell is decreasing. The decrease in current comes from having a battery module act as a power supply and not a regulated source. The constant-current recharge times of the different cells are 2.18 s, 5.16 s and 16.15 s respectively. A summary of the voltage, current and recharge times are listed in Table 2. The temperature rise of each of the cells was not significant, roughly a few degrees C in each of the experiments, and thus is not presented.

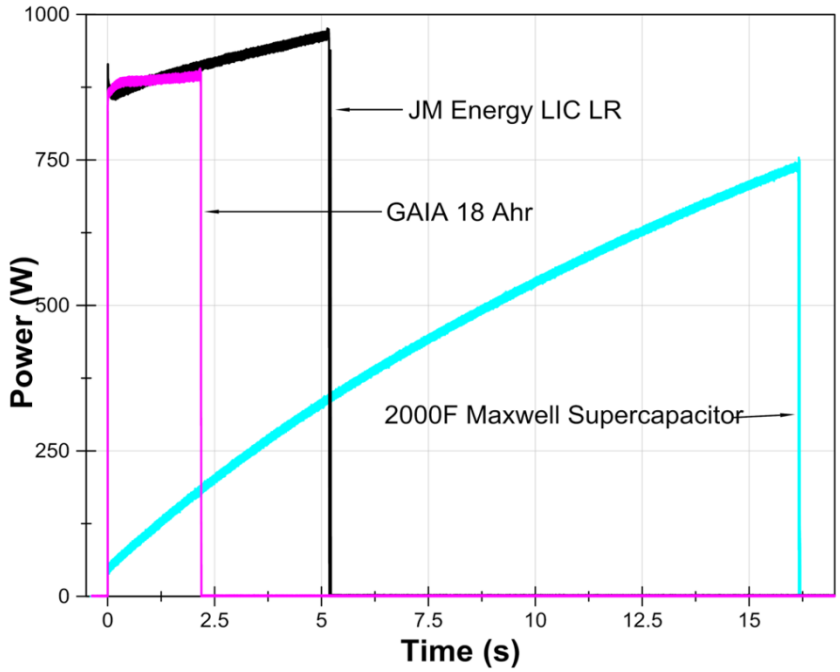

Figure 34 Power into each of the cells during the commissioning experiments.

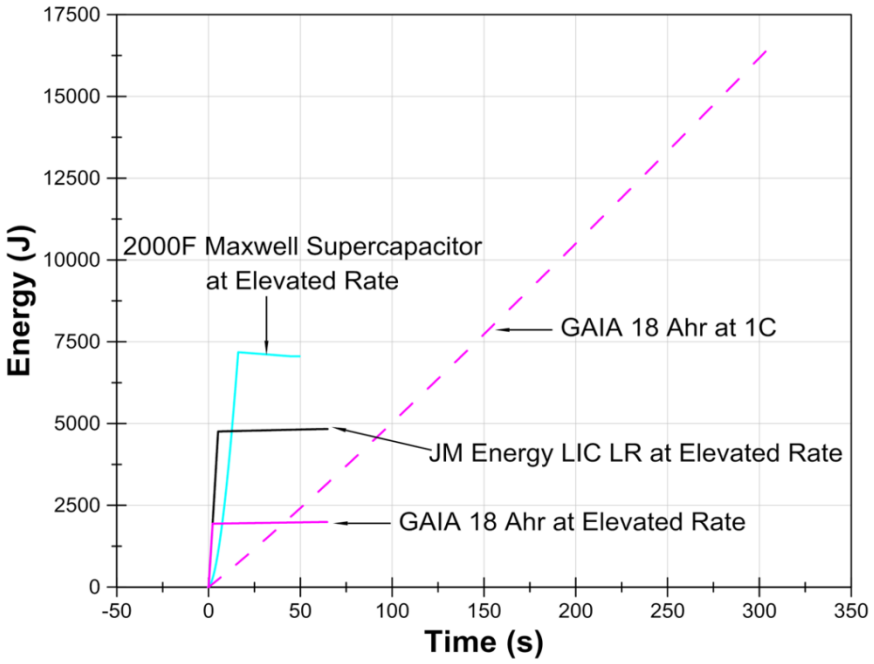

Figure 35 Energy into cells during the commissioning experiments.

For comparison, the cell voltage and capacity recorded during a 1C constant-current recharge of the 18Ahr cell (18 A) is shown in Figure 36. From that plot, it should be noticed that a recharge at 1C takes roughly 310 s compared to the 2.18 s already observed at the 17C recharge rate. Because the lack of a constant voltage phase on these charges, it should be noted that the 1C charges allows the cell to add and extract significantly more energy than the rise from the 17C charge. This voltage rise across the ESR is an order of magnitude larger for the 17C charge causing the cell to reach its cutoff voltage much quicker even though less capacity is added. This means that the voltage quickly drops once the charge stops, as shown in Table 3.

Table 3 Constant current charges of various cells. Note the difference between the 1C charge on the 18Ahr` cell and the high current pulse.

Cell	Initial Voltage (V)	Final Voltage (V)	Charge Current (A)	Charge Time(s)
GAIA 18AHR $LiFePO_4$	2.55	2.76	281	2.18
GAIA 18AHR $LiFePO_4$	2.45	3.2	18	310
2000F Maxwell Supercapacitor	0.04	2.39	289	16.15
JM Energy Lithium-ion Capacitor	2.24	2.87	251	55.56

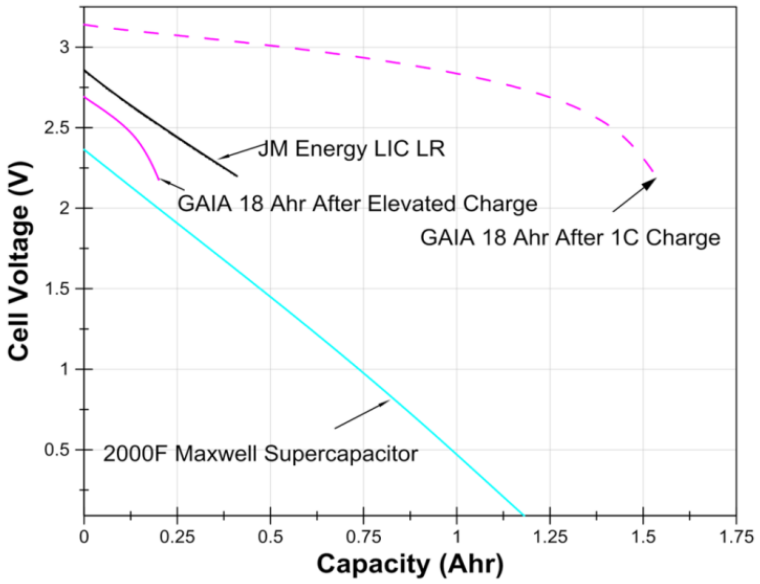

Figure 36 Capacity extracted during the commissioning experiments.

The general conclusion taken from these preliminary results was that the elevated rate constant-current recharge of different types of electrochemical cells is possible and that the capacity added decreases considerably as the charge rate is increased even though the charge time drops significantly. As expected, without a constant voltage phase though, there was not significant capacity added to the cell.

Though the above experiments showed that this setup would work, it was apparent modifications would be needed after the commissioning experiments. One of

the first modifications made to the stand was to exchange the aluminum CVR with a steel CVR in order to get more accurate impedance measurements. This is because the steel had approximately one order of magnitude larger resistance than the aluminum, causing larger voltage drops across the CVR. The 2 μΩ CVR could not measure accurately unless the current was well above 1 kA. The second issue came with the LeCroy probes. Though they worked well, they had the drawback of being on a proprietary system connected to a proprietary oscilloscope. This oscilloscope had a limited sample rate among several other drawbacks. To deal with this, a National Instruments high-speed data acquisition system was procured to sample voltages as well. Additionally, a pair of insulated gate bipolar transistors (IGBTs) were added in anti-series to ensure that no current could flow unless a signal was sent to the switches. Though this fixed a large number of problems, a couple of issues continued which will be discussed later. Even with these limitations , a fair number of useful experiments were performed, most notably the combined recharge and discharge of electrochemical cells. A spice schematic is shown in Figure 37 and Figure 38 shows a photograph of the stand in this configuration.

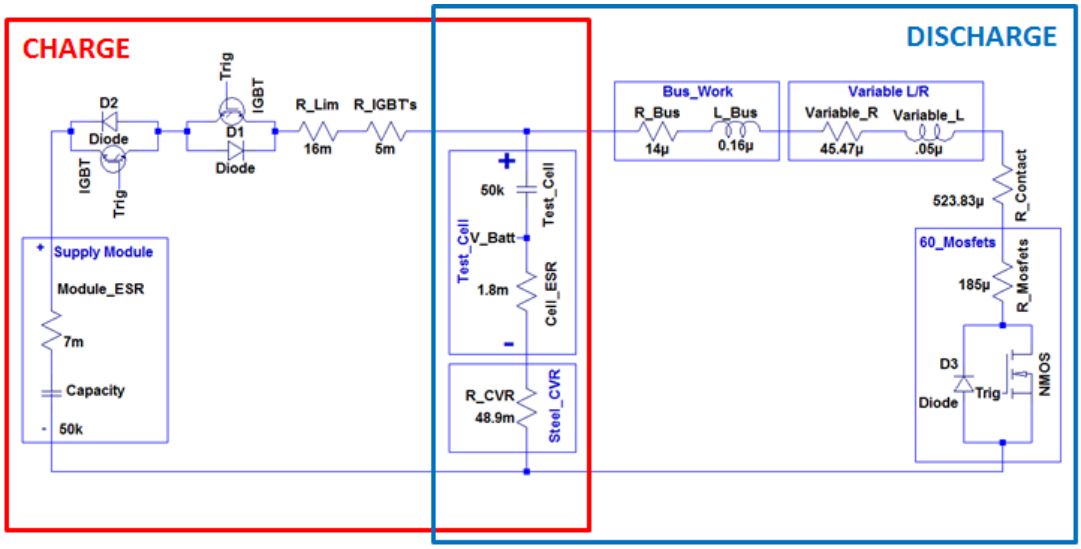

Figure 37 The test stand in a charge/discharge configuration.

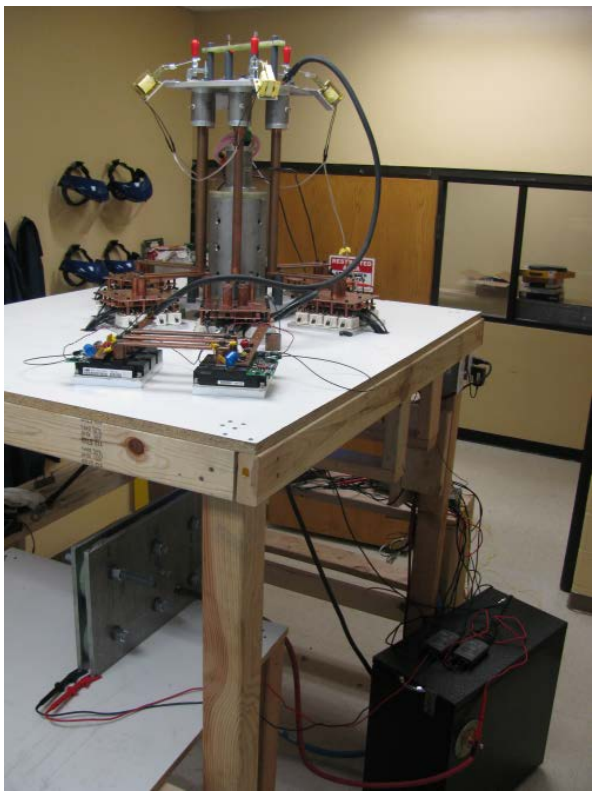

Figure 38 A photograph of the test stand in a charge/discharge configuration.

Since the charge portion has already been described as well as its modifications, the discharge portion of the test stand will be reviewed for completeness. Note that the discharge portion is similar to the charge portion described earlier, with the exception that the cell also connects to a variable inductor and there is no power supply used. The positive terminal of the cell is oriented downward and is connected directly to a 1.58 cm diameter C11000 copper rod, which is one of four conductors that makes up the variable inductor. The variable inductor is essentially a two turn inductor that varies by adjusting the vertical location of two saddle clamp conductors over the conductor length of 0.1 m to 1.5 m. This provides a circuit inductance range of 0.1μH to 2.3μH and resistance of 10μΩ to 425μΩ. The output of the inductor terminates into the aluminum plate located below

the cell. From that point forward, the current travels through the MOSFETs, CVR, and busswork already described into the anode of the cell. This discharge stand was designed to conduct large current pulses, and each SKM111AR has an on-state resistance of roughly 9mΩ giving a theoretical on-state impedance as low as 450μΩ for the entire discharge stand. Note that contact resistance drives this value higher, so the total resistance of the stand typically comes to around 500-700μΩ, though some of this may be mitigated by using shorter copper bars.

4.2 Experimental Simulation of a Pulse Discharge/Recharge

As stated in Chapter 1, one of the major applications for elevated rate recharge considers pulsed power loads. In addition to determining whether or not a particular charge profile damages the battery, there is very little examination of whether or not such things are possible. Though no lifetime studies were made in this particular experiment, it did confirm that pulsed recharges between pulsed discharges (such as a regenerative break) did slightly extend the usable capacity without immediate negative effects.

Now that the justification for the experiment has been given, the charge/discharge profile with an 18Ahr lithium iron phosphate cell will be described. In this particular instance, an 18Ah GAIA cell, initially at 100% SOC, was pulse discharged at 1200 A for 8 seconds with a 3.3 kHz square wave at 50% duty cycle. Next, a 100 ms delay was implemented, after which the cell was recharged for 1.8 s continuously with 16.4V power supply and 25 mΩ current limiting resistor, providing approximately 300A of current to recharge. After another 100 ms delay, whole process was repeated until the threshold of temperature or cell voltage was reached. The threshold for temperature was set at 55°C or greater and cell voltage set at 2.1V or less. The current is presented graphically in Figure 39, Figure 40 shows the voltage, and Figure 41 shows the temperature profile during the combined charge/discharge.

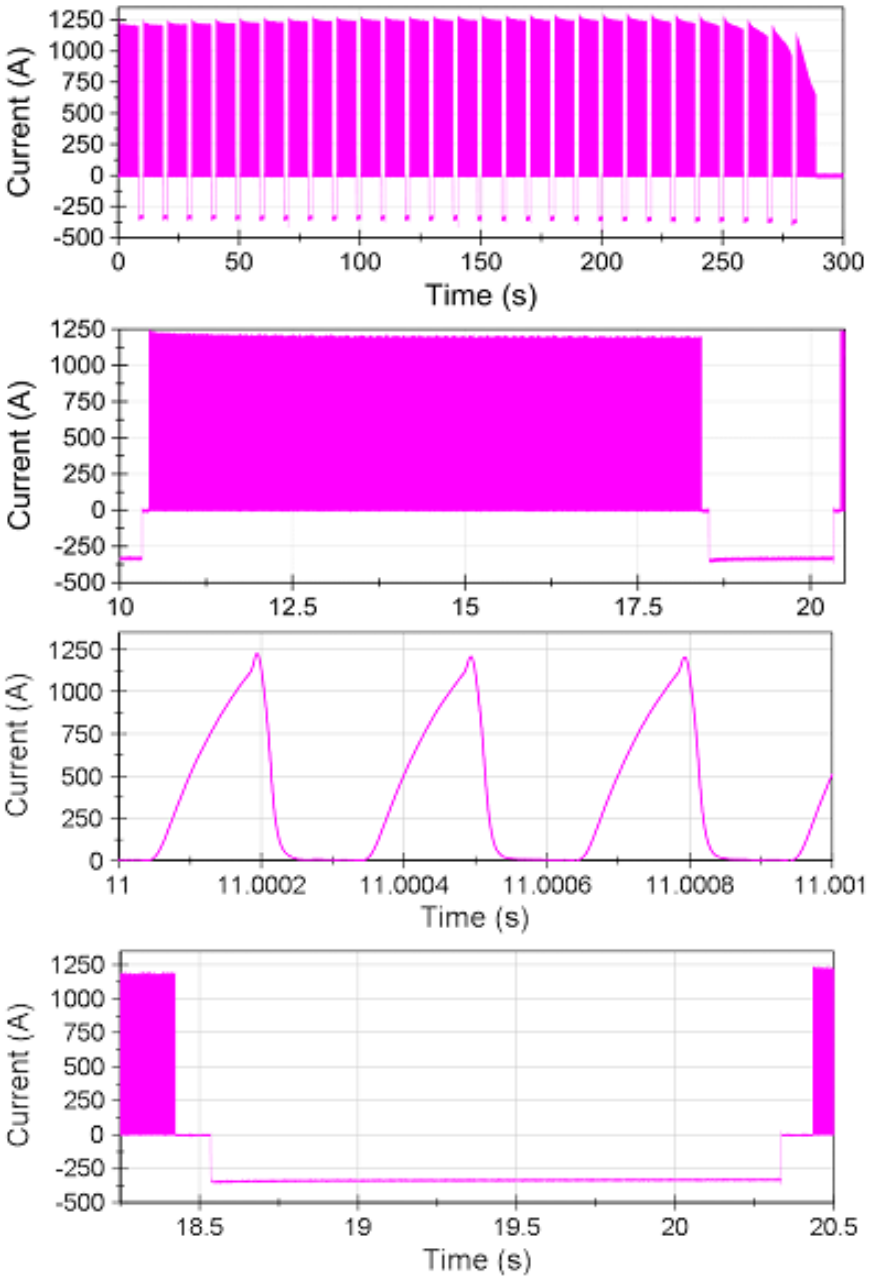

Figure 39 The current in the elevated charge/discharge experiment. The different time scales focus on particular aspects of the experiment.

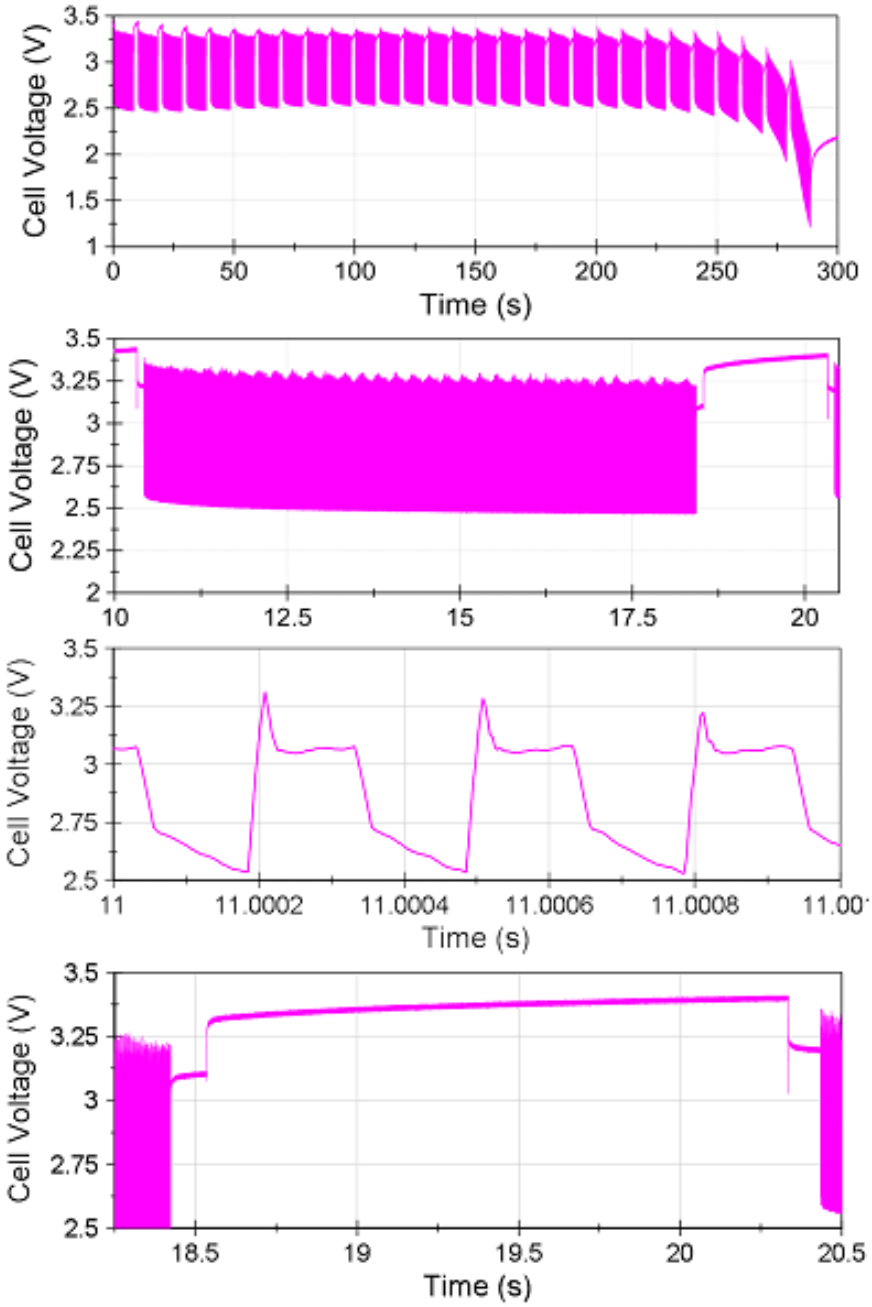

Figure 40 The voltages during the elevated charge/discharge. The different time scales, focus on particular aspects of the experiment.

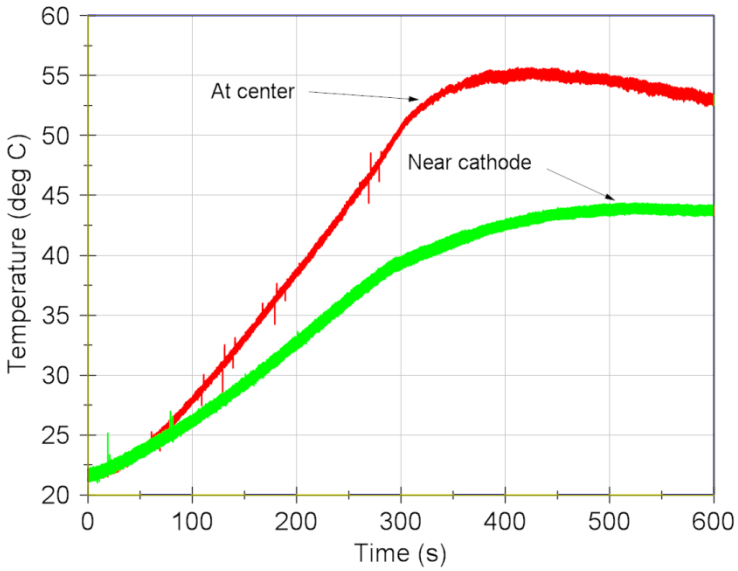

Figure 41 The temperature profile of the combined charge discharge experiment.

The conclusion from this particular experiment was that the test stand is extremely versatile, and could perform a wide variety of charge and discharge profiles, as well as simulate pulsed power sources and loads. However, both IGBTs and MOSFETs function in full saturation or in open circuit, and the inability to provide a linear current eventually caused us to acquire a regulated voltage/current supply provided by Maccor®. The linearly regulated system provides up to 240A on a 5V channel which is sufficient for a 4V lithium-ion cell. For the 3 Ah cell chosen, this means that the cycler can theoretically charge up to 80 C without an issue. Though the sample rate on the cycler itself is only 10 Hz max, samples were taken from the NI data acquisition system during elevated pulse charging tests, allowing for significant resolution.

One the stand and Maccor system had been commissioned, lifetime studies were started. A 3 Ah cell made by Saft was chosen for these tests for several reasons. First, the relatively small capacity means that high C-rates are achievable using small magnitude currents. For example, a 100A pulse corresponded to a 33C rate. Additionally, the cell has a relatively low ESR, meaning that even though the high current

caused a notable voltage increase, it did not thermodynamically stress the electrolyte as discussed previously. One final advantage is that the cell has an NCA chemistry that can be scaled up in terms of capacity, theoretically permitting construction of a power and energy dense cell. Some datasheet properties of the cell selected are shown in Table 4. These experiments will be discussed in detail in the next section.

Table 4 Datasheet properties of Saft 3Ah Cell

Capacity	Mass	Continuous Discharge Power	Specific Energy
3Ah	.21kg	17.3 kW/kg	71 Wh/kg

Chapter 5

Experimental Results

No amount of experimentation can ever prove me right;
a single experiment can prove me wrong.
- Albert Einstein

5.1 Pulsed Elevated Charge Cell # 1

The first test cell experimented with was evaluated using the test stand described in Chapter 4. This data has appeared in [130]. Both a control and variable experiment were performed independently using two identical types of cells. Fifty cycles were performed on each one respectively. The variable cell, which is charged at an elevated pulsed rate, will be described first. In these experiments, two C-rates are used to recharge the cell. As the experiment begins, a peak charge rate of 33C (~100 A) is applied in 3 s increments with 6 s of idle time between pulses. This gives an average overall C rate of around 15C which is acceptable according to Saft. The 33C rate is applied until the cell reaches approximately 3.75V. Once this critical point occurs, a relay opens to increase the series resistance of the circuit. This increase in resistance prevents the overvoltaging of the electrolyte when high charge currents are applied to a partially charged cell. A 10 s delay is implemented at this point so that the control system can confirm that the relay functioned properly, and will either continue or abort the process depending on the result. Assuming normal operation, the increased resistance reduces the recharge rate to roughly 27C. This rate is low enough to prevent the electrolyte from overvoltaging and therefore continues to charge the cell until a 4.0V cell voltage is observed during the last second of the pulse. This indicates that further charging would likely unduly stress the electrolyte, even though the full capacity of the battery has yet to be added. As stated earlier, currents of these magnitudes require consideration of the cell's ESR.

The recharge pulse frequency and duty cycle were chosen for a few reasons. First, the 33% duty cycle reduces the average recharge rate to 11C, which is documented as acceptable by the manufacturer. Also, the long delay between pulses enables the cell voltage to relax and the control system to make an accurate measurement of the cell's SOC. After every ten elevated rate recharge cycles were performed, the variable cell is cycled using a 1C-CC/CV charge and discharge process on the potentiostat. EIS measurements were made on the cell while in the charged and discharged state and the 1C capacity was then evaluated against earlier measurements made. This enables the capacity fade of the cell to be measured under similar conditions as cycle life increases. Figure 42 shows a flowchart of the process for the control and variable cell.

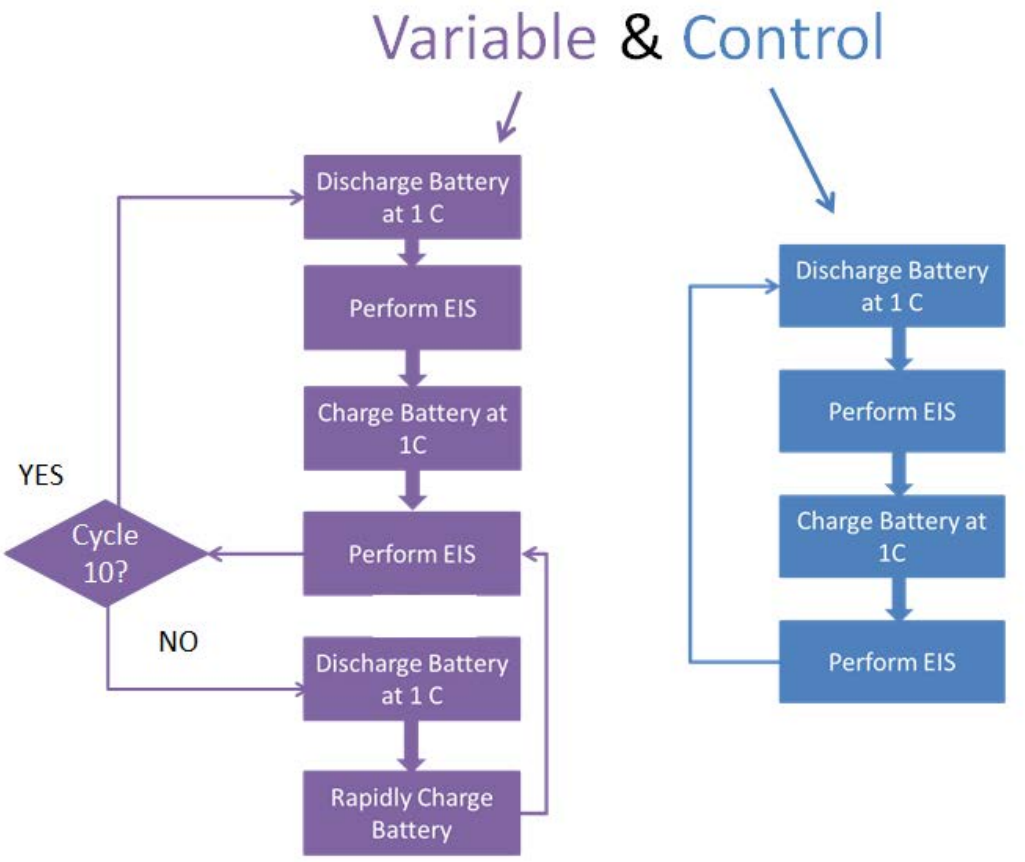

Figure 42 - Experimental Setup for the 1st test cell. The control cell is shown in blue and the variable cell is shown in purple.

The first cell tested underwent fifty cycles. Figure 43 and Figure 44 show plots of the cell voltage and current respectively recorded during the first and fiftieth elevated charge profiles. The temperature near the terminals of the cell and at the center of the cell respectively was recorded during every test, though the difference between the two measurements is nearly indistinguishable. Figure 45 shows the temperature profile of the first and fiftieth recharge experiments where it can be seen that an increase of just over 10˚C is recorded during the experiments. The capacity change in the control cell is negligible and does not merit further discussion. The variable cell does show roughly a

3.7% reduction in the capacity extracted. This is shown graphically in the plot shown in Figure 46 and Figure 47.

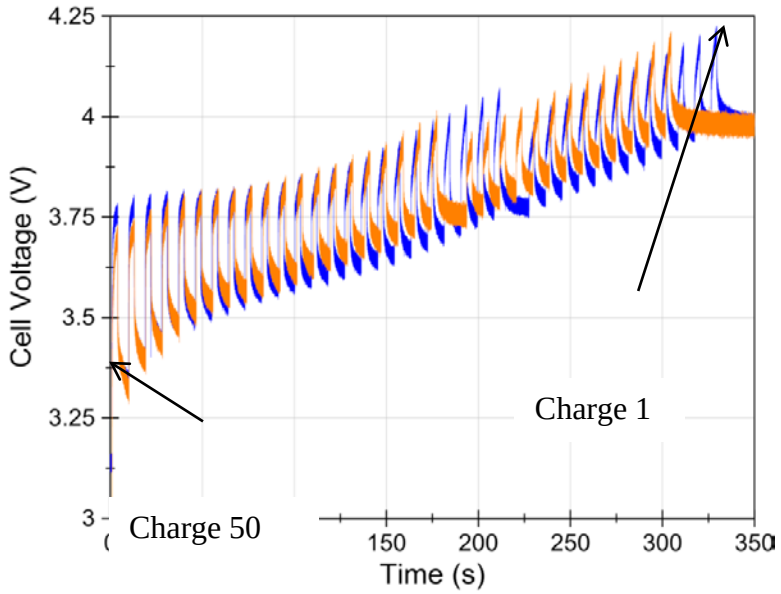

Figure 43 - Cell voltage profiles recorded during the first and fiftieth elevated recharge experiments respectively.

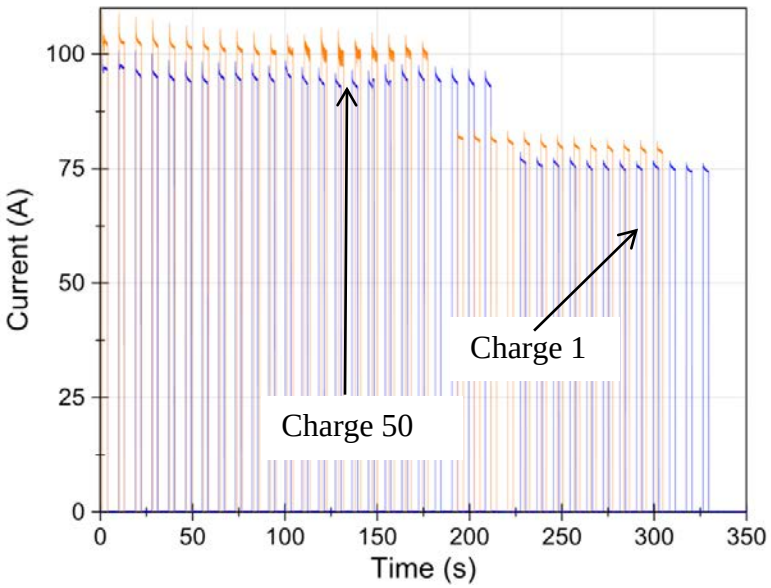

Figure 44 - Cell current profiles recorded during the first and fiftieth elevated recharge experiments respectively.

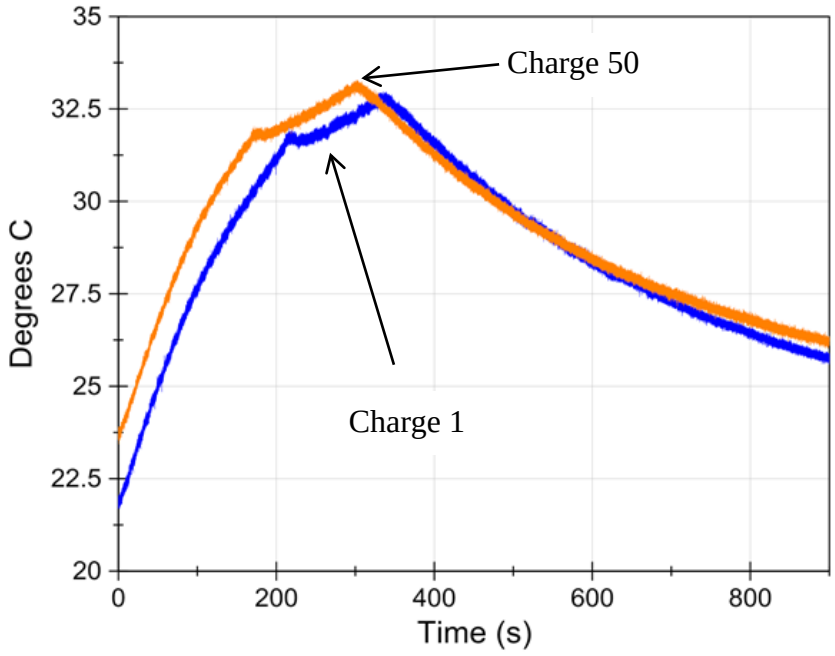

Figure 45 - Cell thermal profiles recorded during the first and fiftieth elevated recharge experiments respectively.

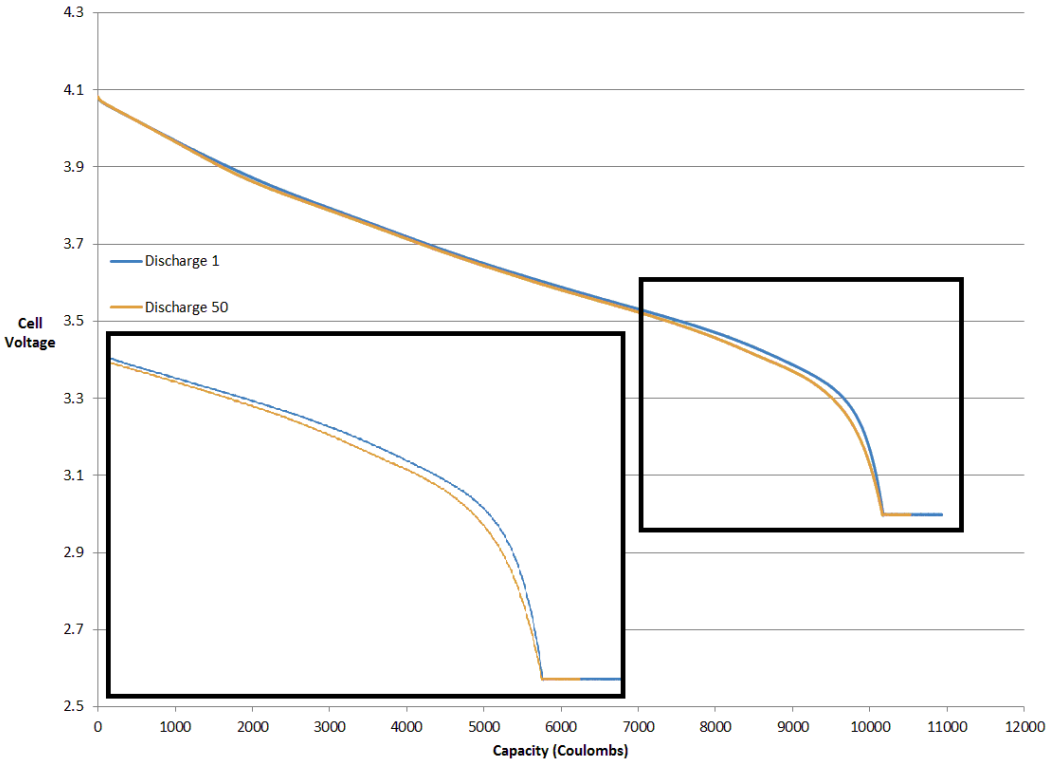

Figure 46 - Comparison of the 1C discharge curves recorded after the first and fiftieth elevated rate cycles of the variable cell.

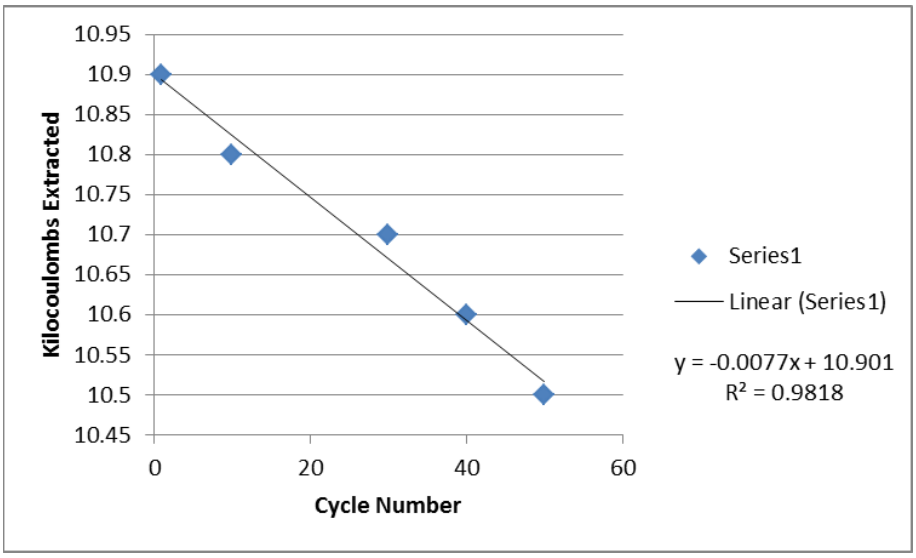

Figure 47 - The 1C capacity fade of a cell undergoing elevated charge.

Table 5 and Table 6 summarize the results of the 1C discharge experiments of the variable and control cells respectively. As shown, the 1C cycles show very little change in the cell over the fifty cycles performed.

Table 5 - Charge/Discharge cycles statistics after N number of elevated charges on the variable cell.

Cycle Number	Kilo-Coulombs Extracted	Kilo-Joules Extracted	Kilo-Joules Into Cell	Energy Efficiency
1	10.9	39.4	40.6	0.97
10	10.8	39.0	40.2	0.97
20	10.6	38.8	39.0	0.99
30	10.7	38.9	39.4	0.99
40	10.6	38.5	39.2	0.98
50	10.5	38.1	38.8	0.98

Table 6 - 1C Charge/Discharge cycle statistics after N number of 1C charges on the control cell.

Cycle Number	Kilo-Coulombs Extracted	Kilo-Joules Extracted	Kilo-Joules Into Cell	Energy Efficiency
1	11.2	40.4	41.7	0.97
10	11.4	41.1	42.2	0.97
20	11.4	41.3	42.1	0.98
30	11.3	40.9	42.1	0.97
40	11.3	40.9	41.9	0.98
50	11.3	40.8	41.9	0.97

The magnified box shown on the lower left corner of Figure 46 more closely shows the slight difference in the two curves. The change in the cell capacity implies that chemical processes have occurred inside the variable cell which have not yet occurred inside of the control cell. To help understand what this change might be, the EIS curves have been shown in Figure 48 and Figure 49 respectively.

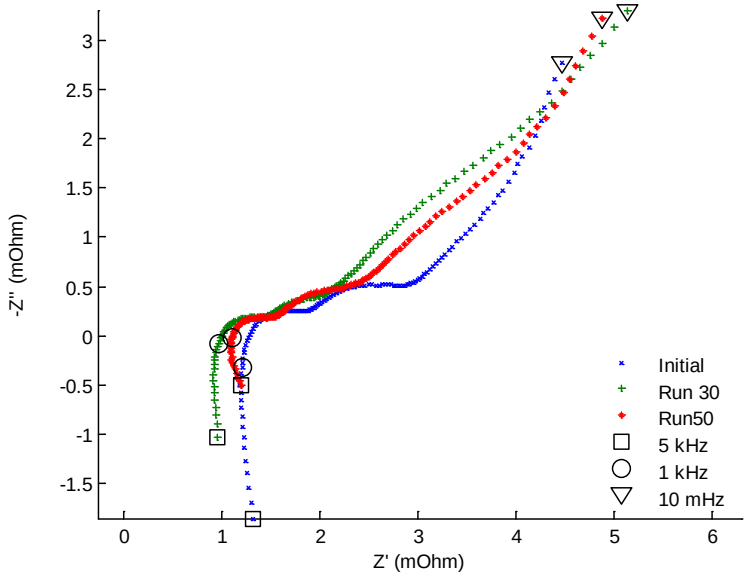

Figure 48 - EIS measurements made on the variable cell.

The frequency is swept from from 5 kHz to 10 mHz using a signal with an RMS value of 10mV. The cell's potential is approximately 4.0V DC near 100% SOC.

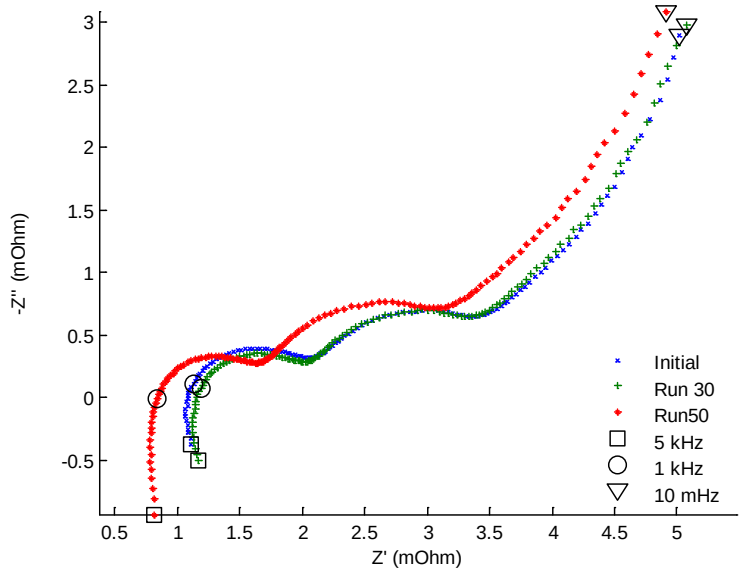

Figure 49 - EIS measurements made on the control cell.

The frequency is swept from 5 kHz to 10 Hz using a signal with an RMS value of 10mV at approximately 4.0V DC near 100% SOC.

As seen in both figures, the EIS measurements appear to shift from a state of higher impedance to lower impedance along the real axis as cycling progresses. In the case of the variable cell however, the cell begins to increase impedance after the 30th cycle, implying that the variable cell is aging quicker than the control cell. The shapes of the EIS curves are representative of that typically seen from lithium-ion batteries. Though this has been stated in Chapter 3, the general shape of an EIS curve for a lithium-ion battery will be reviewed here. There two semi-circles and a high frequency and low frequency tail. The mid frequency semi-circle represents the charge carrier relaxation and particle to particle contact resistance resulting from the formation of passivation layer on the electrode surface [3,132], which a number of electrochemists refer to as a thin film or SEI layer. Because the shape and size of the first loop does not change significantly as

the number of cycles increases, it is implied that the passivation layer remains consistent as cycling occurs [132,121]. The low frequency loop results from the RC circuit inherent to the double layer capacitance and solution/charge transfer resistance [121,133,134]. Overall, the shape of the EIS curves remains consistent from both cells suggesting that there is no substantial change in the electrochemical nature of either of the cells as cycling occurs.

Further testing would have been performed on this cell, however a concern with calendar aging of the cell was noted. In order to ensure the effects of calendar aging were minimized with respect to cyclic aging much as possible, a second cell was tested in a similar manner as the first.

5.2 Pulsed Elevated Charge Cell # 2

Unlike the first test cell, which was performed on the test stand, the second set of experiments were performed using the the Maccor® cycler. The process was approximately the same for both test cells, except the cut off voltage for this cell was 4.1V rather than 4.0V. A baseline was performed, followed by a fixed number of elevated charge/rated discharge cycles, followed by another baseline. This time, approximately 400 cycles were performed. It is worth noting that 400 cycles was chosen as the end point as a another identical cell, which was pulsed discharged at high rates exhibited 20% capacity fade after 400 cycles. For the sake of completeness, a voltage, current, and thermal profile of the 1^{st} and 400^{th} charges will be shown in Figure 50 through Figure 52.

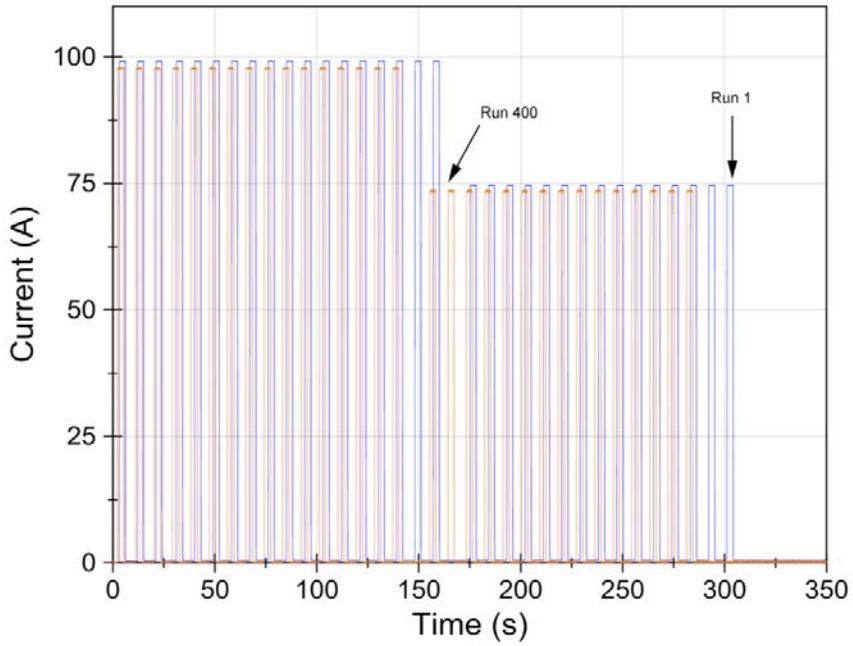

Figure 50 - The current profile of elevated charge 1 and 400, compared side by side.

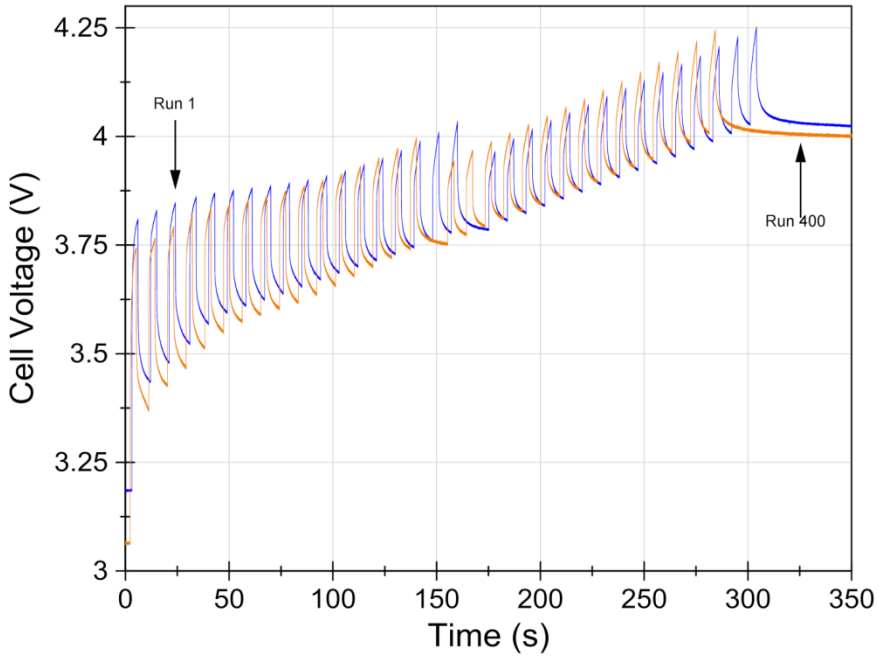

Figure 51 - The cell voltage profile for elevated charge 1 and 400 compared side by side.

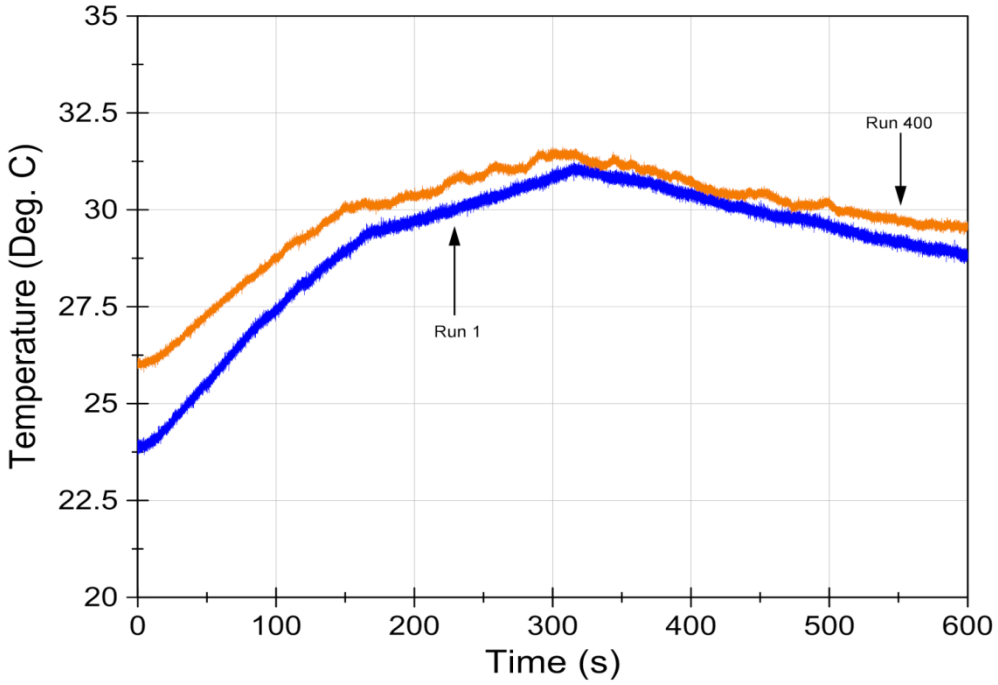

Figure 52 - Thermal Profile of elevated charge 1 and 400 compared side by side.

As expected, run 400 shows significant capacity loss compared to run 1. The only metric where run 400 displays slightly superior performance is in the thermal profile, because the increase in temperature is slightly smaller. This is only attributed to the fact that less current traverses the cell, which implies that less energy enters system, preventing the larger temperature rise seen in run 1. As with the prior experiment, the 1C control cell did not significantly alter its behavior over 400 cycles. The decrease in capacity is expected for the elevated charge cell. It is worth noting that the capacity fade follows a near linear trend after the first several cycles, which Figure 63 will show later. The 1C baseline discharge cycles are shown in Figure 53.

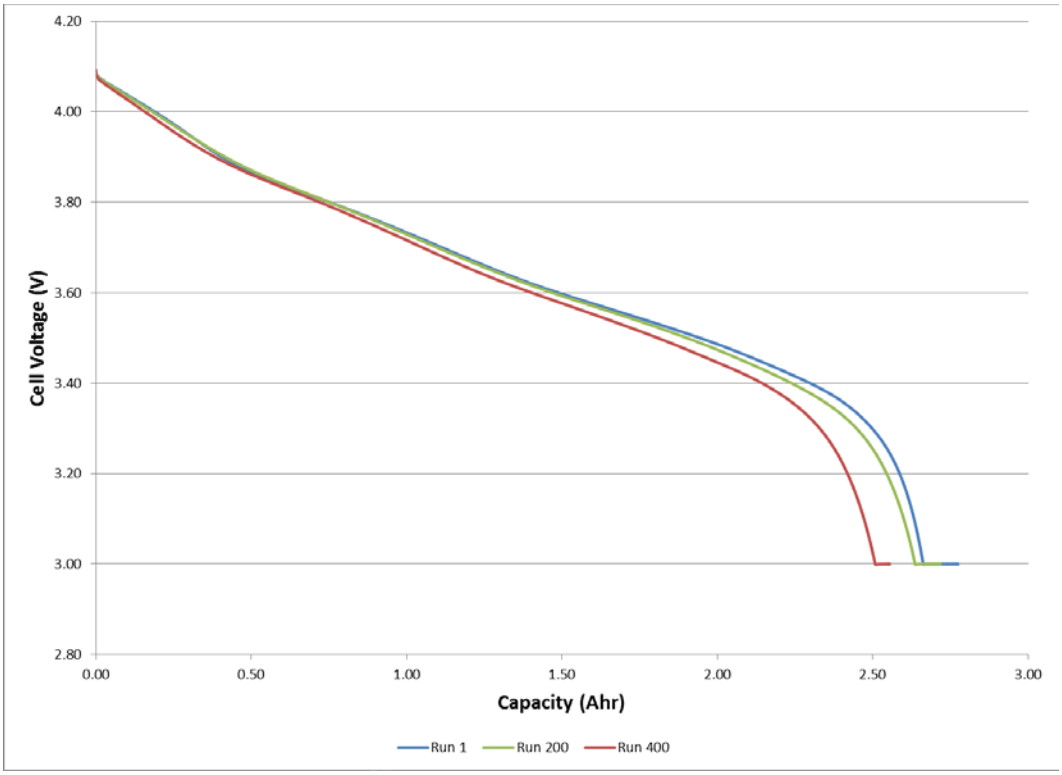

Figure 53 – The 1C discharges on the 2nd elevated pulsed charge cell.

The variable cell's capacity decreases by 9.5% from the maximum value, which occurred at cycle 50. Though the decrease in capacity is expected, joule counting and coulomb counting cannot paint the entire picture of what is causing the cell to age. In order to do this, a qualitative look at the EIS curves is necessary. Figure 54 The EIS curves of the variable cell after cycles 400, 200, and the initial case. 54(a) shows the complete curve, 54(b) shows the zoomed in section on the SEI layer. displays the EIS curves of the initial run, run 200, and run 400. Figure 55 displays the normalized experimental and normalized simulated data generated by an equivalent circuit model for run 200.

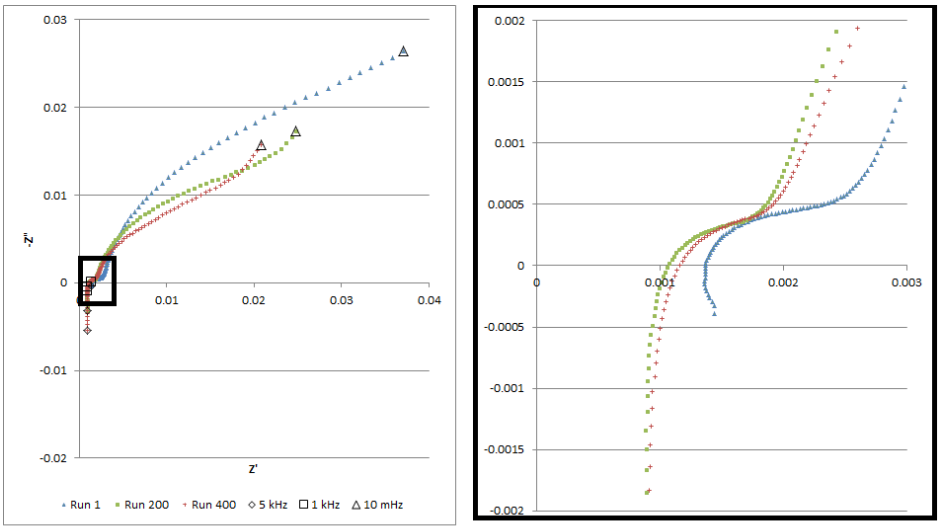

Figure 54 The EIS curves of the variable cell after cycles 400, 200, and the initial case. 54(a) shows the complete curve, 54(b) shows the zoomed in section on the SEI layer.

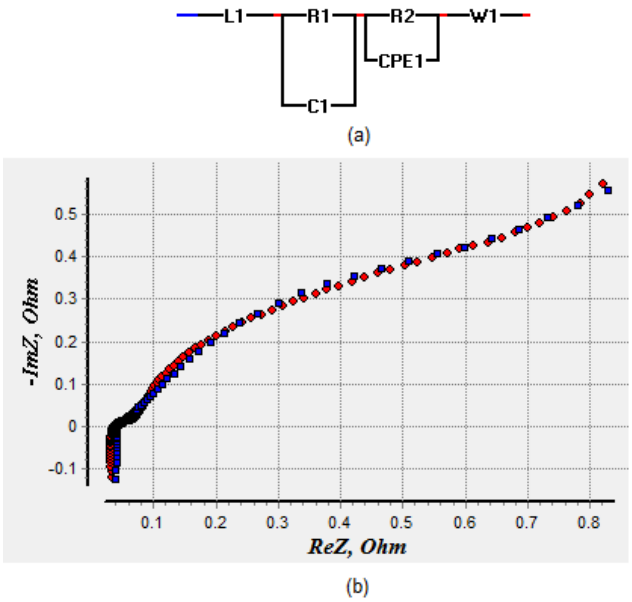

Figure 55 The equivalent circuit schematic (a) and the results of simulated and experimental results of run 200(b).

The experimental data is red and the simulated data is blue. This EIS data is normalized by the maximum value of impedance magnitude |Z|, which is why the values differ significantly from Figure 54.

The variable cell grew slightly more inductive over the cycle life of the battery. This strongly implies that the shape of one or both electrodes is changing. Because the shape of the mid-frequency semicircle in Figure 54 does not change significantly, this likely suggests the cathode is changing shapes rather than the anode. However, without a post-mortem examination of the cell, it is not possible to completely exclude anode changes at the time of this writing, especially given the fact that it is well known that the anode changes volume during cycling. One other consistent factor is the decrease in the radius of the low frequency semicircle, implying that the cell has become less capacitive. This also implies that the RC double layer has become less capacitive. The most likely cause of this is the change in electrode shape since it corresponds with the cell becoming more inductive. The other possibility is that a large amount of salt formation has occurred, and there is not as much charge present in the electrolyte. This forces us to take a look at what the math suggests. If one models this battery as seen in Figure 55, the first inductance term describes the overall inductance of the cell, the first parallel combination of a resistor and capacitor models the SEI layer, the resistor in parallel with a constant phase element (CPE) models the electric double layer, and the Warburg (W) impedance models the semi-infinite diffusion of lithium-ions. The values for selected runs are shown in Table 7 which correspond with the runs shown in Figure 54.

Table 7 Values for modeling normalized equivalent circuit

Run	L	R1	R2	C1	|CPE|	∠ CPE	Warburg
Initial	3.00E-08	0.03	0.3	1.00E-06	120	89	0.04
200	2.00E-07	0.03	0.3	1.00E-06	75	84	0.04
400	7.00E-06	0.03	0.3	1.00E-06	75	76	0.04

Note that the mathematical model also implies that the overall inductance of the system is increasing. Since the values are normalized, the resistance of the model does not significantly change over cycle life. The other significant difference is the CPE. The

magnitude of the CPE is significantly higher during the first run, and the CPE acts like a near ideal capacitor. As the cycle life increases though, the CPE becomes less capacitive and more resistive, further suggesting that there is a decrease in the charge available to the double layer. In short, the cell that underwent pulsed elevated recharge had a significantly higher capacity fade than their control cell, and the likely culprit is either salt formation or the changing shape of one of the electrodes.

5.4 Continuously Elevated Charge Cell

In addition to the elevated pulsed charge, another set of experiments were performed in which a cell was charged at an elevated rate continuously rather than pulsed. This cell underwent a 33 A CC charge until the voltage reached 3.75V followed by a 25 A charge until the cell reached 4.1V. This particular current rate was chosen because it is the same as the average current value described in the pulsed current experiments. Figure 56, Figure 57, and Figure 58 show the voltage, current, and temperature of run 1 and 400 respectively. Like the second pulsed cell, the first charge had more charge placed into it than the final charge. This increased energy was not enough to significantly alter the temperature profile, which is shown in Figure 58. The EIS measurements are shown in Figure 59.

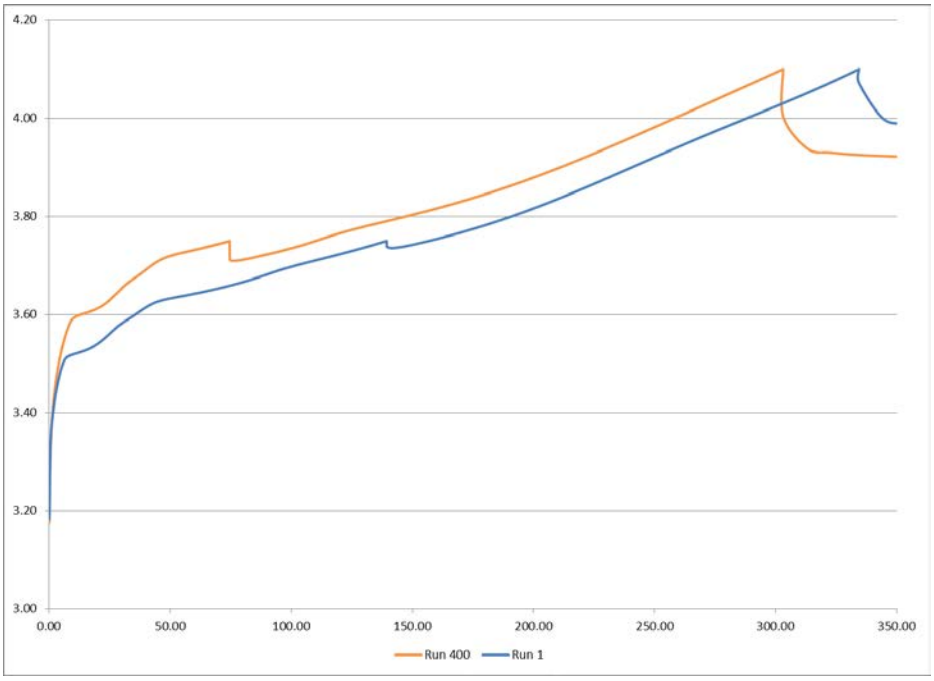

Figure 56 - The voltage profile of a non-pulsed elevated charge.

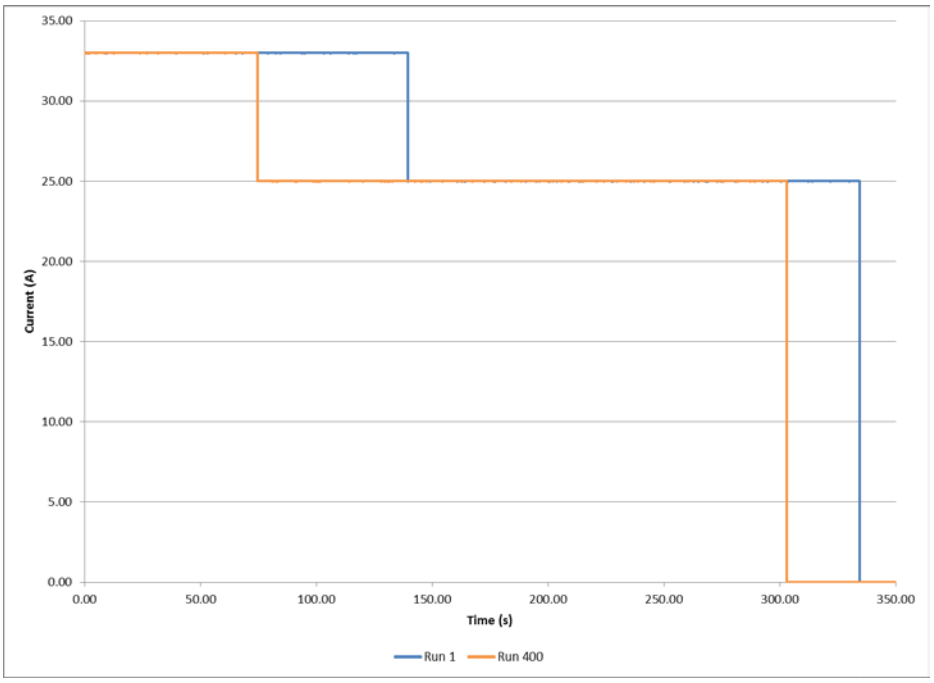

Figure 57 - The current profile of an elevated charge.

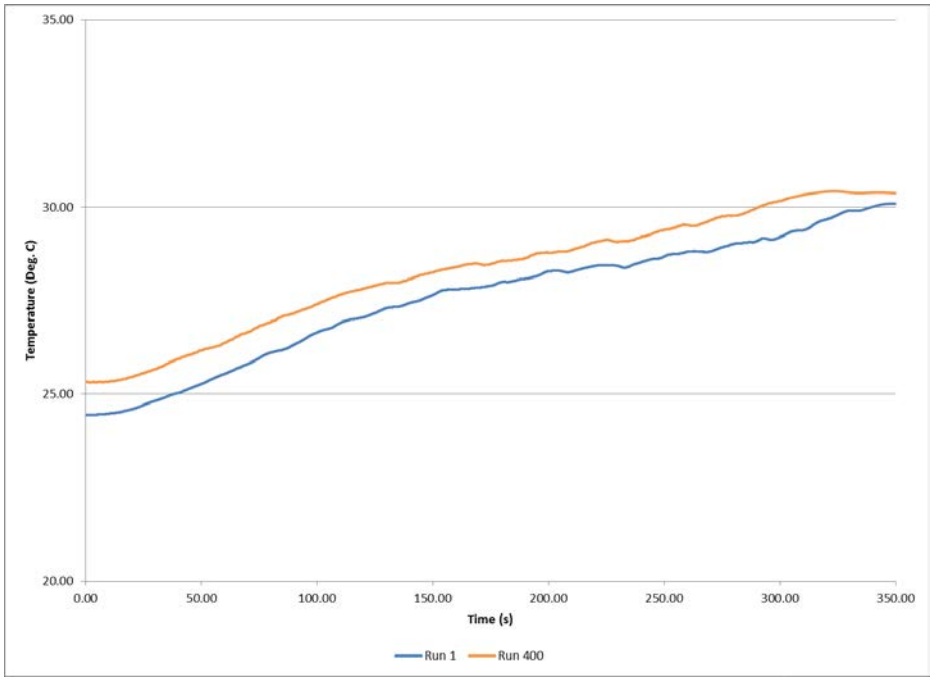

Figure 58 - Temperature profile of the elevated charge for runs 1 and 400.

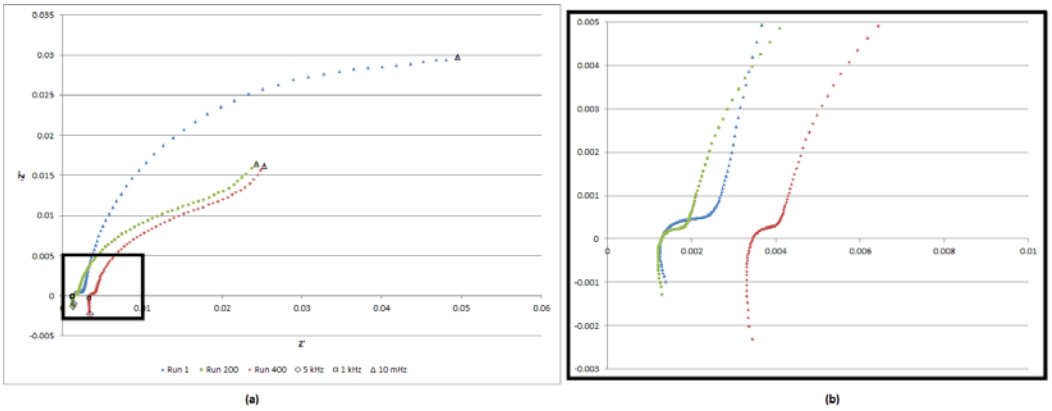

Figure 59 - EIS curves of the elevated cell for runs 1, 200 and 400. Part (a) shows the entire frequency sweep, and part (b) zooms in on the area showing the SEI layer.

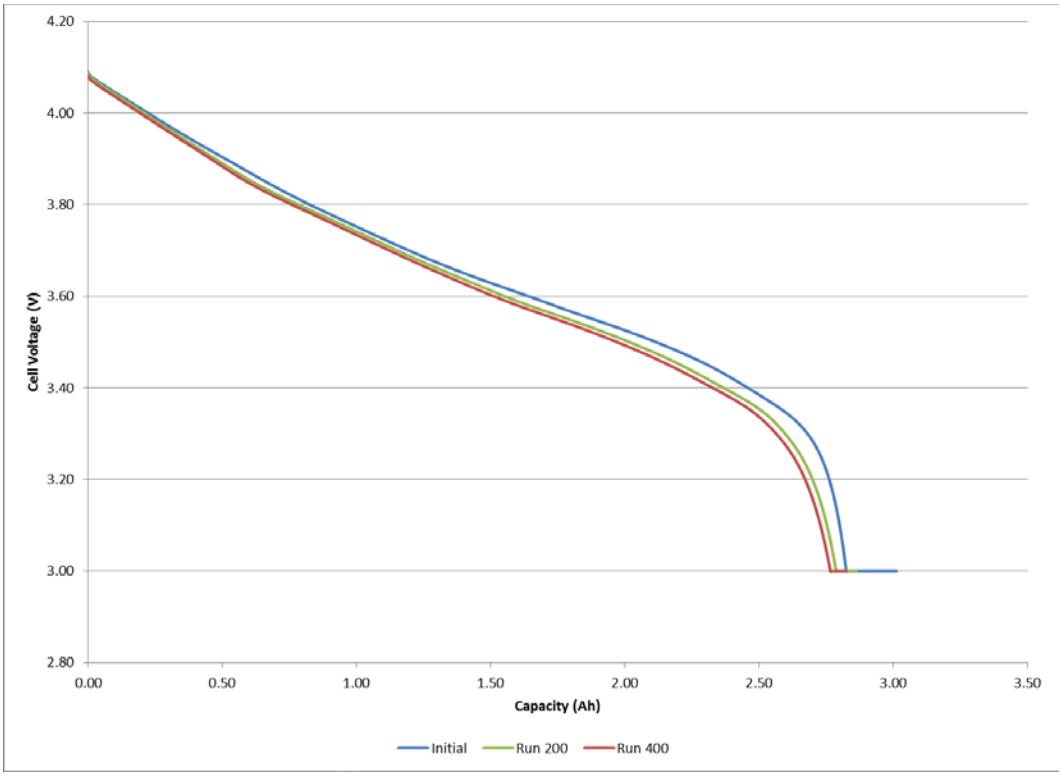

Figure 60 - The 1C discharges on the steady elevated rate charge cell.

Note that the elevated charge cell has noticeably increased resistance between cycle 1 and cycle 400. This is also verified by the EIS curve shifting to the right in Figure 59. This DC impedance increase is significantly more than the cell that underwent pulsed elevated charge, even though the pulsed cell has more capacity loss. This implies that the diffusion time allowed in the pulsed charge slightly mitigates impedance growth, even though there is a greater loss in capacity. The 1C discharge curves for the elevated charge cell are shown in Figure 60. This cell, though having less capacity fade than the pulsed charge cell has significantly higher power fade, as the measurable increase in the ESR shows. The likely cause of this is a decrease in surface area of the electrodes, which would also account for the decreasing capacitance of the RC double layer seen in Figure 59. Though the cell does appear to become slightly more inductive as well, the

extent is not as much in the pulsed charged cell. This hypothesis cannot be confirmed without a post-mortem examination.

5.5 Control Cell

In order to have a valid baseline comparison, a control cell that only underwent 1C charge and discharge was experimentally performed as well. As one may expect, using a cell at its ratings is less detrimental than using a cell at high currents. This cell did not significantly alter from its original capacity, though it did fade to about two percent of its maximum capacity. The 1C discharge curve is shown in Figure 61 and the EIS curves are shown in Figure 62. Note that the control cell did appear to become slightly more resistive in its SEI layer, though the amount is within the error of measurement.

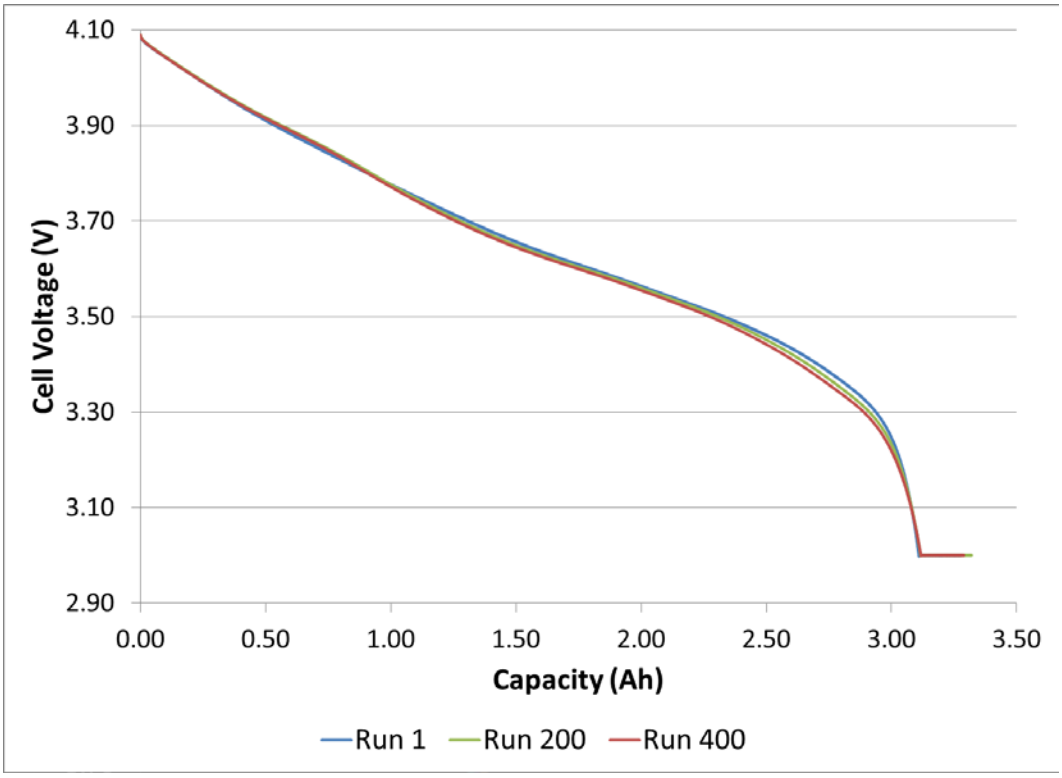

Figure 61 -1C discharges of the control cell

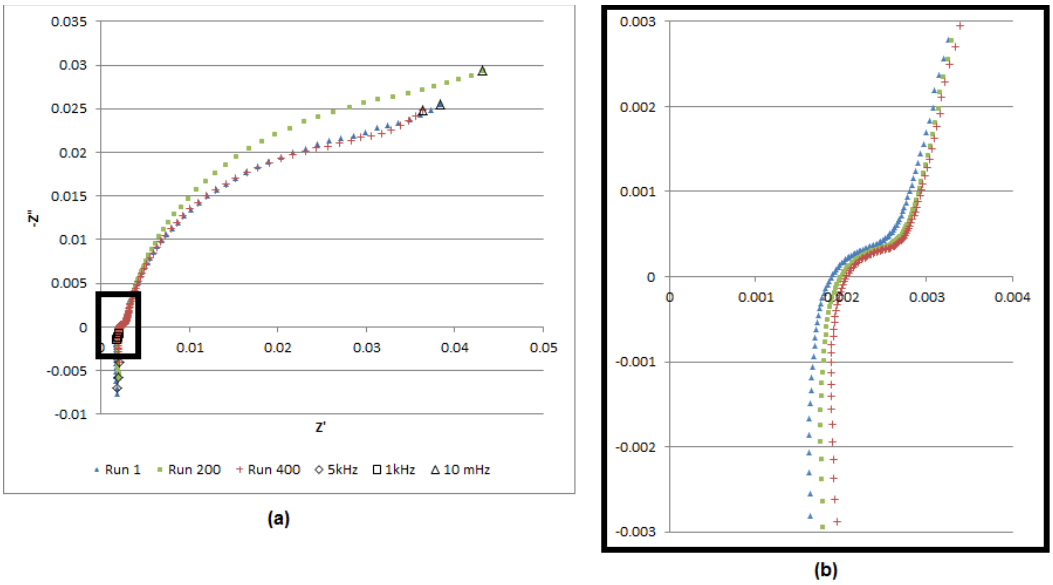

Figure 62 – The control cell EIS curves over 400 cycles.

5.6 Capacity Fade Summary

Table 8 shows how the pulsed elevated cell aged as measured from its 1C baseline cycles. Table 9 shows similar information for the elevated charge cell and shows similar data for the control cell. Figure 63 shows how these cells compared over 400 cycles graphically.

Table 8 - The 1C baselines on the pulsed elevated charge cell.

Run #	Ahr Extracted	Whr Extracted	Whr Added	Energy Efficiency
1	2.77	10.05	10.38	0.968
10	2.82	10.18	10.44	0.975
20	2.83	10.25	10.45	0.981
30	2.83	10.25	10.43	0.983
40	2.82	10.19	10.59	0.962
50	2.83	10.24	10.47	0.978
75	2.81	10.16	10.43	0.974
100	2.79	10.12	10.38	0.975
125	2.79	10.12	10.31	0.981
150	2.76	9.99	10.26	0.974
175	2.72	9.84	10.18	0.967
200	2.72	9.85	10.17	0.969
225	2.70	9.79	10.1	0.969
250	2.68	9.73	9.88	0.985
275	2.66	9.66	9.96	0.970
300	2.64	9.59	9.85	0.973
350	2.6	9.42	9.66	0.975
400	2.56	9.34	9.64	0.969

Table 9 - 1C Baselines on the elevated charged cell.

Run #	Ahr Extracted	Whr Extracted	Whr Added	Energy Efficiency
1	3.01	10.9	11.18	0.975
50	3	10.86	11.14	0.975
100	2.97	10.74	11.1	0.968
150	2.92	10.56	10.84	0.974
200	2.86	10.39	10.61	0.979
250	2.87	10.41	10.67	0.976
300	2.84	10.31	10.72	0.962
350	2.83	10.23	10.53	0.972
400	2.82	10.24	10.61	0.965

Table 10 - 1C data for the control cell

Run #	Ahr Extracted	Whr Extracted	Whr Added	Energy Efficiency
1	3.10	11.35	11.58	0.980
10	3.09	11.30	11.55	0.978
20	3.10	11.33	11.55	0.980
30	3.10	11.32	11.56	0.980
40	3.09	11.32	11.54	0.980
50	3.10	11.33	11.56	0.980
75	3.11	11.36	11.59	0.980
100	3.10	11.34	11.58	0.980
125	3.14	11.45	11.64	0.984
150	3.12	11.38	11.62	0.980
175	3.14	11.45	11.66	0.981
200	3.12	11.38	11.62	0.980
225	3.12	11.44	11.62	0.985
250	3.11	11.36	11.62	0.978
300	3.11	11.36	11.60	0.979
350	3.10	11.32	11.58	0.977
400	3.10	11.29	11.54	0.978

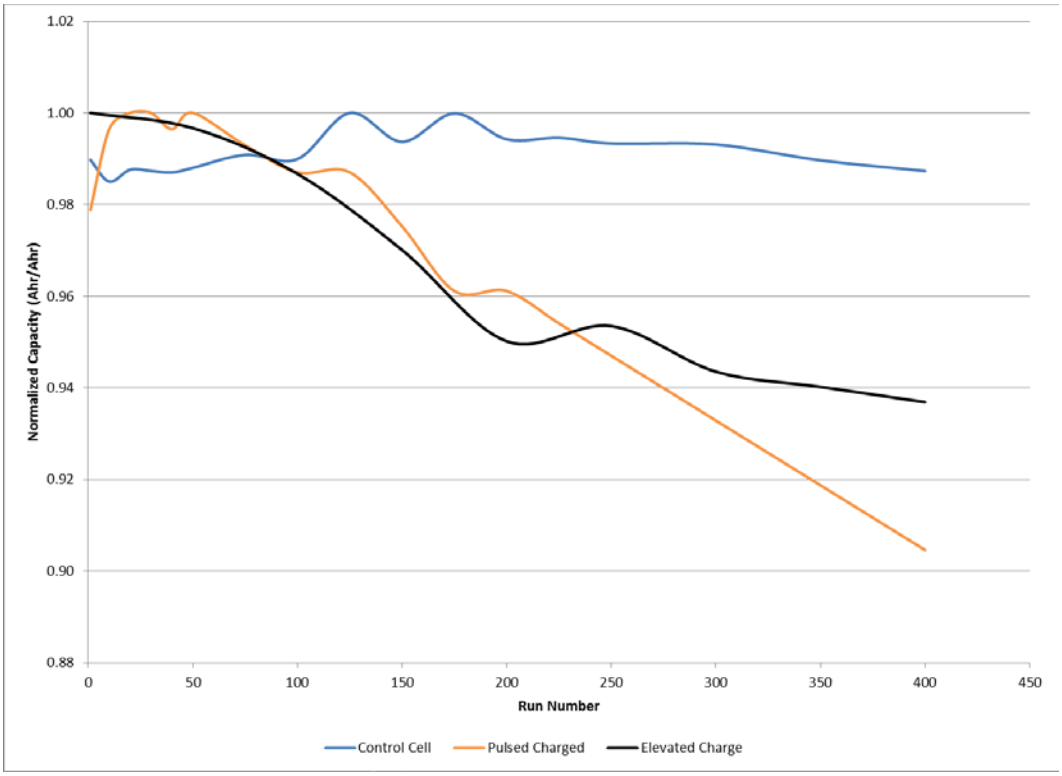

Figure 63 - The capacity loss versus cycle life for the control cell, elevated charge cell, and pulsed elevated charge cell.

These values were taken from the 1C charge and discharge curves for the control and variable cell. Note the capacity value is normalized with respect to its maximum value, not its original value.

As expected, the control cell had the least capacity fade. Though the AC and DC resistance of the elevated charge cell was slightly higher, the capacity fade in the pulsed elevated charge was also slightly higher. This suggests a correlation between the magnitude of current and capacity fade, which further suggests that this process is diffusion limited. Figure 64 suggests this as well, with evidence taken from an elevated discharge cycle life testing procedure.

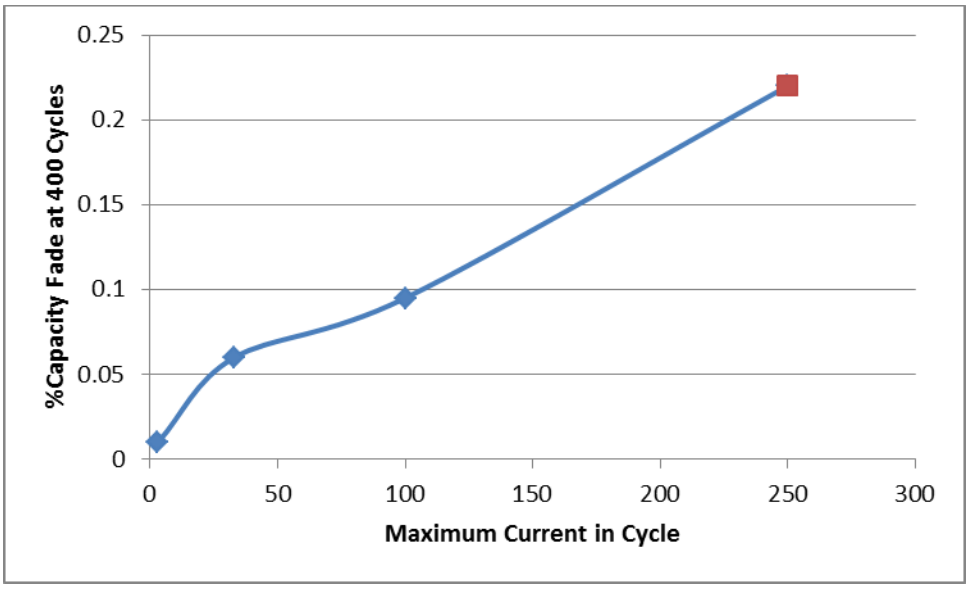

Figure 64 - The capacity fade at 400 cycles versus the maximum current during either a charge/discharge procedure.

The blue diamonds correspond to elevated charge with a rated discharge. The red box corresponds to an elevated discharge with a rated charge. Though the resolution is low, a linear appearance relating current magnitude to cycle life fade appears for the NCA cells in this work.

Chapter 6

Modeling

Pure mathematics is, in its way, the poetry of logical ideas
- Albert Einstein

6.1 Modeling Background

Over the years a number of different battery models have been developed. Which model to used depends on a number of conditions. The simplest model of an electrochemical cell is an ideal voltage source. One modest tweak to this circuit is a resistor placed in series with the voltage source, modeling the ESR. One may also take a simple Norton equivalent circuit of the aforementioned model to have a current source rather than a voltage source. Both Thévenin and Norton models allow relatively quick computations when a number of factors are known or are going to be relatively stable. For example, in DC circuit models that feed relatively steady loads, this model is near ideal. A typical example of where this model could be used comes from steady loads with only an off or an on state, with very little change in voltage or current demand from the electrochemical cell. Though this model has ease of use as well as simplicity, it lacks the ability to prognosticate causes of battery failure, as well as take into account transients. For modeling circuit elements with cheap alkaline or nickel metal hydride batteries though, this model works well enough for a large number of test cases. The two models are shown in Figure 65.

A common transfer function used for modeling electrochemical cells is bode and Nyquist modeling. Though these models are incredibly accurate, they require a large amount of information to be known and used. While getting activity and other various chemical properties of a cell in an electrical system is a non-trivial task, a number of people have tried to make circuit models out of them [135]. These circuit models have a number of interesting properties, but they all have an issue with circuit modeling. They

invariably use a concept called Warburg impedance or a constant phase element. From an electrochemical modeling perspective, this makes a large amount of sense.

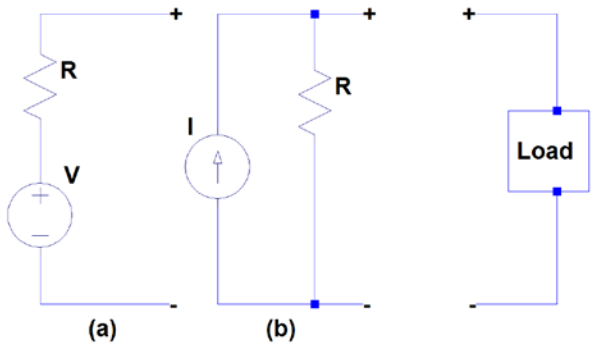

Figure 65 - Simple DC models of batteries with resistance.

The Thévenin voltage model is shown in (a) and the Norton equivalent is shown in (b). The simplicity and relative straight forwardness of this model has made it extremely popular to use with cells that may be easily replaced, such as alkaline and nickel-metal hydride cells.

The EIS curve in Chapter 5 made use of these elements, and they greatly aided in determining the more likely causes of failure. From an electrical engineering perspective this concept has a significant number of drawbacks. A Warburg impedance models the semi-infinite diffusion across an electrode and accounts for surface roughness. Though it is possible to determine the Warburg impedance from electrochemical impedance spectroscopy, it is not possible to directly convert it into simple analog circuit elements. Constant phase elements are simple enough to describe mathematically, and can be approximated by a series of RC or RL circuits. Consequently, a number of people have tried to convert their constant phase elements as well as Warburg impedances into a series of RLC circuits, though the success of this approach varies from battery to battery.

Another common approach to batteries is to model them as a combination of RC circuits[136], shown in Figure 66. This allows relatively easy circuit simulation and

calculation, and works well if the parameters can be determined through a series of tests. With advancements in computing, more authors have made the resistances and capacitances a function of state of charge. While this allows for more accuracy, it increases the complexity of the system[137].

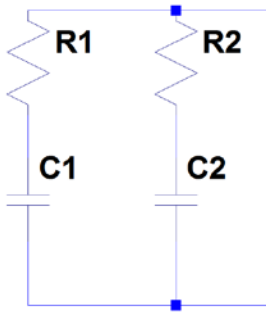

Figure 66 - An RC model of a battery.

Note that depending on the type of modeling done as well as the transients intended to model, many RC paths may exist. Also note that in this model the capacitance must be large enough to function similar to a battery. This particular method of modeling works extremely well on supercapacitors.

Because of the complexity of batteries, a large amount of research has been done concerning modeling them as artificial neural networks (ANN). There are a number of methods for constructing an artificial neural network, the most common methods being the Gauss-Newton and Levenberg–Marquardt algorithms. A full discourse on these ANNs would take a long time, for the sake of completeness the mathematics behind the Levenberg–Marquardt are qualitatively discussed, though a more thorough discussion may be found in [138,139]. Artificial neural networks are a way of performing a particular form of mathematical problem where the solution and the inputs are known, but the system is not. In order to try to solve the system, an ANN takes a number of decision points called neurons and assigns them various weights. Using an iterative method of

forward and backward solving problems, all ANNs try to minimize the error function, which is the difference between the target output and the inputs multiplied by the weights. The smaller the error function, the closer a network is to an approximate solution. The other mathematical trick deals with convergence. The Levenberg–Marquardt algorithm converges, as described in Equation 6. Once the error does not reduce further, the ANN is said to have converged as much as possible.

$$w_{k+1} = w_k - (J_K^T * J_K + \mu I)^{-1} * J_k e_k$$

Equation 6 - The weight convergence of a Levenberg–Marquardt ANN.

W refers to the weights, J refers to the Jacobian, I is the identity matrix, e is the error, and μ a non-zero positive value that determines the step size [140].

Artificial neural networks have two large drawbacks. First, ANNs require large amounts of data in order to accurately predict battery behavior. If the amount of data collected is too small, they will have large prediction errors. Second, ANNs are non-linear. Though it does make sense having a non-linear model predict a non-linear device, a large number of mathematical operations cannot be performed due to this property of neural networks.

6.2 EIS Modeling

6.2.1 EIS Spectrum Modeling

A large amount of data exists for modeling EIS curves. In the models described herein, all EIS measurements were taken at room temperature between 0 - 10% SOC at 3.2 VDC. The near discharged state was chosen for two reasons. The first is that the changes were slightly easier to track for these particular cells. The second is that the resistance is slightly higher in the discharged state. From a practical perspective, one always wants to assume the cell has more resistance than less.

Most EIS curves graphically display the real impedance versus imaginary impedance. EIS based modeling has primarily been physics based, where chemists have used white-box modeling in an effort define every interaction in the cell at a very basic level. Though not a white box model itself, an equivalent circuit model was presented in Chapter 5 with respect to aging characteristics.

6.2.2 Bode Modeling

While equivalent circuit modeling is useful, most electrical engineers use black box modeling, where the input acts as a function of output and the exact circuit parameters are unknown. In this particular case, rather than model EIS curves as a function of real impedance versus imaginary impedance, a method of modeling impedance versus frequency, as well as phase versus frequency, will be discussed. This is commonly referred to as Bode plots. This is useful because a large amount of electrical equipment operate at a fixed frequency. If one can predict how a battery or battery module will act at 1kHz, 400Hz, and 50/60 Hz or other fixed frequencies, circuit modeling becomes much simpler due to phasor mathematics.

For those unfamiliar with the term, phasor math is a simplification of the Laplace Transform of a circuit element at a fixed frequency. This allows DC analysis of circuits on AC systems by transforming capacitors and inductors into resistors multiplied by the imaginary number j, which is defined as the square root of negative 1. In phasor circuit analysis, capacitors have a negative j value whereas inductors have a positive j value. Depending on the textbook, some people may refer to the imaginary number as i, however in electrical engineering this is uncommon because i typically refers to current. This means that certain elements may be lumped together to perform circuit analysis. A brief example will follow in order to illustrate the point. Say a 60Hz system has a 120V sinusoidal voltage source in parallel with a 1mF capacitor and a 1 Ohm resistor.

Because the resistor is frequency independent, its Laplace transform into a phasor does not change values. Since the voltage is simply a sinusoid, its Laplace transform simply goes to the magnitude of the source. Note that in this example, RMS values are not given for the sake of clarity.

When solving AC circuits, picking a reference is mandatory. The convention uses either the source or the load as the 0 degree reference point, though it is arbitrary. Usually, choosing the reference can ease some of the calculations. In this particular example, we are arbitrarily choosing the voltage source as the reference because it is in parallel with all of the elements. This means that the only thing remaining to solve is the current.

The Laplace transform of a capacitor is 1/C*s. A Fourier transform of that same element is 1/jwC. Because phasors act at a fixed frequency, the phasor simplifies to j/(2*pi*frequency). This theoretically transforms the 1mF capacitor into as a resistor with a magnitude of 2.7j*Ω. Paralleling the two elements impedances gives a total impedance of approximately 0.8756 Ω - 0.3301*j Ω. Taking 120 and dividing by the total resistance gives a total of 128 at an angle of 20 degrees leading the voltage. This verifies because capacitance causes the voltage to lead the current, generating a leading power factor. Conversely, inductors do the opposite generating a lagging power factor. A unity power factor is where the voltage and current is perfectly in phase with one another, which is a characteristic of purely resistive systems. A SPICE schematic of the circuit in question, as well as the plot is shown in Figure 67.

Note that all of this math was performed in order to turn a time dependent AC circuit into a DC circuit with no elements any more complex than a resistor. As one might expect, reducing time dependent sinusoids into a simple DC circuit with imaginary and real impedances can greatly reduce the calculation overhead on any number of

applications. This technique is most commonly used in power systems, where a relatively well controlled grid frequency allows this sort of math to take place with a fairly large degree of accuracy given the scale and scope of the power system. Phasor math can be used in other places, but again it is primarily used in power system analysis.

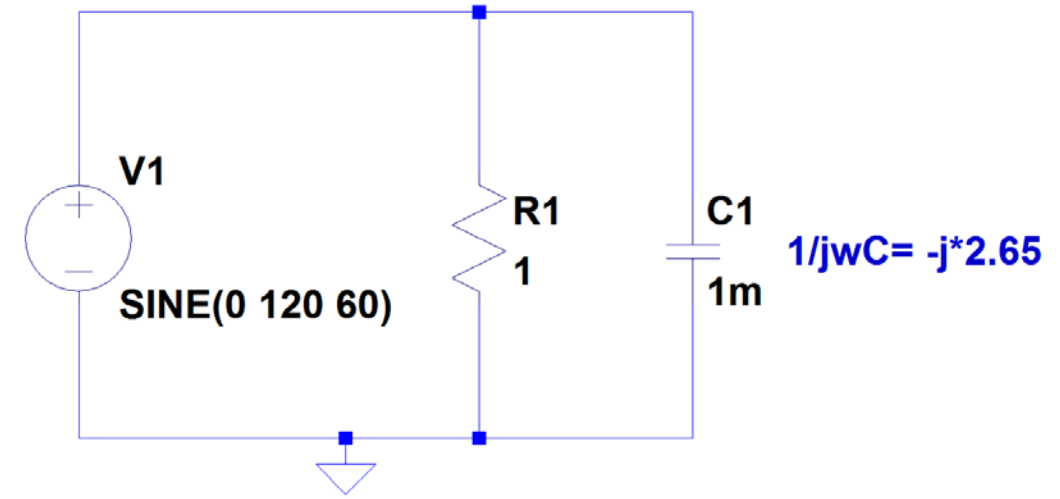

(a)

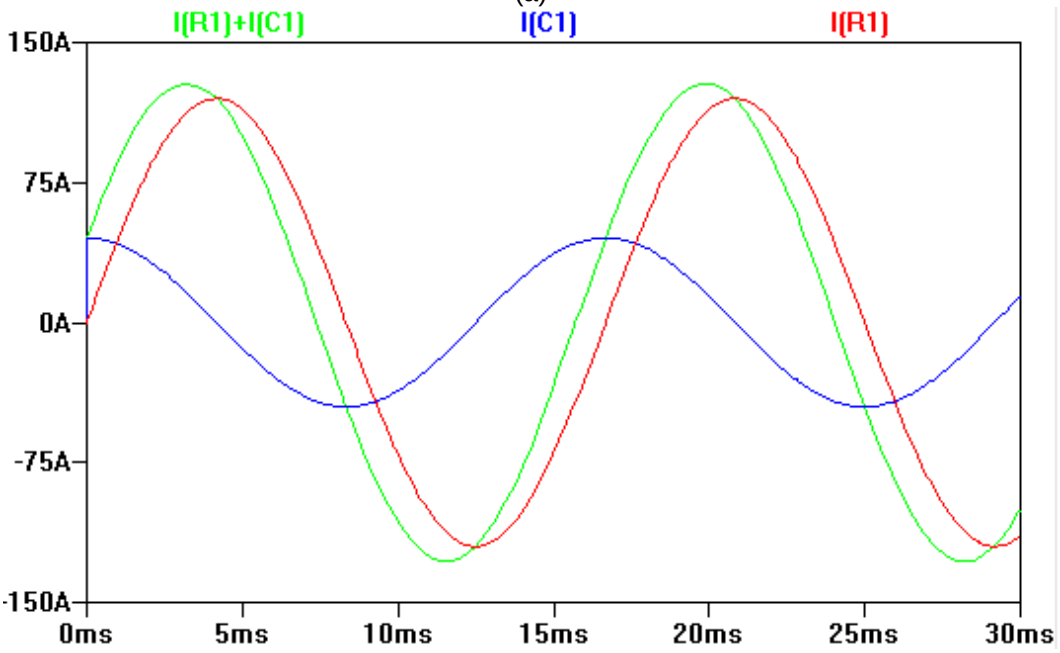

(b)

Figure 67 - SPICE circuit schematic (a) and simulation results (b) of example phasor math. .

The current verifies the magnitude and phase shift calculated above. Due to Kirchoff's current law, the current through the sinusoidal source is written as I(C1)+I(R1), verifying that the sum of currents into a node is equivalent to the sum of the currents exiting. Note that the phasor represents a sinusoid even though it is merely written as a complex number with a real and imaginary component. With the aforementioned applications in mind, Figure 68 and Figure 69 show the magnitude and phase of the Saft 3Ah cell at a particular frequency before its first run.

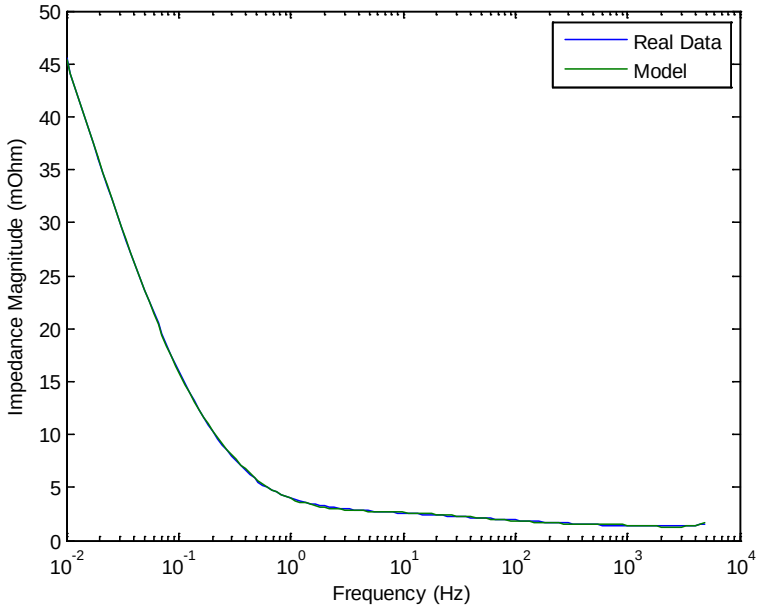

Figure 68 - Empirical Model for Impedance Magnitude as a function of frequency for the first run.

As one might expect, there is a strong dependency on frequency, phase and impedance. Here, EIS measurements were taken up to 20kHz, but no data above 5kHz is shown on these graphs. The reason being is that there are a large amount of parasitic inductances that stray into the cables. The cutoff point was chosen to be 5kHz because the 0.5 meters of 22AWG wire has less than one µH of inductance. This means that any

inductance measured is more likely to be real, especially for the larger current carrying wires. These models are derived from a set of empirical data. In this case, the equations take the form of a summation of coefficients multiplied by the logarithm of the frequencies raised to a specific power, shown in Equation 7.

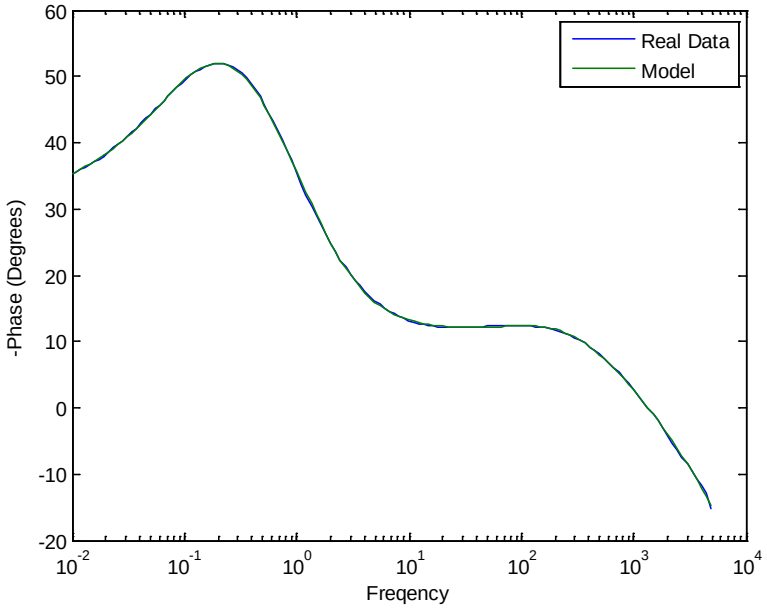

Figure 69 - Phase plot of the 1st EIS run versus frequency.
It should be noted that both of the above models are derived from an empirical basis.

$$|Z(frequency)| = \sum_{i=1}^{n} p_i * \ln(freqeuncy))^{n-i}$$

Equation 7 – Simplified form of the representation of model estimating the magnitude of frequency. p_i is a coefficient, and Z is the magnitude in milliohms.

This equation may be expanded out into whatever order someone devises, allowing for more general modeling of systems that might behave oddly over a wide number of frequencies. Likewise, the phase element is described by a slightly modified Fourier expansion, dealing with the common logarithm of the frequency rather than the

frequency itself which is shown in Equation 8. As with other expansions, it may be expanded in order to model more complex behaviors at higher frequencies.

$$-Phase(frequency) = \sum_{i=1}^{n} a_i * \sin(b_i * \ln(freqency) + c_i)$$

Equation 8 - The modified Fourier expansion that models the phase of the bode plot.

This shows the mathematical breakdown of the aforementioned models. As stated before, these models are empirically derived. Note that neither Equation 7 nor Equation 8 had a function of cycle life. In order to show a function of cycle life, both equations must be expanded out and have the coefficients act as a function of cycle life, as shown in Equation 8 and Equation 9. The coefficients are calculated on an empirical basis. Appendix A describes these data points in further detail.

$$|Z(frequency, n)| = p_1(n)\ln(frequency)^8 + p_2(n)\ln(frequency)^7 + \ldots + p_8(n)\ln(frequency)^1 + p_9(n)$$

Equation 9 - The frequency magnitude dependent upon cycle life, derived from Equation 7.

$$-Phase(frequency, n) = a_1(n) * \sin\big(b_1(n) * \ln(frequency) + c_1(n)\big) + a_2(n) * \sin\big(b_2(n) * \ln(frequency) + c_2(n)\big) + \ldots + a_4(n) * \sin(b_4(n) * \ln(frequency) + c_4(n))$$

Equation 10 - The frequency phase dependent upon cycle life, derived from equation Equation 8

To prove this method works, this model was used to model the 150th run, shown below in Figure 70 and Figure 71. However, this form of modeling requires a large amount of data to model one point at the state of charge. Other state of charge points may be mapped using the same method.

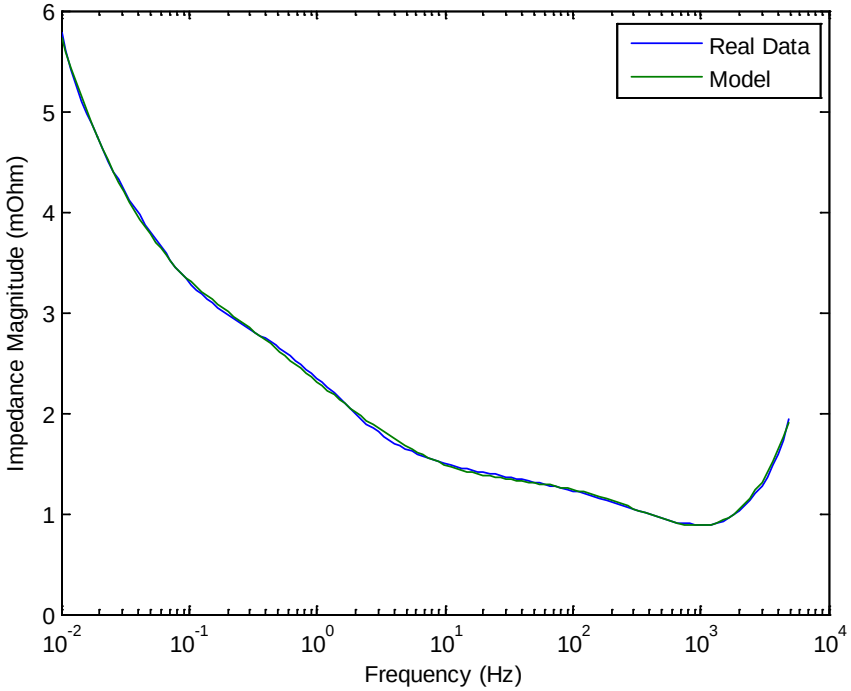

Figure 70 - The EIS data of cycle 150 as well as the model.

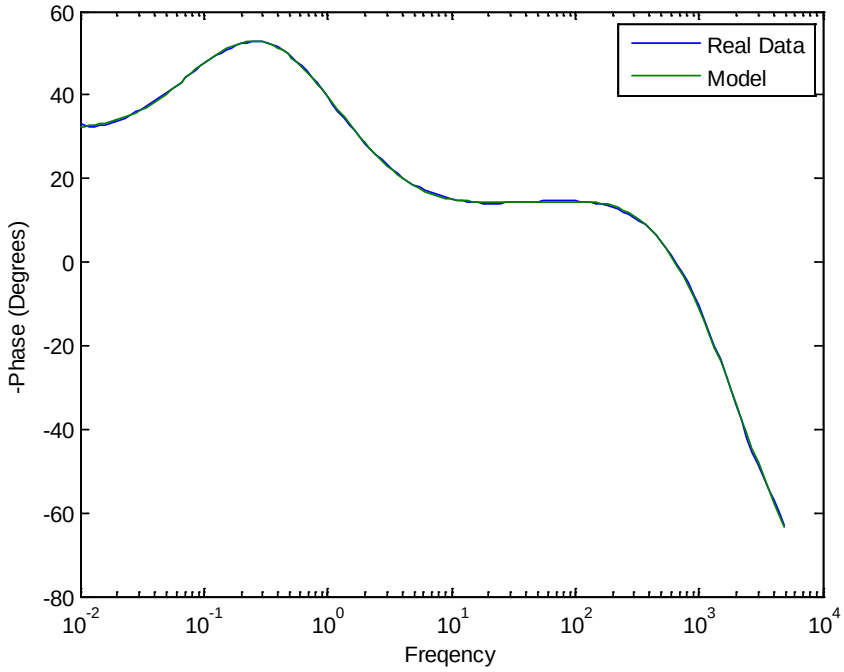

Figure 71 - The EIS phase data at cycle 150 as well as the model.

This empirical data is heavily dependent upon the natural logarithm of the frequency. Logarithms also have significant work done in the chemical field called Tafel equations and slopes [141]. For those unfamiliar with the term, a Tafel equation is merely a simplification of the Butler Volmer equation where a relatively large amount of current travels through an electrochemical system. Tafel slopes are typically used to find the exchange current density, and are typically plots the voltage versus the common logarithm of the current. Other authors have used similar methods to calculate the area of an interface using this method as well [142]. As always, it is possible to change from the common logarithm of any real number greater than zero to the natural logarithm of the same number, as seen in Equation 11.

$$\log_{10} x = 0.4343 \ln x$$

Equation 11 - Equation to convert the natural log to the common log.

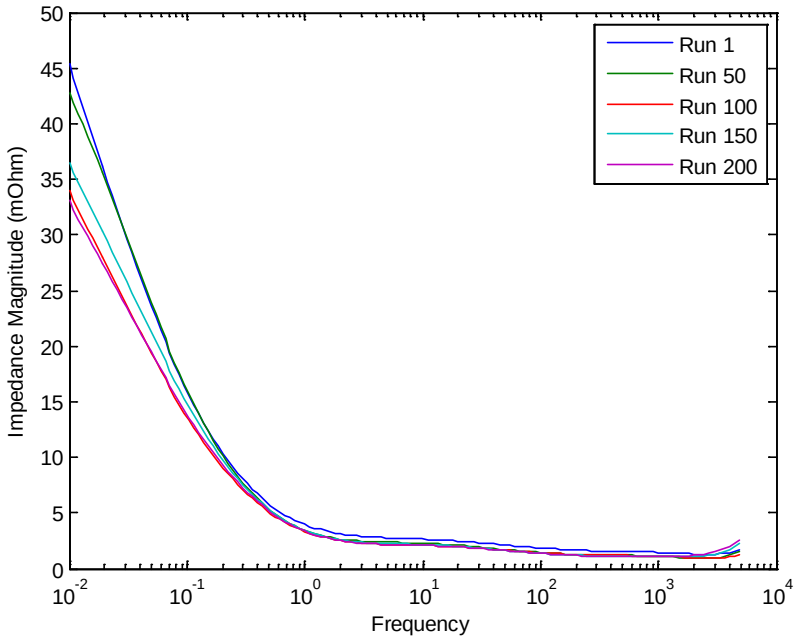

Figure 72 - The EIS models of various runs.

6.3 Modeling the Voltage and Current In an Elevated Charge

Unlike EIS measurements, an elevated charge rapidly changes values. The SOC changes from approximately zero to one hundred percent in about five minutes. This means that both the state of health and state of charge affect battery life. Modeling one state without taking into account the other will lead to a number of inaccuracies. Though a number of papers before have looked at various ways to model batteries, when applied to this particular research the margin of error was large. Compared to a discipline like electric engineering, where there have been commercial processes available for a decade that has accuracies to two microns on silicon [143], electrochemistry is somewhat imprecise. Research and development has gotten far more accurate with respect to silicon etching, but that particular process was chosen as an example because anyone may use it without having access to their own clean room. In terms of electrochemistry, this matter is compounded when using manufactured cells, where even though large amounts of the process are automated, it is not unheard of for cells to vary by significant fractions of an amp hour. Regardless, modeling of a single elevated charge may be modeled as a function of SOC. The inputs into this model are the capacitance as a function of state of charge, the resistance as a function of state of charge, the current as a function of time, and the initial voltage. Note that state of charge and time are both strongly correlated with each other in a pulsed experiment such as this, and are not independent variables due to the state of charge being directly related to the integral of the input current. This particular method of modeling takes the EIS curves, calculates the change in capacitance and resistance as a function of state of charge, and finally calculates the battery voltage as an RC circuit. Note that in the following figures, state of health is not considered a major factor. Figure 73 shows the capacitance versus time and Figure 74 shows the resistance versus time.

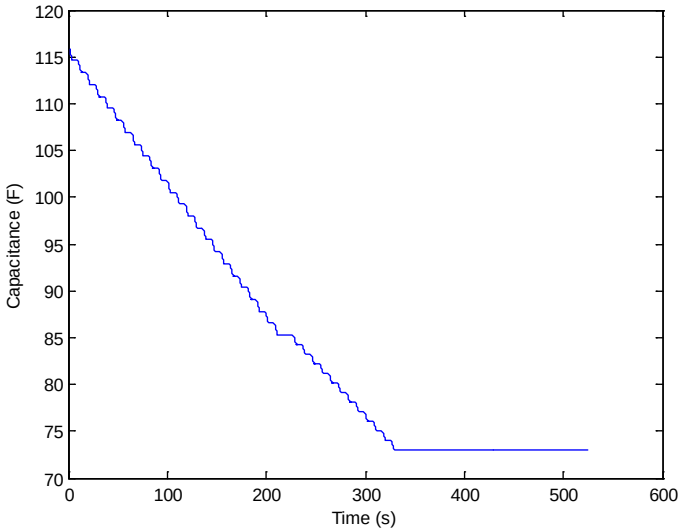

Figure 73 - Capacitance versus time for the model of Run 1.
The state of charge and time values are directly correlated, allowing capacitance to be modeled as a function of time, which is significantly easier to simulate in a time based simulation program like spice. This particular model uses Matlab® software to calculate values. Note that as the state of charge increases, the capacitance decreases.

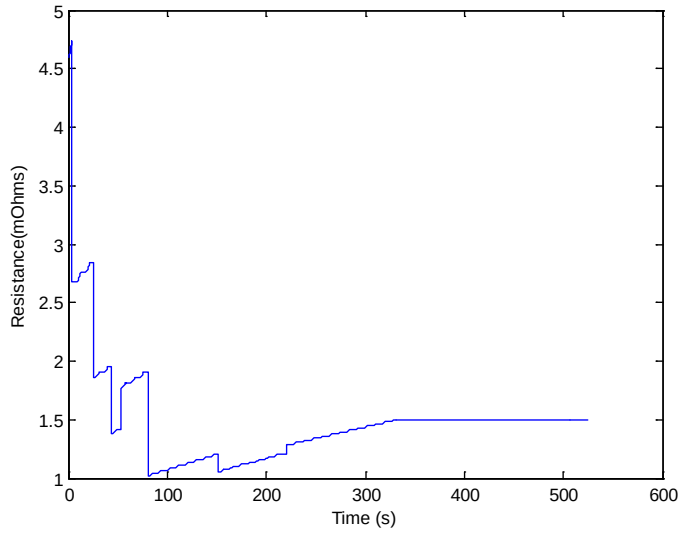

Figure 74 - Resistance versus time for the model of Run 1.
This is the highly non-linear resistance of the model. The drop around 100 seconds correlates to the current dropping from 100A to 75A. Note the highly non-linear behavior.

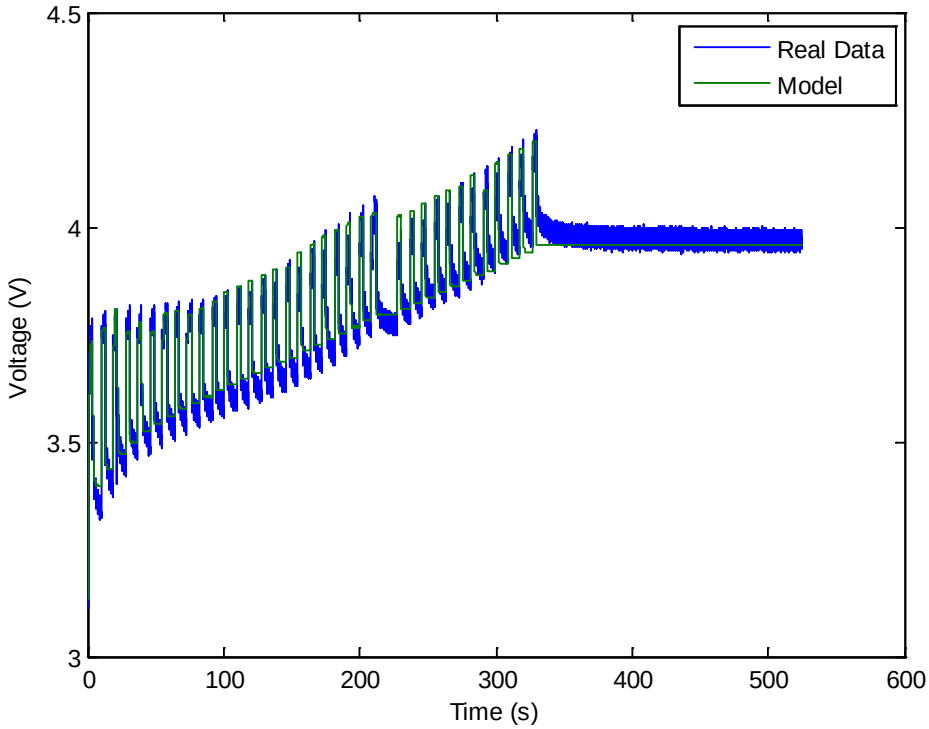

Figure 75 - The model and real data for the initial run on test cell 1.

Before going into state of health, Figure 75 shows the actual and predicted voltage data. If a small number of cycles is desired, this method may be practical for modeling it. As the number of cycles increases though, the state of health becomes more of a factor. To account for this, an artificial neural network is used to estimate any change in the state of health. Though seemingly small, the state of health does have noticeable effect after a critical number of cycles have been reached. Once that critical number has been reached, one must either retrain the network for that particular state of health, or retrain the neural network so that it has a higher error across all runs. In this particular work, the former method was chosen due to its relative simplicity. The neural network had twenty neurons in one hidden layer, and one output layer. It was solved using Levenberg–Marquardt method. Note that the neural network is simply a state of

health estimator, and must be used in conjunction with the modeling method described above in an RC circuit. The mean of the state of health model plus the circuit model yields the overall model. In order to prove this works, In order to prove this method works, the model of run 40 is shown in Figure 76.

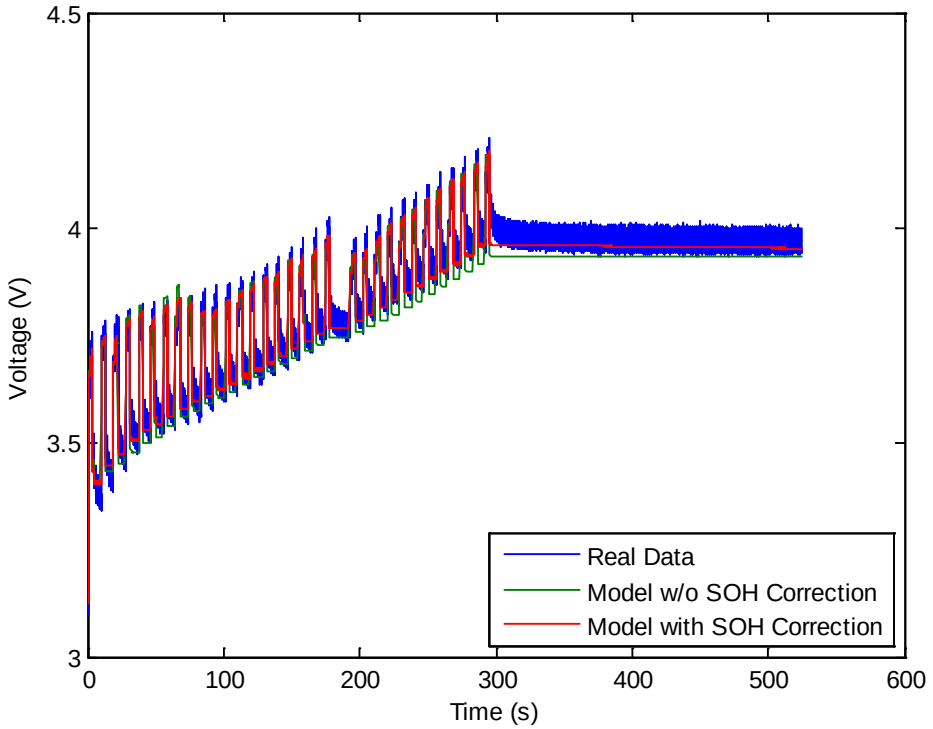

Figure 76 - The model with and without cell SOH correction provided by the ANN for run 40.

One final note, is that this model is largely empirical and requires large amounts of data in order to obtain the resistance and capacitance as a state of charge, as well as train the neural networks to monitor the state of health. Also note that this model does require a known current waveform for an input to generate an output, and is non-linear. Though the RC model without the SOH modification will approximately predict what will

happen to the cell if a 200A pulse is used in lieu of a 100A pulse, the neural network would have to be retrained.

Chapter 7

Conclusions, Contributions, and Future work

Since no man knows the future, who can tell him what is to come?
- Solomon

7.1 Conclusions

Elevated recharge of electrochemical energy storage devices has a number of applications. Time shifting supply and demand on the electric grid, quickly recharging portable electronic devices, and charging hybrids and all electric vehicles in a timely manner are all general engineering challenges that rapidly charging an electrochemical device can help with. Other major applications include quickly recharging high power pulsed power applications.

This work has presented a brief review of secondary cell technology, a method for rapidly charging an electrochemical cell, and a method for modeling a pulsed elevated charge cell's characteristics as a function of cycle life. Like all things, rapid charging of an electrochemical cell incurs a cost elsewhere, in this particular case it happens to be how fast the cell ages. Here, pulsed elevated charge and continuously elevated charge profiles were applied to two identical 3 Ah cells. Both caused the cells to age faster than a nominal 1C charge/discharge cycle with the higher peak to average rate of the pulsed recharge aging the cell faster than the uniform peak to average rate of the high continuously charged cell. The most likely cause of capacity fade is limitations in the diffusion process, since the age rate was proportional to the current magnitude. Lithium-ions have approximately ten thousand times more times mass than an electron and consequently cannot move as fast or be intercalated as quickly into the electrode materials. This means that even though the electrical current is flowing into the battery, a certain amount of lithium is either getting fed into the solid-electrolyte interface layer or causing lithium-ions to form salts in the electrolyte rather than diffusing across the

electrodes. This is most obvious in the coulomb counting of the cells as a function of cycle life, which shows a measurable decreasing trend for the cells that underwent an elevated charge.

It is also interesting to note that even though the elevated charge cell less capacity fade than the pulsed discharge cell, it had more power loss. The measurable increase in DC resistance as well as the RC double layer implies a high probability that the surface area of the electrode decreased.

The other potential cause of accelerated aging could be material degradation due to electrical stress placed on the battery, but this is less probable due to the fact that the voltage does not exceed 4.3 Volts. This value is well below the threshold of electrolyte decomposition, and should not cause significant gas generation or other mechanical failures.

7.2 Contributions

This thesis has contributed to the general field of elevated charging of lithium batteries. Very few papers exist that investigate high C-rate charge. This thesis has shown a significant amount of work in that respect. Though there are a number of papers describing elevated discharge, relatively few papers describe elevated charging and those that do generally have C-rates less than ten. This thesis has looked at how high current charging effects battery life.

Another contribution of this thesis comes from accumulation of both a large array of chemical and electrical engineering knowledge. Despite the close correlation both fields have in electrochemical cells, the phenomena that the two disciplines study varies widely. A piece of literature that can be readily read both by chemists and electrical engineers will go a long way towards advancing battery technology as well as its applications.

In a more esoteric field, this thesis has also contributed in the study of NCA cells, particularly with the state of health being directly proportional to the cycle number when undergoing a pulsed elevated charge or an elevated charge. This remarkably simple relationship suggests that a more fundamental relationship exists between battery aging and current magnitude.

7.3 Future Work

Future work may include studying rapid discharge of electrochemical cells at an elevated rate in order to get a more complete picture of how elevated discharge effects cells as compared to elevated charge. Other future work may include a post mortem examination to verify the concerns with lithium diffusion directly correlating to the magnitude of the current.

A large amount of future work could go towards optimizing the charge profile. In this work, the charge profile was selected because the elevated charge procedure generally stayed below 4.3 Volts and charged the cell in approximately five minutes. It would be worthwhile to investigate if a different current profile could charge the battery more fully, faster, or both. It might be possible to reduce the time to charge the cell, especially if a higher magnitude current is used during the 1^{st} stage, though concerns about lithium diffusion remain. Other parameters that could be optimized include having a more than two stages to the charge or simply changing the duty cycle or period of the waveform. In addition to the cycle profile, temperature modifications could be made as well. The tests in this thesis were done at approximately 298 Kelvin. Determining if batteries age in a similar manner at 318 Kelvin or 273 Kelvin may provide some further insights into how lithium-ion cells age.

One final area where future work could go is to make a more general model of lithium cells. The work described herein is for a particular model and brand of battery.

Expanding it into either a general model for an NCA battery or a general lithium-ion battery could generate a large amount of interest.

Appendix A

Bode EIS Values

These graphs are used to define the coefficients in Equation 8 and Equation 9 as a function of cycle number. The points on the graph represent the ideal expansion taken from Equation 7 and Equation 8, without regard for the prior tests. The smoothed line is the Fourier fit/interpolation of all the points. Run 40 was excluded because it was an outlier.

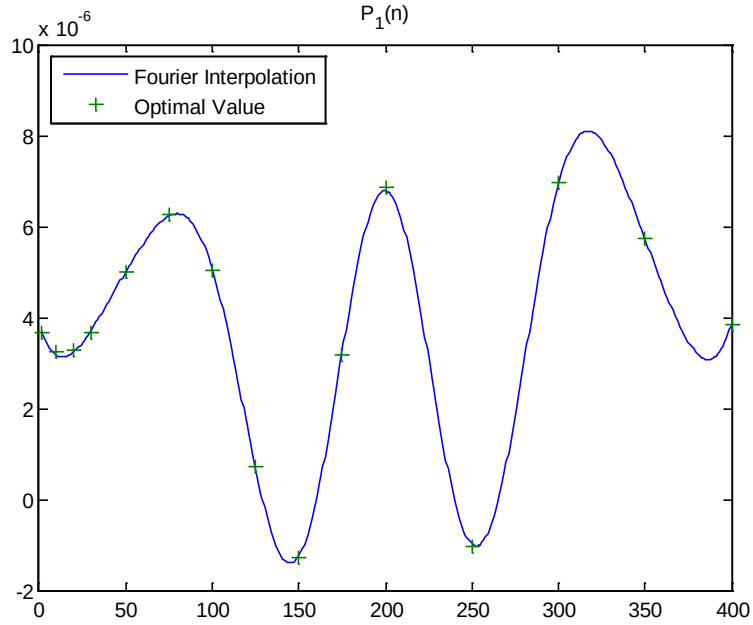

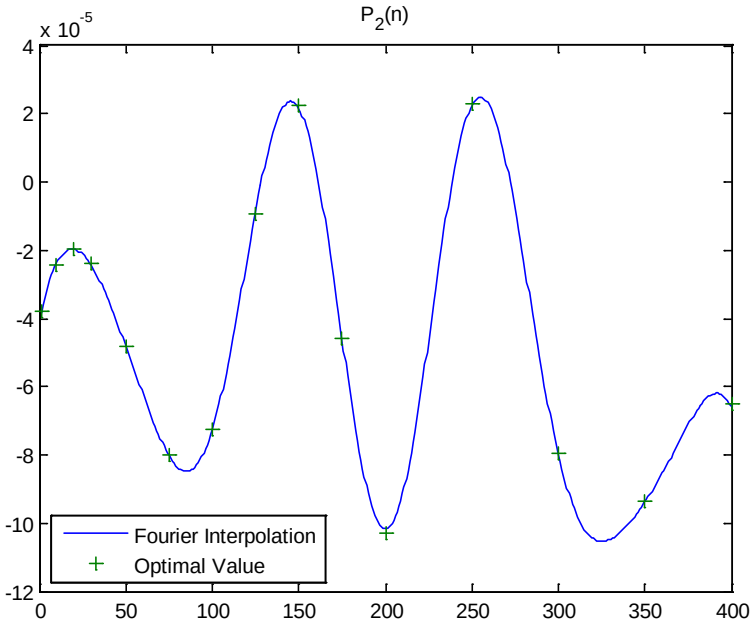

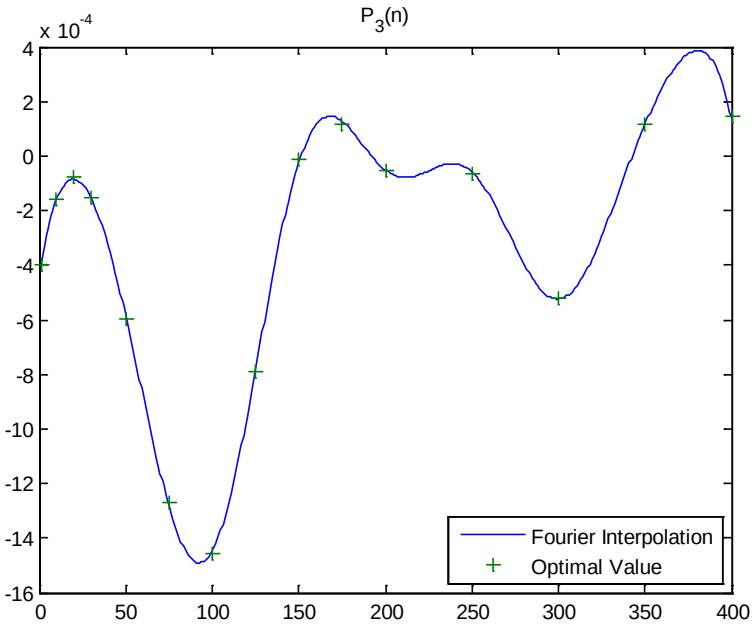
P3(n)
x 10-4
4
2
0
-2
-4
-6
-8
-10
-12
-14
-16
0
50
100
150
200
250
300
350
400
Fourier Interpolation
Optimal Value

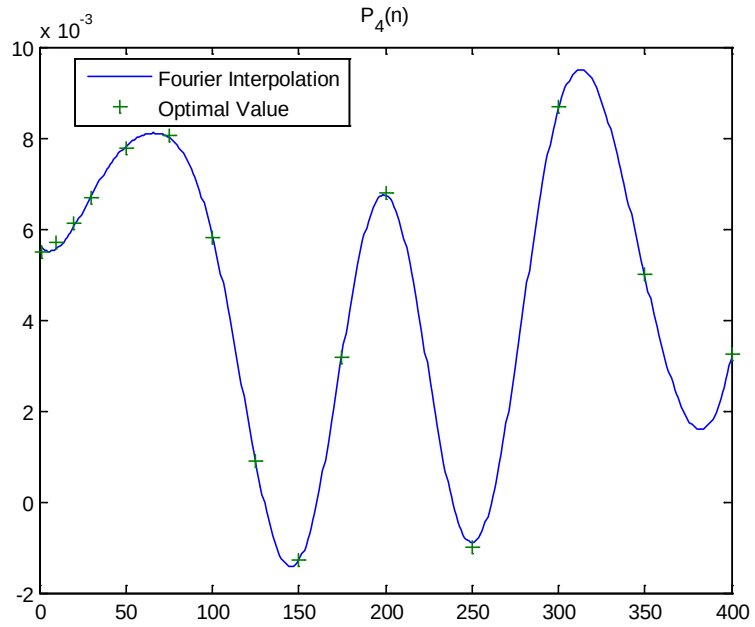
P4(n)
x 10-3
10
8
6
4
2
0
-2
0
50
100
150
200
250
300
350
400
Fourier Interpolation
Optimal Value

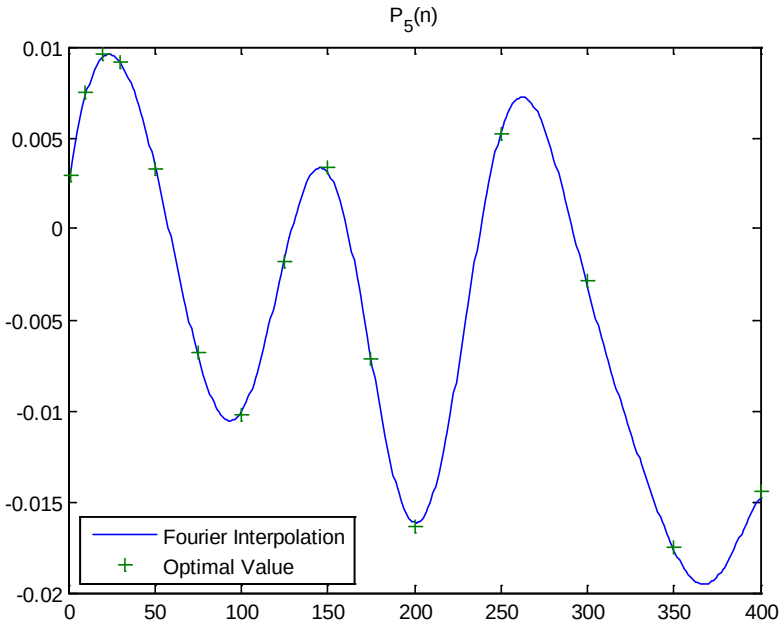
P5(n)
0.01
0.005
0
-0.005
-0.01
-0.015
-0.02
0
50
100
150
200
250
300
350
400
Fourier Interpolation
Optimal Value

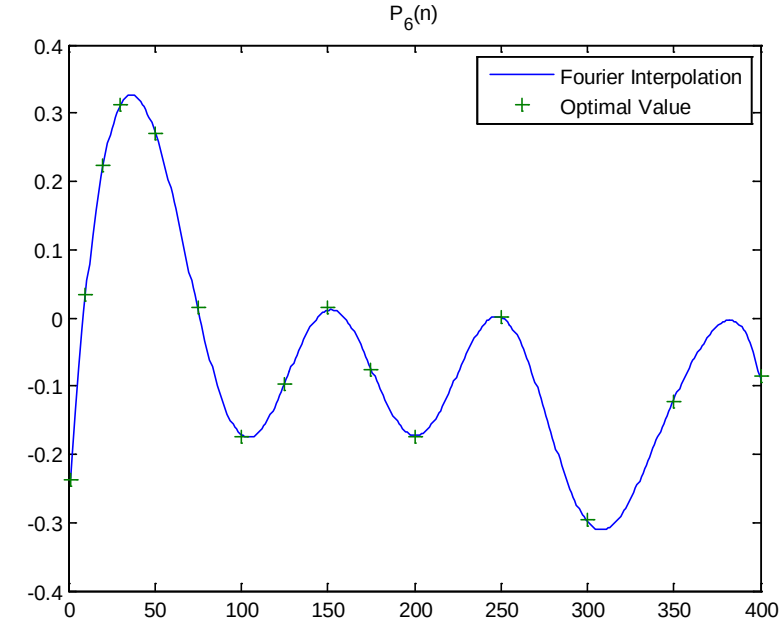
P6(n)
0.4
0.3
0.2
0.1
0
-0.1
-0.2
-0.3
-0.4
0
50
100
150
200
250
300
350
400
Fourier Interpolation
Optimal Value

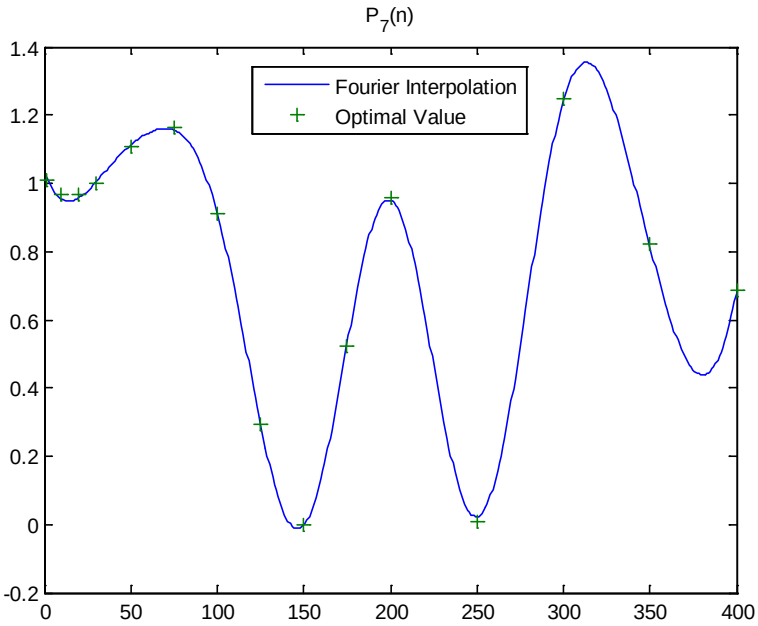
P7(n)
Fourier Interpolation
Optimal Value
1.4
1.2
1
0.8
0.6
0.4
0.2
0
-0.2
0
50
100
150
200
250
300
350
400

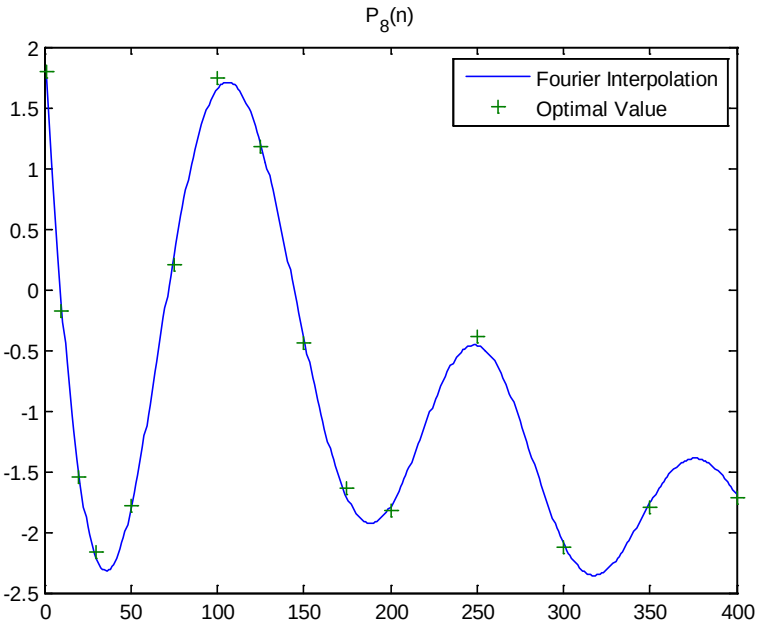
P8(n)
Fourier Interpolation
Optimal Value
2
1.5
1
0.5
0
-0.5
-1
-1.5
-2
-2.5
0
50
100
150
200
250
300
350
400

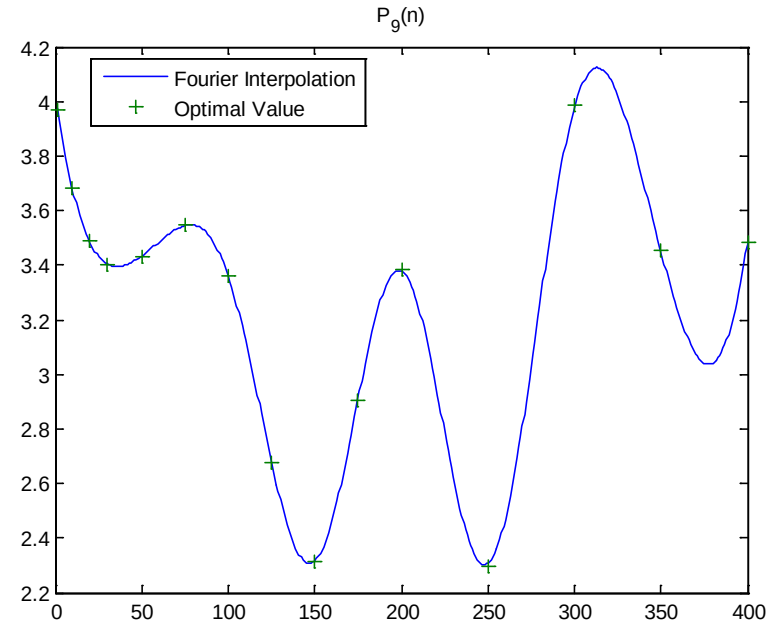
$P_9(n)$
Fourier Interpolation
Optimal Value
4.2
4
3.8
3.6
3.4
3.2
3
2.8
2.6
2.4
2.2
0
50
100
150
200
250
300
350
400

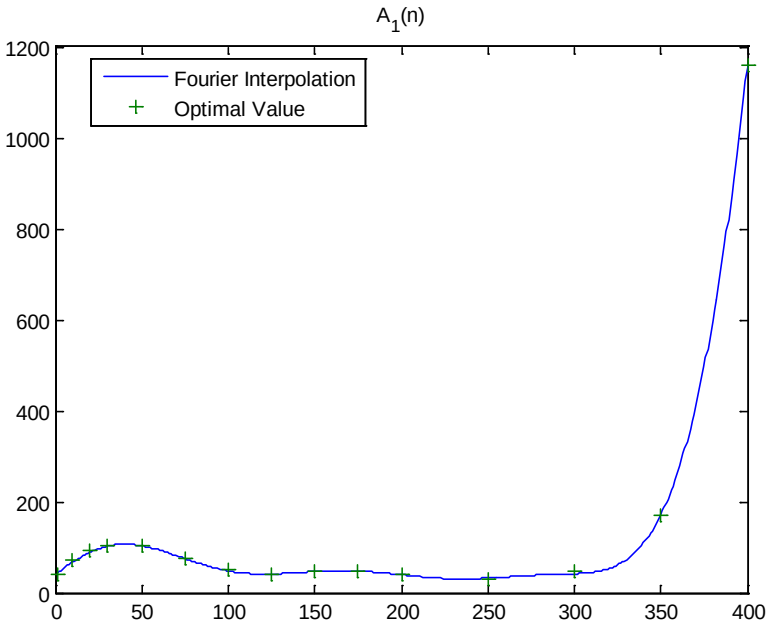
$A_1(n)$
Fourier Interpolation
Optimal Value
1200
1000
800
600
400
200
0
0
50
100
150
200
250
300
350
400

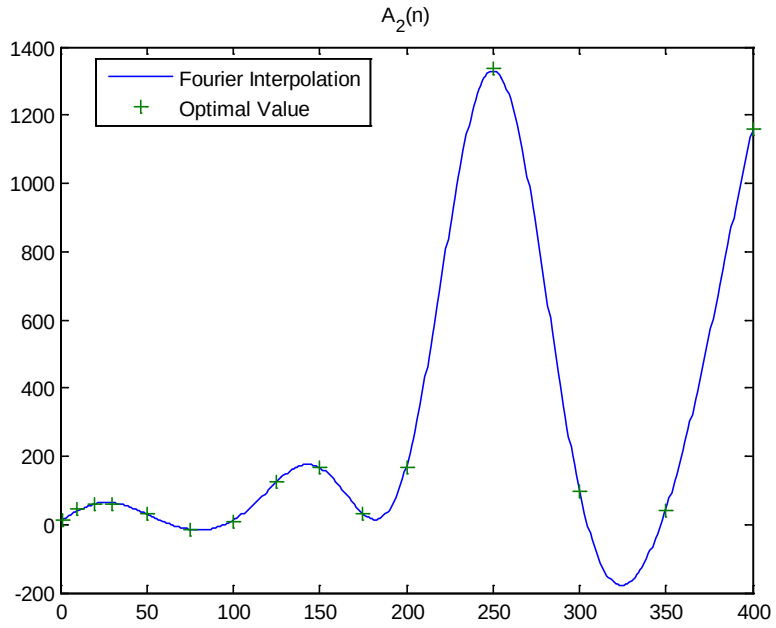
A2(n)
Fourier Interpolation
Optimal Value
1400
1200
1000
800
600
400
200
0
-200
0
50
100
150
200
250
300
350
400

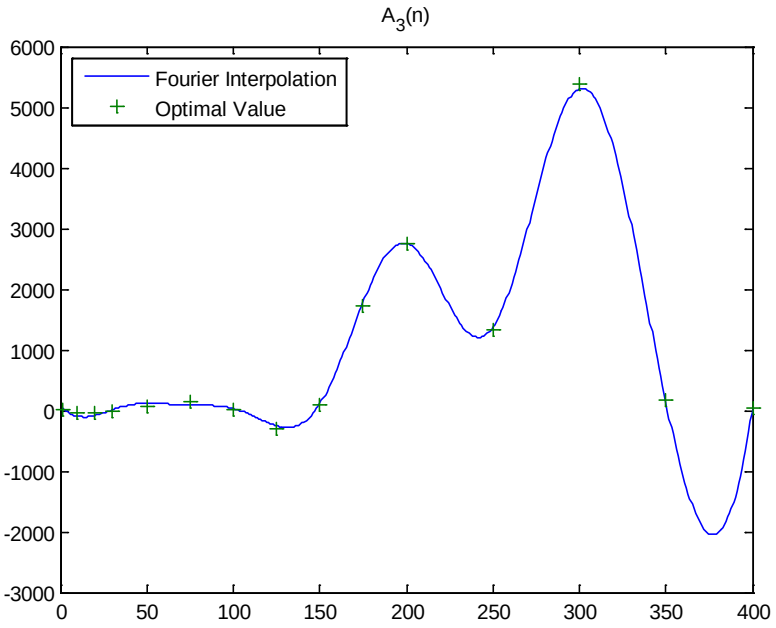
A3(n)
Fourier Interpolation
Optimal Value
6000
5000
4000
3000
2000
1000
0
-1000
-2000
-3000
0
50
100
150
200
250
300
350
400

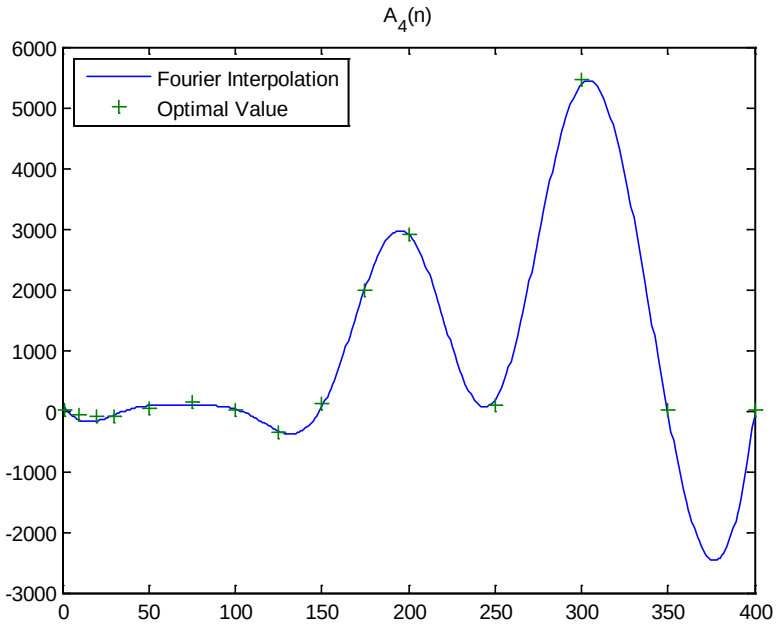
$A_4(n)$
Fourier Interpolation
Optimal Value
6000
5000
4000
3000
2000
1000
0
-1000
-2000
-3000
0
50
100
150
200
250
300
350
400

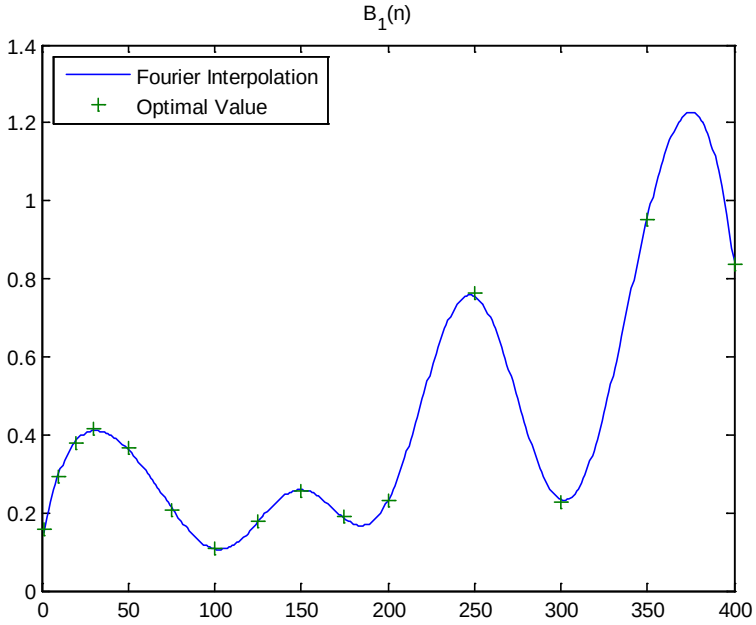
$B_1(n)$
Fourier Interpolation
Optimal Value
1.4
1.2
1
0.8
0.6
0.4
0.2
0
0
50
100
150
200
250
300
350
400

.

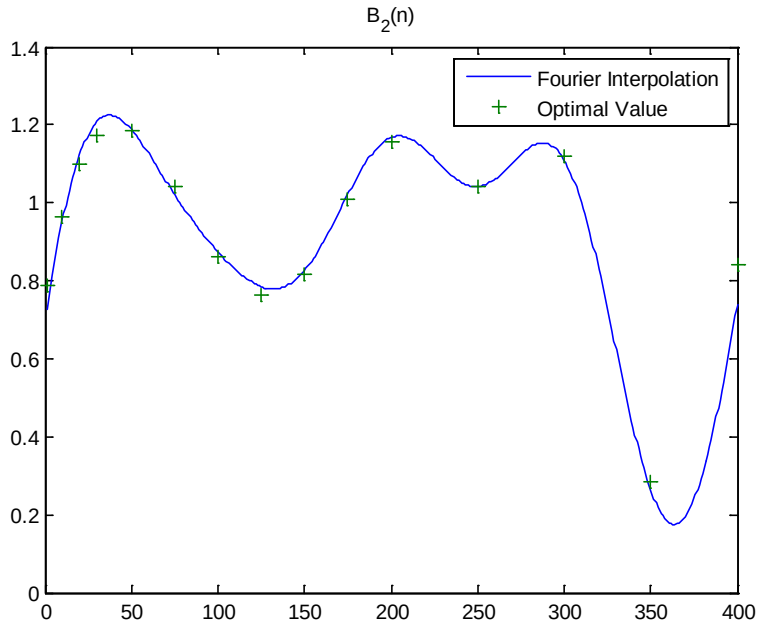
B2(n)
Fourier Interpolation
Optimal Value
1.4
1.2
1
0.8
0.6
0.4
0.2
0
0
50
100
150
200
250
300
350
400

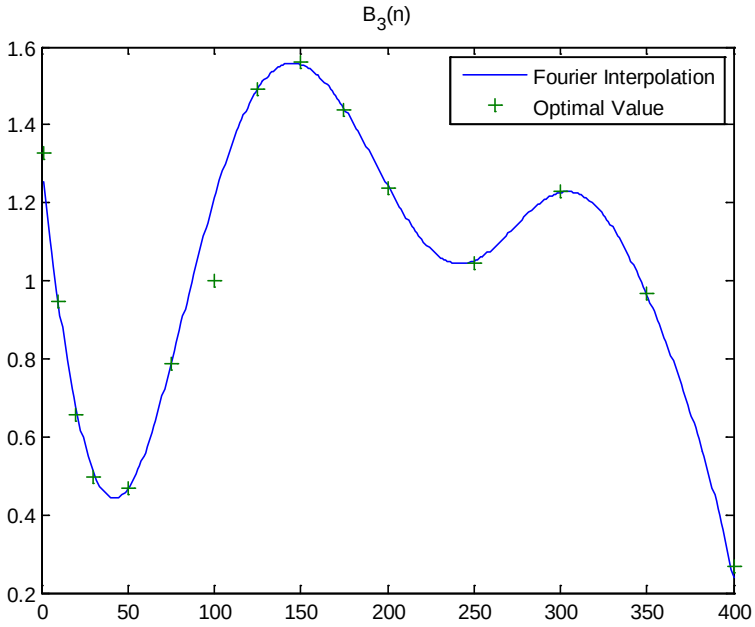
B3(n)
Fourier Interpolation
Optimal Value
1.6
1.4
1.2
1
0.8
0.6
0.4
0.2
0
50
100
150
200
250
300
350
400

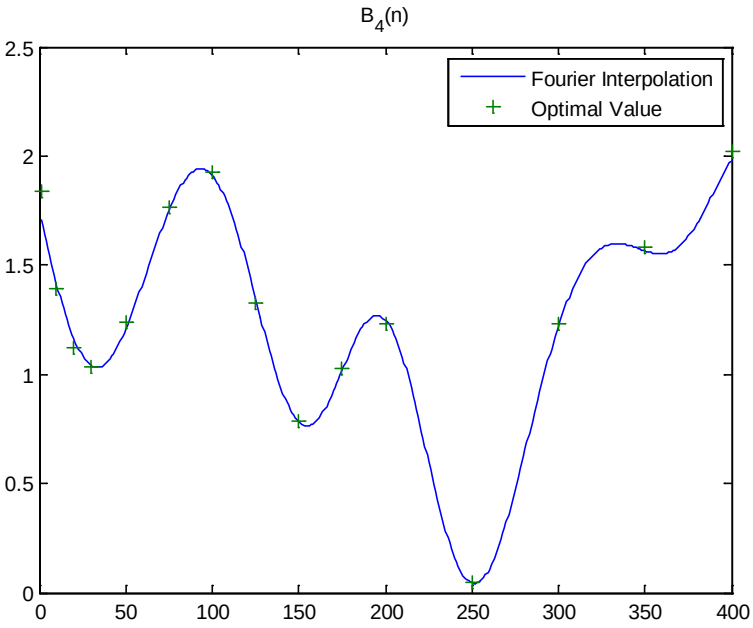
$B_4(n)$
Fourier Interpolation
Optimal Value
2.5
2
1.5
1
0.5
0
0
50
100
150
200
250
300
350
400

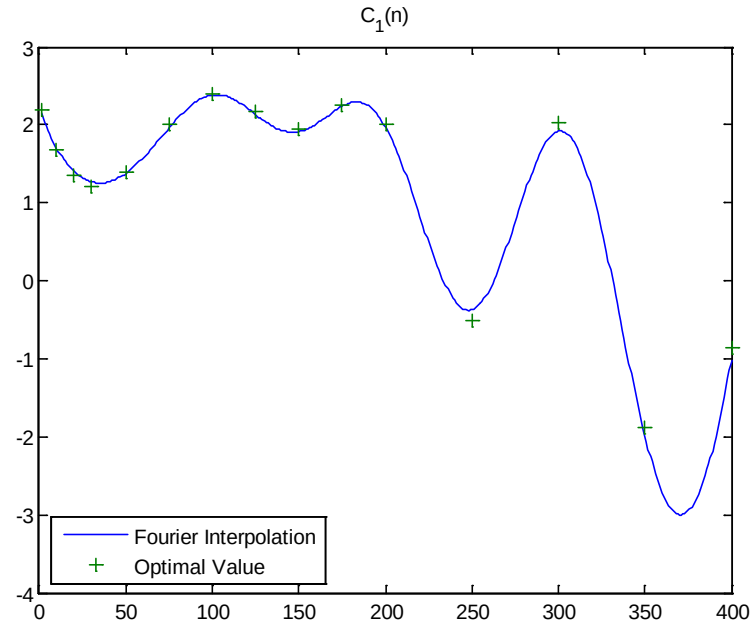
$C_1(n)$
Fourier Interpolation
Optimal Value
3
2
1
0
-1
-2
-3
-4
0
50
100
150
200
250
300
350
400

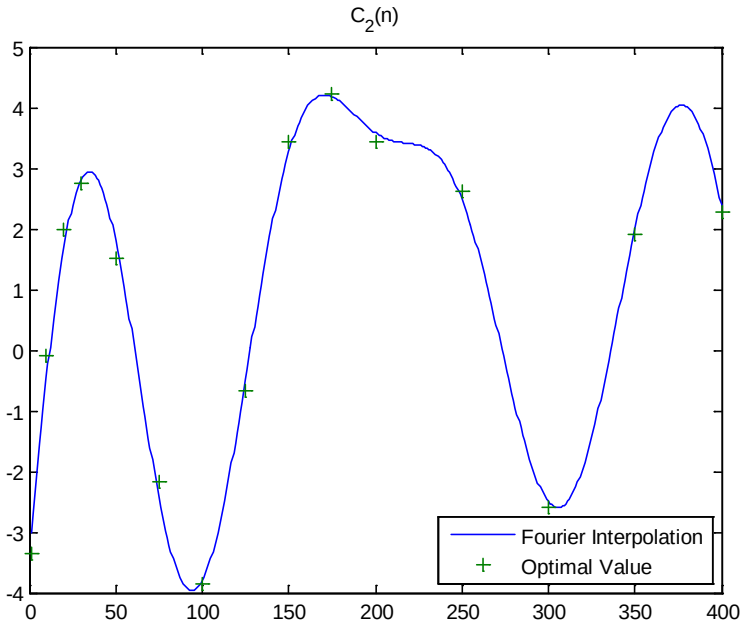
C2(n)
5
4
3
2
1
0
-1
-2
-3
-4
0
50
100
150
200
250
300
350
400
Fourier Interpolation
Optimal Value

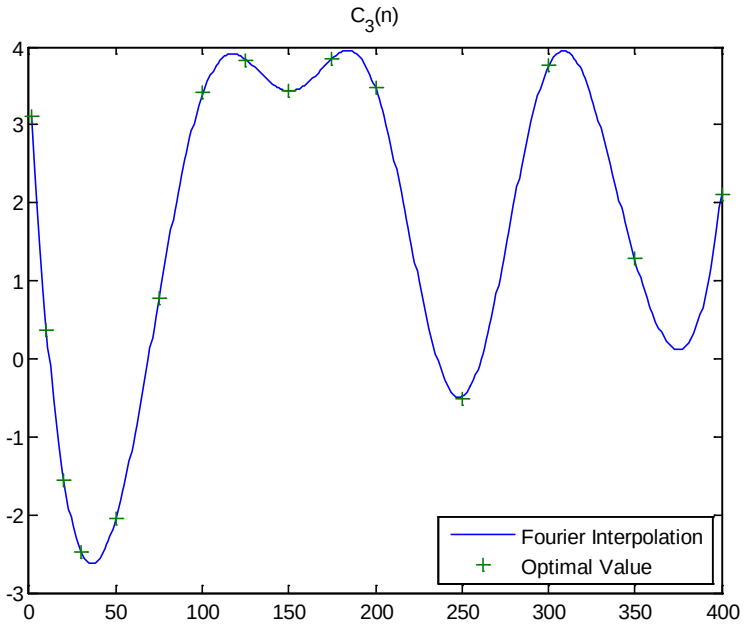
C3(n)
4
3
2
1
0
-1
-2
-3
0
50
100
150
200
250
300
350
400
Fourier Interpolation
Optimal Value

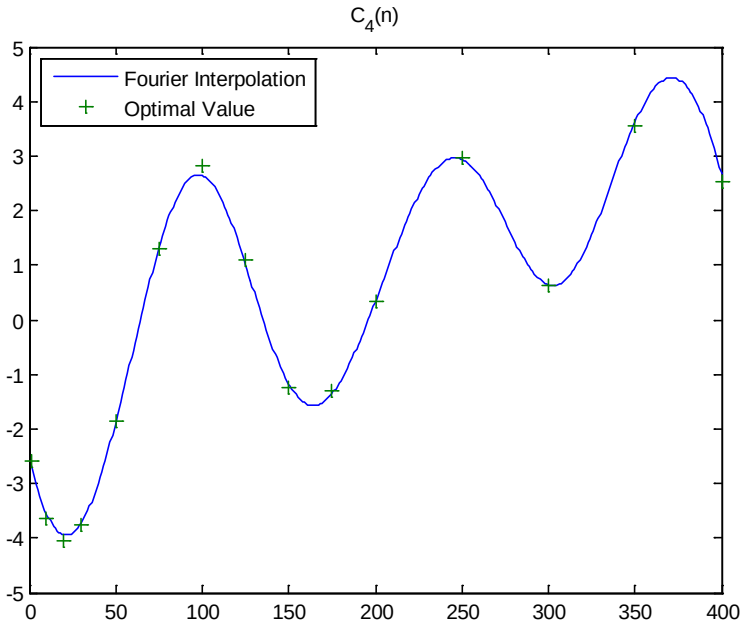
C4(n)
Fourier Interpolation
Optimal Value
5
4
3
2
1
0
-1
-2
-3
-4
-5
0
50
100
150
200
250
300
350
400

References

1. Dr. Schaefer, Laura. University of Pittsburgh. Couse Notes ME 1065:. *Thermal Analysis and Design.* Online. Accessed 9/26/2013. http://me1065.wikidot.com/chevrolet-volt
2. Saft America, Inc., Space & Defense Division. “Data sheet for the Saft VL 5U - Ultra high power cell,” *Saft, Doc N° 54073-2-1009*, Edition: October 2009, www.saftbatteries.com.
3. JM Energy. “ Lithium Ion Capacitor Presentation, ULTIMO,” http://www.jmenergy.co.jp/en/product.html, JM Energy Corporation, Copyright(C), July 2010.
4. J Crook. “Exclusive: IEEE Forms Power Matters Alliance to Determine Wireless Power Standards”. *Tech Crunch*. 9 January 2012. Online. Accessed 10/2/2013. http://techcrunch.com/2012/01/09/exclusive-ieee-forms-power-matters-alliance-to-determine-wireless-power-standards/
5. Schamiloglu, E.; Schoenbach, K.H.; Vidmar, R.J., ‘On the Road to Compact Pulsed Power: Adventures in Materials, Electromagnetic Modeling, and Thermal Management,’ *14th International IEEE Pulsed Power Conference*, Vol. 1, 2003, pp. 3 – 8.
6. C. Brissot, M. Rosso, J.-N. Chazalviel, S. Lascaud, “Dendritic growth mechanisms in lithium/polymer cells,” *Journal of Power Sources*, Volumes 81–82, September 1999, Pages 925-929
7. John B. Goodenough and Youngsik Kim. “Challenges for Rechargeable Li Batteries” *Chemistry of Materials* 2010 22 (3), 587-603
8. J Dumas. “ERCOT Market Nodal Market”. Presentation given May 1st, 2013. UT Arlington, Part of lecture notes on Power System Dispatch by Dr. Shoultz.

9. Dr. Lee, Wei-Jen. University of Texas at Arlington. Fall 2011. Course Notes EE 5309. *Renewable Energy*..
10. Lampton, C. “How Regenerative Breaking Works”. www.howstuffworks.com. Online. Accessed 10/2/2013.
11. Asimakopoulos, P.; Boumis, B.T.; Patsias, C.E.; Safacas, A.; Mitronikas, E., "Experience derived from the conversion of a conventional car to a hybrid electric vehicle -analysis of the powertrain," *Power Electronics Electrical Drives Automation and Motion (SPEEDAM), 2010 International Symposium on* , vol., no., pp.1040,1045, 14-16 June 2010
12. Shuhei Miura, Hideo Honma, “Advanced copper electroplating for application of electronics,” *Surface and Coatings Technology*, Volumes 169–170, 2 June 2003, Pages 91-95, ISSN 0257-8972,
13. Wei-Ping Dow, Ming-Yao Yen, Sian-Zong Liao, Yong-Da Chiu, Hsiao-Chun Huang, “Filling mechanism in microvia metallization by copper electroplating” *Electrochimica Acta*, Volume 53, Issue 28, 30 November 2008, Pages 8228-8237
14. Ki Baek Song; Kew Yong Sung; Wook Jeon; Yoon Jung; Mung Chul Choi; Eun-Ha Choi, "The diagnostics of high-power microwave from virtual cathode oscillator with the coupled line band pass filter," *Vacuum Electronics, 2003 4th IEEE International Conference on* , vol., no., pp.186,, 28-30 May 2003
15. Engel, T.G.; Neri, J.M.; Nunnally, W.C., "Efficiency and Scaling of Constant Inductance Gradient DC Electromagnetic Launchers," *Magnetics, IEEE Transactions on* , vol.42, no.8, pp.2043,2051, Aug. 2006.
16. Wells, B.T.; Stevenson, R.C.; McElroy, J.; Noh, J.; Ramadoss, S.; Gunow, G.A.; Hammig, M.D., "Defeating IEDs, SNM and contraband secreting via long range gamma-ray imaging of neutron interrogated materials," *Nuclear Science*

Symposium Conference Record (NSS/MIC), 2009 IEEE , vol., no., pp.668,675, Oct. 24 2009-Nov. 1 2009

17. Jang, S.R.; Ryoo, H.J.; Jin, Y.-S.; Ahn, S.H.; Rim, G.-H., "Application of pulsed power system for water treatment of the leachate," *Pulsed Power Conference, 2009. PPC '09. IEEE* , vol., no., pp.980,983, June 28 2009-July 2 2009
18. Schamiloglu, E.; Schoenbach, K.H.; Vidmar, R.J., 'On the Road to Compact Pulsed Power: Adventures in Materials, Electromagnetic Modeling, and Thermal Management,' 14th International IEEE Pulsed Power Conference, Vol. 1, 2003, pp. 3 – 8
19. Mankowski, J., Kristiansen, M. "A Review of Short Pulse Generator Technology," *IEEE Transactions on Plasma Science*, vol.28, no.1, pp.102-108 (2000).
20. Domonkos, M.T.; O'Loughlin, J.P.; Tran, T.; Turchi, P.; Brown, D.; Gregg, C.W.; Parker, J.; Montoya, T.; Slenes, K., "Stacked, Parallel-Plate Solid-Dielectric Blumlein Lines for Compact Pulsed Power," *Plasma Science, 2007. ICOPS 2007. IEEE 34th International Conference on* , vol., no., pp.368,368, 17-22 June 2007
21. Domonkos, M.T.; Heidger, S.; Brown, D.; Parker, J.V.; Gregg, C.W.; Slenes, K.; Hackenberger, Wes; Seongtae Kwon; Loree, E.; Tran, T., "Submicrosecond Pulsed Power Capacitors Based on Novel Ceramic Technologies," *Plasma Science, IEEE Transactions on* , vol.38, no.10, pp.2686,2693, Oct. 2010
22. Mangalvedekar, H. A.; Paithankar, A. S.; Chakravarthy, D. P.; Dixit, K.P.; Barve, D. N., "Ferrite core based pulse power modulator," *Dielectrics and Electrical Insulation, IEEE Transactions on* , vol.18, no.4, pp.1158,1162, August 2011
23. Birtwhistle, D.; Stokes, A.D., "Dielectric recovery of short gaps following current interruption: with particular application in sulphur hexaflouride," *Properties and*

Applications of Dielectric Materials, 1994., Proceedings of the 4th International Conference on , vol.1, no., pp.143,146 vol.1, 3-8 Jul 1994

24. Zorngiebel, V.; Spahn, E.; Buderer, G.; Welleman, A.; Fleischmann, W., "Compact High Voltage IGBT Switch for Pulsed Power Applications," *Electromagnetic Launch Technology, 2008 14th Symposium on* , vol., no., pp.1,5, 10-13 June 2008
25. Welleman, A.; Leutwyler, R., "Solutions with Solid State Switches for Pulse Modulators," *IEEE International Power Modulators and High Voltage Conference, Proceedings of the 2008* , vol., no., pp.29,32, 27-31 May 2008
26. A. Väyrynen, J. Salminen, “Modular li-ion battery systems for electric and hybrid powertrains” in: *ICPC 2011, 6th AVL International Commercial Powertrain Conference*, Graz, Austria, 25–26 May 2011.
27. Arndt, M. “Building a better battery” *Businessweek*, (4044), 71 . 2007.
28. Fassin, D., & Naudé, A. (2004). “Plumbism reinvented: childhood lead poisoning in France” 1985-1990. *American Journal Of Public Health*, 94(11), 1854-1863.
29. International Battery Council. “Battery Recylcing”. Online. Accessed 8/1/2013. http://batterycouncil.org/?page=Battery_Recycling
30. James, J. E.; Aidman, G.; Aidman, E. I.; Orsino, J. A., "Bifunctional aircraft lead-acid battery," *Battery Conference on Applications and Advances, 1991. Proceedings of the Sixth Annual* , vol., no., pp.95,95, 1991
31. Allen, Raymond; Neri, Jesse, "A Battery Powered, 200-KW Rapid Capacitor Charger for a Portable Railgun in Burst Mode Operation at 3 RPS," *Plasma Science, 2007. ICOPS 2007. IEEE 34th International Conference on* , vol., no., pp.867,867, 17-22 June 2007

32. J. Cherng, P. Rao. “Bipolar Lead Acid Battery”. US Patent # 5348817A. Sept. 20, 1994.
33. G.K. Bowen, W.C. Delaney, M.D. Eskra. “Lead acid bipolar battery plate and method of making the same US Patent # 4900643. Apr 8, 1988
34. LaFollette, R.M., "Design and performance of high specific power, pulsed discharge, bipolar lead acid batteries," *Battery Conference on Applications and Advances, 1995., Proceedings of the Tenth Annua*l , vol., no., pp.43,47, 10-13 Jan 1995
35. M. Saakes, R. Woortmeijer, D. Schmal, “Bipolar lead–acid battery for hybrid vehicles” *Journal of Power Sources*, Volume 144, Issue 2, 15 June 2005, Pages 536-545
36. M. Coux, X. Muneret, P. Lenain, J.L. Wojkiewicz, J. Renard, “Bipolar Lead/Acid Batteries: Effect of Membrane Conductivity on Performance” *Journal of Power Sources*, Volume 78, Issues 1–2, March 1999, Pages 115-122
37. The Advanced Lead Acid Consortium. “The Advanced Lead-Acid Battery Bipolar Designs – A Commercial Reality”. Online. Accessed 8/21/2013. http://www.alabc.org/publications/bipolar-designs
38. Vidas, R.A.; Miles, R.C.; Korinek, P.D., "The bipolar lead acid battery at Johnson Controls Inc," *Power Sources Symposium, 1990., Proceedings of the 34th International* , vol., no., pp.351,354, 25-28 Jun 1990
39. M. Schriber. “Relativity Powers Your Car Battery”. *Physics Review Focus*, 27 (2). Jan. 14 2011.
40. Hariharan B, “Bipolar Lead Acid Batteries: Opportunities Amongst the Automotive Segment”. *Frost and Sullivan Market Insight*, April 2004. Online.

Acessed 8/12/2013. URL: http://www.frost.com/sublib/display-market-insight.do?id=17944096

41. Rodney M. LaFollette and Douglas N. Bennion “Design Fundamentals of High Power Density, Pulsed Discharge, Lead Acid Batteries” *Journal of the Electrochemical Society* 1990 137(12): 3693-3701
42. F.A Fleming, P Shumard, B Dickinson, “Rapid recharge capability of valve-regulated lead-acid batteries for electric vehicle and hybrid electric vehicle applications,” *Journal of Power Sources,* Volume 78, Issues 1–2, March 1999, Pages 237-243, ISSN 0378-7753,
43. P.T Moseley, “Research results from the Advanced Lead–Acid Battery Consortium point the way to longer life and higher specific energy for lead/acid electric-vehicle batteries,” *Journal of Power Sources*, Volume 73, Issue 1, 18 May 1998, Pages 122-12
44. P.T Moseley, A Cooper, “Progress towards an advanced lead–acid battery for use in electric vehicles,” *Journal of Power Sources,* Volume 78, Issues 1–2, March 1999, Pages 244-250, ISSN 0378-7753,
45. A. Kirchev, M. Perrin, E. Lemaire, F. Karoui, F. Mattera,” Studies of the pulse charge of lead-acid batteries for PV applications: Part I. Factors influencing the mechanism of the pulse charge of the positive plate,” *Journal of Power Sources*, Volume 177, Issue 1, 15 February 2008, Pages 217-225, ISSN 0378-7753,
46. A. Kirchev, A. Delaille, M. Perrin, E. Lemaire, F. Mattera, “Studies of the pulse charge of lead-acid batteries for PV applications: Part II. Impedance of the positive plate revisited,” *Journal of Power Sources*, Volume 170, Issue 2, 10 July 2007, Pages 495-512,

47. Angel Kirchev, Florence Mattera, Elisabeth Lemaire, Kien Dong, “Studies of the pulse charge of lead-acid batteries for photovoltaic applications: Part IV. Pulse charge of the negative plate,” *Journal of Power Sources*, Volume 191, Issue 1, 1 June 2009, Pages 82-90
48. Ralph M. Sullivan, Christopher G. Hoffman, Gopalakrishna M. Rao, “Orbital performance of AMPTE/CCE nickel-cadmium batteries with a large number of charger-induced, very small, charge/discharge cycles,” *Journal of Power Sources*, Volume 69, Issues 1–2, November–December 1997, Pages 27-36.
49. Akihiro Taniguchi, Noriyuki Fujioka, Munehisa Ikoma, Akira Ohta, “Development of nickel/metal-hydride batteries for EVs and HEVs” *Journal of Power Sources*, Volume 100, Issues 1–2, 30 November 2001, Pages 117-124, ISSN 0378-7753,
50. Cole, J.H.; Eskra, M.; Klein, M., "Bipolar nickel-metal hydride batteries for aerospace applications," *Aerospace and Electronic Systems Magazine, IEEE* , vol.15, no.1, pp.39,45, Jan 2000
51. Eskra, M.; Ralston, P.; Klein, M.; Johnson, W.; Erbacher, J.; Newman, B., "Nickel-metal hydride replacement for VRLA and vented nickel-cadmium aircraft batteries," *Applications and Advances, 2001. The Sixteenth Annual Battery Conference on , vol., no.,* pp.11,15,2001
52. N. Vassal, E. Salmon, and J.-F. Fauvarque “Nickel/Metal Hydride Secondary Batteries Using an Alkaline Solid Polymer Electrolyte” *Journal of the Electrochemical Society* 1999 146(1): 20-26
53. Cole, J.H.; Eskra, M.; Klein, M., "Bipolar nickel-metal hydride batteries for aerospace applications," *Aerospace and Electronic Systems Magazine, IEEE* , vol.15, no.1, pp.39,45, Jan 2000

54. Eskra, M.; Ralston, P.; Klein, M.; Johnson, W.; Erbacher, J.; Newman, B., "Nickel-metal hydride replacement for VRLA and vented nickel-cadmium aircraft batteries," *Applications and Advances, 2001. The Sixteenth Annual Battery Conference on , vol., no.,* pp.11,15,2001
55. Viera, J. C.; Gonzalez, M.; Anton, J.C.; Campo, J.C.; Ferrero, F. J.; Valledor, M., "NiMH vs NiCd Batteries under High Charging Rates," *Telecommunications Energy Conference, 2006*. INTELEC '06. 28th Annual International , vol., no., pp.1,6, 10-14 Sept. 2006
56. Zinder, David A., "Fast Charging Systems for NiCd Batteries," *Industry and General Applications, IEEE Transactions on* , vol.IGA-4, no.5, pp.555,560, Sept. 1968
57. Philips Semiconductor Ltd, “NiMH and NiCd battery management,” *Microprocessors and Microsystems*, Volume 19, Issue 3, 1995, Pages 165-174.
58. Gonzalez, M.; Perez, M.A.; Diaz, J.; Ferrero, F. J., "Ni-Cd and Ni-MH battery optimized fast-charge method for portable telecommunication applications," *Telecommunications Energy Conference,, 18th International* , vol., no., pp.522,529, 6-10 Oct 1996
59. S.R. Sivakkumar, A.G. Pandolfo, “Evaluation of lithium-ion capacitors assembled with pre-lithiated graphite anode and activated carbon cathode” *Electrochimica Acta*, Volume 65, 30 March 2012, Pages 280-287, ISSN 0013-4686,
60. Glenn G. Amatucci, Fadwa Badway, Aurelien Du Pasquier, and Tao Zheng “An Asymmetric Hybrid Nonaqueous Energy Storage Cell” *Journal of the Electrochemical Society* 2001 148(8): A930-A939; doi:10.1149/1.1383553
61. A Rand, David "A journey on the electrochemical road to sustainability". *Journal of Solid State Electrochemistry*, Vol 15, No 7-8, pp 1579-1622. July, 2011.

62. V. Aravindan*a, N. Shubhab, W. Chui Linga and S. Madhavi. " Constructing high energy density non-aqueous Li-ion capacitors using monoclinic TiO2-B nanorods as insertion host" *Journal of Material. Chemistry A*, 2013, 1, 6145-6151.
63. Hongtao Liu, Ping He, Zhiying Li, Yang Liu, Jinghong Li," A novel nickel-based mixed rare-earth oxide/activated carbon supercapacitor using room temperature ionic liquid electrolyte" *Electrochimica Acta*, Volume 51, Issue 10, 1 February 2006, Pages 1925-1931, ISSN 0013-4686.
64. Saft Industrial Group. "Saft Nickel Capacitor". Document No. 21870-2-0313. March 2013 Edition.
65. Kold Ban International. "KA Power 12 Volt Specifications.". Online. Acessed 9/4/2013. http://www.koldban.com/Kapower_Specifications_s/29.htm
66. Kold Ban International. "KA Power White Paper". Online. Accessed 8.20/2013. http://www.koldban.com/Kapower_White_Paper_s/30.htm
67. R.D. Rauh, S.B. Brummer, "The effect of "additives on lithium cycling in propylene carbonate," *Electrochimica Acta*, Volume 22, Issue 1, January 1977, Pages 75-83, ISSN 0013-4686,10.1016/0013-4686(77)85057-3.
68. Free Press Distribution Service. "Breaking world record on a charger by using lithium-ion battery". May, 2011. Online. Acessed 10/1/2013. URL: http://www.prlog.org/11488430-breaking-world-record-on-charger-by-using-lithium-ion-battery.html
69. J.-M. Tarascon& M. Armand, "Issues and challenges facing rechargeable lithium batteries" *Nature*. Vol. 414, pp 359-367. November 2001
70. Liu, Dr. Fuqiang. University of Texas at Arlington. Spring 2013. Course Notes MSE 5390. *Materials for Energy*.

71. Uday Kasavajjula, Chunsheng Wang, A. John Appleby, “Nano- and bulk-silicon-based insertion anodes for lithium-ion secondary cells”. *Journal of Power Sources*, Volume 163, Issue 2, 1 January 2007, Pages 1003-1039, ISSN 0378-7753, 10.1016/j.jpowsour.2006.09.084.
72. Gold Peak Industries. [handbook] (November 2003) (PDF). “Lithium Ion technical handbook”. Online. Accessed 2/14/2013. http://www.gpbatteries.com/html/pdf/Li-ion_handbook.pdf
73. Higgins, Tim. Bloomberg. Oct 2012. ‘GM Lithium Battery Explosion Sparks Fire at Company Lab’
74. Deborah J. Hankinson, Jan Almlöf, “Cluster models for lithium intercalated graphite: electronic structures and energetics” *Journal of Molecular Structure: THEOCHEM*, Volume 388, 11 December 1996, Pages 245-256, ISSN 0166-1280, 10.1016/S0166-1280(96)80038-8.
75. Nippon Graphite Industries, Ltd. “About Graphite”. Online. Acessed 10/1/2013. URL: http://www.n-kokuen.com/e/whatis/
76. Yu-Sheng Lin, Jenq-Gong Duh, “Facile synthesis of mesoporous lithium titanate spheres for high rate lithium-ion batteries” *Journal of Power Sources*, Volume 196, Issue 24, 15 December 2011, Pages 10698-10703, ISSN 0378-7753, 10.1016/j.jpowsour.2011.09.007.
77. Toshiba Corporation. “SCIB 20 Amp Hour cell”. Datasheet. Online. Retreived 2/5/2013. http://www.toshiba.com/ind/data/tag_files/SCiB_Brochure_5383.pdf
78. B.A. Boukamp, G.C. Lesh, R.A. Huggins”All-solid lithium electrodes with mixed-conductor matrix”. *Journal of the Electrochemical Society*, 128 (4) (1981), p. 725

79. Yu-Sheng Lin, Jenq-Gong Duh, Deng-Tswen Shieh, Mo-Hua Yang, Effect of pH value on electrochemical property of tin compounds loaded graphite anodes for Li-ion battery applications, *Journal of Alloys and Compounds*, Volume 490, Issues 1–2, 4 February 2010, Pages 393-398, ISSN 0925-8388, 10.1016/j.jallcom.2009.10.016.

80. Y.Y. Tang, X.H. Xia, Y.X. Yu, S.J. Shi, J. Chen, Y.Q. Zhang, J.P. Tu, "Cobalt nanomountain array supported silicon film anode for high-performance lithium ion batteries" *Electrochimica Acta*, Volume 88, 15 January 2013, Pages 664-670, ISSN 0013-4686, 10.1016/j.electacta.2012.10.119.

81. B. Fuchsbichler, C. Stangl, H. Kren, F. Uhlig, S. Koller, "High capacity graphite–silicon composite anode material for lithium-ion batteries" *Journal of Power Sources*, Volume 196, Issue 5, 1 March 2011, Pages 2889-2892, ISSN 0378-7753, 10.1016/j.jpowsour.2010.10.081.

82. Sigma-Aaldrich. 'Material Safety Data Sheet Lithium Hexaflourophosphate'. Published 11/05/2012. Online. Accessed 4/18/2013. http://www.sigmaaldrich.com/catalog/product/aldrich/201146?lang=en&region=US

83. ESTREM, Chemicals Inc. 'Material Safety Data Sheet Lithium Hexaflouroarsenate'. Published 8/15/2011. Online. Accessed 4/18/2013. http://www.strem.com/catalog/msds/03-1250

84. Science Lab.com. 'Material Safety Data Sheet Lithium Percholorate anhydrous'. Published 6/09/2012. Online. Accessed 4/18/2013. http://www.sciencelab.com/msds.php?msdsId=9924516

85. Acros Organics N.V. ‘Material Safety Data Sheet Ethylene Carbonate, 99+%’. Published 11/20/2008. Online. Accessed 4/18/2013. Achttps://fscimage.fishersci.com/msds/09022.htm
86. Liu, Z.; Fu, W.; Payzant, E. A.; Yu, X.; Wu, Z.; Dudney, N. J.;Kiggans, J.; Hong, K.; Rondinone, A. J.; Liang, C. “Anomalous High Ionic Conductivity of Nanoporousβ-Li3PSL”. *Journal of the American Chemical Society*. 2013,135, 975–978.
87. Anantha Iyenger Gopalan, Padmanabhan Santhosh, Kalayil Manian Manesh, Jin Hee Nho, Sang Ho Kim, Chul-Gyun Hwang, Kwang-Pill Lee, “Development of electrospun PVdF–PAN membrane-based polymer electrolytes for lithium batteries” *Journal of Membrane Science*, Volume 325, Issue 2, 1 December 2008, Pages 683-690, ISSN 0376-7388, 10.1016/j.memsci.2008.08.047.
88. Andreas Hofmann, Michael Schulz, Thomas Hanemann, “Gel electrolytes based on ionic liquids for advanced lithium polymer batteries” *Electrochimica Acta*, Volume 89, 1 February 2013, Pages 823-831, ISSN 0013-4686, 10.1016/j.electacta.2012.10.144.
89. Takahito Itoh, Yukihiro Mitsuda, Takayuki Ebina, Takahiro Uno, Masataka Kubo, “Solid polymer electrolytes composed of polyanionic lithium salts and polyethers” *Journal of Power Sources*, Volume 189, Issue 1, 1 April 2009, Pages 531-535, ISSN 0378-7753, 10.1016/j.jpowsour.2008.10.113.
90. Mitsubishi Electric. ‘MITSUBISHI HVIGBT MODULES CM900HG-90H’. Datasheet. Published May 2009. Online. Acessed 4/18/2013.
91. H. Buqa, A. Würsig, J. Vetter, M.E. Spahr, F. Krumeich, P. Novák, “SEI film formation on highly crystalline graphitic materials in lithium-ion batteries” *Journal*

of Power Sources, Volume 153, Issue 2, 28 February 2006, Pages 385-390, ISSN 0378-7753, 10.1016/j.jpowsour.2005.05.036.

92. Anthony Barré, Benjamin Deguilhem, Sébastien Grolleau, Mathias Gérard, Frédéric Suard, Delphine Riu, “A review on lithium-ion battery ageing mechanisms and estimations for automotive applications,” *Journal of Power Sources*, Volume 241, 1 November 2013, Pages 680-689,
93. Celgard Corporation. “Products: Celgard® Lithium Battery Separators”. Online. Accessed 3/1/2013. http://www.celgard.com/Products.aspx
94. Bo Xu, Danna Qian, Ziying Wang, Ying Shirley Meng, “Recent progress in cathode materials research for advanced lithium ion batteries” *Materials Science and Engineering: R: Reports*, Volume 73, Issues 5–6, May–June 2012, Pages 51-65, ISSN 0927-796X, 10.1016/j.mser.2012.05.003.
95. Shao-Horn, Yang, Laurence Croguennec, Claude Delmas, E. Chris Nelson, and Michael A. O'Keefe. "Atomic resolution of lithium ions in LiCoO2." *Nature materials* 2, no. 7 (2003): 464-467.
96. Yoshiaki Nitta, Kazuhiro Okamura, Masatoshi Nagayama, Akira Ohta, “Lithium manganese oxides for rechargeable lithium batteries,” *Journal of Power Sources*, Volume 68, Issue 1, September 1997, Pages 166-172, ISSN 0378-7753, 10.1016/S0378-7753(96)02548-7.
97. Yoshinari Makimura, Tsutomu Ohzuku, “Lithium insertion material of LiNi1/2Mn1/2O2 for advanced lithium-ion batteries” *Journal of Power Sources*, Volumes 119–121, 1 June 2003, Pages 156-160, ISSN 0378-7753, 10.1016/S0378-7753(03)00170-8.

98. R.J. Brodd (ed.), Batteries for Sustainability: “Selected Entries from the Encyclopedia of Sustainability Science and Technology,” Springer Science and Business Media. New York 2013
99. Opel, Matthias. "Spintronic oxides grown by laser-MBE." *Journal of Physics D: Applied Physics* 45.3 (2011): 033001. http://iopscience.iop.org/0022-3727/45/3/033001
100. Ki-Soo Lee, Seung-Taek Myung, Hyun Joo Bang, Sukjin Chung, Yang-Kook Sun, “Co-precipitation synthesis of spherical Li1.05M0.05Mn1.9O4 (M = Ni, Mg, Al) spinel and its application for lithium secondary battery cathode” *Electrochimica Acta*, Volume 52, Issue 16, 30 April 2007, Pages 5201-5206, ISSN 0013-4686, 10.1016/j.electacta.2007.02.029.
101. Xifei Li, Youlong Xu, Chunlei Wang, “Suppression of Jahn–Teller distortion of spinel LiMn2O4 cathode” *Journal of Alloys and Compounds,* Volume 479, Issues 1–2, 24 June 2009, Pages 310-313, ISSN 0925-8388, 10.1016/j.jallcom.2008.12.081.
102. J. Molenda, D. Pałubiak, J. Marzec, “Transport and electrochemical properties of the LiyCrxMn2−xO4 (0<x<0.5) cathode material” *Journal of Power Sources*, Volume 144, Issue 1, 1 June 2005, Pages 176-182, ISSN 0378-7753, 10.1016/j.jpowsour.2004.11.065.
103. Kwang Joo Kim, Jung Han Lee, “Effects of nickel doping on structural and optical properties of spinel lithium manganate thin films”, *Solid State Communications*, Volume 141, Issue 2, January 2007, Pages 99-103, ISSN 0038-1098, 10.1016/j.ssc.2006.08.044.
104. Dragana Jugović, Dragan Uskoković, “A review of recent developments in the synthesis procedures of lithium iron phosphate powders” *Journal of Power*

Sources, Volume 190, Issue 2, 15 May 2009, Pages 538-544, ISSN 0378-7753, 10.1016/j.jpowsour.2009.01.074.

105. Kuperman, A.; Levy, U.; Goren, J.; Zafransky, A.; Savernin, A., "Battery Charger for Electric Vehicle Traction Battery Switch Station," *Industrial Electronics, IEEE Transactions on* , vol.PP, no.99, pp.1,1, 0 doi: 10.1109/TIE.2012.2233695

106. V. Svoboda, H. Doering, J. Garche, “The influence of fast charging on the performance of VRLA batteries” *Journal of Power Sources*, Volume 144, Issue 1, 1 June 2005, Pages 244-254, ISSN 0378-7753, 10.1016/j.jpowsour.2004.12.026.
107. Fu-Ming Wang, Hsin-Yi Wang, Meng-Han Yu, Yi-Ju Hsiao, Ying Tsai, “Differential pulse effects of solid electrolyte interface formation for improving performance on high-power lithium ion battery” *Journal of Power Sources*, Volume 196, Issue 23, 1 December 2011, Pages 10395-10400, ISSN 0378-7753,
108. Nelson, R.F.; Rinehart, R.; Varley, S., "Ultrafast pulse discharge and recharge capabilities of thin-metal film battery technology," *Pulsed Power Conference, 1997. Digest of Technical Papers*. 1997 11th IEEE International , vol.1, no., pp.636,641 vol.1, June 29 1997-July 2 1997 doi: 10.1109/PPC.1997.679411
109. M.Luisa Soria, Joaquín Chacón, J.Carlos Hernández, Daniel Moreno, Araceli Ojeda, “Nickel metal hydride batteries for high power applications” *Journal of Power Sources*, Volume 96, Issue 1, 1 June 2001, Pages 68-75, ISSN 0378-7753, http://dx.doi.org/10.1016/S0378-7753(00)00677-7.
110. Lu Zhang, “AC impedance studies on sealed nickel metal hydride batteries over cycle life in analog and digital operations” *Electrochimica Acta*, Volume 43, Issues 21–22, 1 July 1998, Pages 3333-3342, ISSN 0013-4686, http://dx.doi.org/10.1016/S0013-4686(98)00056-5.

111. Jixiao Zhang, Jingxian Yu, Chuansin Cha, Hanxi Yang,"The effects of pulse charging on inner pressure and cycling characteristics of sealed Ni/MH batteries" *Journal of Power Sources*, Volume 136, Issue 1, 10 September 2004, Pages 180-185, ISSN 0378-7753, http://dx.doi.org/10.1016/j.jpowsour.2004.05.008.

112. Jun Li, Edward Murphy, Jack Winnick, Paul A Kohl, "The effects of pulse charging on cycling characteristics of commercial lithium-ion batteries" *Journal of Power Sources*, Volume 102, Issues 1–2, 1 December 2001, Pages 302-309, ISSN 0378-7753,

113. Frederick W. Grover, *Inductance Calculations: Working Formulas and Tables,Dover* Publications, Inc., New York, 1946

114. Dr. Liu,Fuqiang. *Personal Interview.* Professor of Material Science at the University of Texas at Arlington. 9/30/2013.

115. Barsoukov, E. and Macdonald, J. R. (eds) (2005) Index, in Impedance Spectroscopy: Theory, Experiment, and Applications, Second Edition, John Wiley & Sons, Inc., Hoboken, NJ, USA

116. Sheng Shui Zhang, "The effect of the charging protocol on the cycle life of a Li-ion battery" *Journal of Power Sources*, Volume 161, Issue 2, 27 October 2006, Pages 1385-1391, ISSN 0378-7753,

117. Wetz, D.A.; Novak, P.M.; Shrestha, B., "Development of a power electronic test stand for the elevated rate recharge of electrochemical energy storage devices," *Applied Power Electronics Conference and Exposition (APEC), 2012 Twenty-Seventh Annual IEEE* , vol., no., pp.2159,2166, 5-9 Feb. 2012

118. Norio Takami, Hiroki Inagaki, Yoshinao Tatebayashi, Hidesato Saruwatari, Keizoh Honda, Shun Egusa, "High-power and long-life lithium-ion batteries using

lithium titanium oxide anode for automotive and stationary power applications" *Journal of Power Sources*, ISSN 0378-7753, 10.1016/j.jpowsour.2012.11.055.

119. H. Huang, T. Faulkner, J. Barker, M.Y. Saidi, "Lithium metal phosphates, power and automotive applications" *Journal of Power Sources*, Volume 189, Issue 1, 1 April 2009, Pages 748-751, ISSN 0378-7753, 10.1016/j.jpowsour.2008.08.024. (
120. M Broussely, S Herreyre, P Biensan, P Kasztejna, K Nechev, R.J Staniewicz, "Aging mechanism in Li ion cells and calendar life predictions" *Journal of Power Sources*, Volumes 97–98, July 2001, Pages 13-21, ISSN 0378-7753, 10.1016/S0378-7753(01)00722-4.
121. J. Vetter, P. Novák, M.R. Wagner, C. Veit, K.-C. Möller, J.O. Besenhard, M. Winter, M. Wohlfahrt-Mehrens, C. Vogler, A. Hammouche, "Ageing mechanisms in lithium-ion batteries" *Journal of Power Sources*, Volume 147, Issues 1–2, 9 September 2005, Pages 269-281, ISSN 0378-7753, 10.1016/j.jpowsour.2005.01.006.
122. Rachid Yazami, Yvan F Reynier, "Mechanism of self-discharge in graphite–lithium anode" *Electrochimica Acta*, Volume 47, Issue 8, 1 February 2002, Pages 1217-1223, ISSN 0013-4686, 10.1016/S0013-4686(01)00827-1.
123. C. Li, H.P. Zhang, L.J. Fu, H. Liu, Y.P. Wu, E. Rahm, R. Holze, H.Q. Wu, "Cathode materials modified by surface coating for lithium ion batteries' *Electrochimica Acta*, Volume 51, Issue 19, 20 May 2006, Pages 3872-3883, ISSN 0013-4686, 10.1016/j.electacta.2005.11.015.
124. M Wohlfahrt-Mehrens, C Vogler, J Garche, "Aging mechanisms of lithium cathode materials," *Journal of Power Sources*, Volume 127, Issues 1–2, 10 March 2004, Pages 58-64.

125. P. Novak, D.A. Wetz, and B. Shrestha, 'Fast Recharge of Electrochemical Energy Storage Devices at Pulsed Elevated Rates,' *IEEE Transactions on Plasma Science*, Vol. 40, No. 10, Part: 1, 2012, pp. 2416 - 2424.
126. B. Shrestha, D.A. Wetz, and P. Novak, 'Pulsed Elevated Rate Discharge of Electrochemical Energy Storage Devices,' *IEEE Transactions on Plasma Science, Vol. 40*, No. 10, Part: 1, 2012, pp. 2462 - 2469.
127. Data sheets for the GAIA 18 Ahr Lithium-ion cell, http://www.gaia-akku.com/fileadmin/user_upload/downloads/cells/18AhHP_LFP.pdf, October 28, 2011.
128. Maxwell Technologies Datasheets for K2 Series Ultracapacitors, http://www.maxwell.com/ultracapacitors/products/large-cell/bcap0650.asp, © 2010 Maxwell Technologies, Inc.
129. Datasheets for JM Energy's Lithium Ion Capacitors. http://www.jmenergy.co.jp/en/product.html. Copyright(C) 2009.JM Energy Corporation
130. Peter Michael Novak, David Alan Wetz, and Biju Shrestha. "Cycling Fatigue Induced on Electrochemical Energy Storage Cells as a Result of High C Pulsed Charging" *Electrochemical Society Transactions*. 2013 50(26): 175-186;
131. P. Arora, B. N. Popov, and R. E. White. "Electrochemical Investigations of Cobalt-Doped LiMn2 O 4 as Cathode Material for Lithium-Ion Batteries" *Journal of the Electrochemical Society*. 1998 145(3): 807-815; doi:10.1149/1.1838349
132. M. D. Levi, G. Salitra, B. Markovsky, H. Teller, D. Aurbach, Udo Heider, and Lilia Heider "Solid-State Electrochemical Kinetics of Li-Ion Intercalation into Li1 − x CoO2: Simultaneous Application of Electroanalytical Techniques SSCV, PITT,

and EIS" *Journal of the Electrochemical Society*.1999 146(4): 1279-1289; doi:10.1149/1.1391759

133. Rodrigues, Shalini, Munichandraiah, N., Shukla, A. K. "AC impedance and state-of-charge analysis of a sealed lithium-ion rechargeable battery". *Journal of Solid State Electrochemistry*. 1999. Pgs 397-405.
134. F Croce, F Nobili, A Deptula, W Lada, R Tossici, A D'Epifanio, B Scrosati, R Marassi, "An electrochemical impedance spectroscopic study of the transport properties of LiNi0.75Co0.25O2" *Electrochemistry Communications*, Volume 1, Issue 12, 1 December 1999, Pages 605-608, ISSN 1388-2481,
135. Eckhard Karden, Stephan Buller, Rik W. De Doncker, "A frequency-domain approach to dynamical modeling of electrochemical power sources" *Electrochimica Acta*, Volume 47, Issues 13–14, 25 May 2002, Pages 2347-2356, ISSN 0013-4686, 10.1016/S0013-4686(02)00091-9.
136. V.H. Johnson, "Battery performance models in ADVISOR*" Journal of Power Sources*, Volume 110, Issue 2, 22 August 2002, Pages 321-329, ISSN 0378-7753, 10.1016/S0378-7753(02)00194-5.
137. V.H. Johnson, A.A Pesaran, T. Sack. "Temperature-Dependent Batery Models for High-Power Lithium-Ion Batteries". NREL. Presentation. Online. http://www.nrel.gov/vehiclesandfuels/energystorage/pdfs/evs17poster.pdf
138. K. Levenberg, "A method for the solution of certain problems in least squares" *Quarterly of Applied Mathematics*, 5, 164–168, 1944
139. D. Marquardt, "An algorithm for least-squares estimation of nonlinear parameters" *SIAM Journal on Applied Mathematics*, 11(2), 431–441, June 1963.

140. Hao Yu and B. M. Wilamowski, “Levenberg–Marquardt Training” Industrial Electronics Handbook, vol. 5 – Intelligent Systems, 2nd Edition, chapter 12, pp. 12-1 to 12-15, CRC Press 2011.
141. Agnieszka Kapałka, György Fóti, Christos Comninellis, “Determination of the Tafel slope for oxygen evolution on boron-doped diamond electrodes, “*Electrochemistry Communications*, Volume 10, Issue 4, April 2008, Pages 607-610
142. E.X Sun, W.B Nowak, “Electrochemical characteristics of Ti–6Al–4V alloy in 0.2 N NaCl solution: I. Tafel slopes in quasi-passive state” *Corrosion Science*, Volume 43, Issue 10, October 2001, Pages 1801-1816, ISSN 0010-938X,
143. MEMSCAP Corporation. “Polymumps”. Online. Accesssed 8/22/2013. http://www.memscap.com/products/mumps/polymumps

Biographical Information

Peter Novak was born in Houston, Texas. He earned a Bachelor of Science in 2007 from Colorado School of Mines and worked for Fluor Daniel as a design electrical engineer for two years before going to graduate school at the University of Texas at Arlington. He is a member of the IEEE, and has actively published in their literature. His research interests include polyphase power, pulsed power, and electrochemistry.

---

i